Computational Studies of Environmentally-Related Topics: Part I. Elucidating Mechanisms of Rhenium-Mediated Carbon Dioxide Conversion Part II. Investigating Vinyl Radical and Methyl Peroxy Radical Combustion Intermediates

by

Jay Agarwal

(Under the direction of Henry F. Schaefer III)

Abstract

Combustion processes are a major contributor of pollutants in the atmosphere; they emit particles of soot, and greenhouse gases like carbon dioxide and nitrogen oxides. Reducing the environmental impact of combustion is central to protecting the environment and mitigating unwanted climate change. Many solutions have been proposed, including increasing the efficiency of combustion to reduce soot formation or lowering the combustion temperature to avoid forming nitrogen oxides. Additionally, the conversion or sequestration of CO_2 has been suggested. In each case, fundamental research is required to identify suitable conditions and materials. Herein, we present research that contributes to the understanding of elementary combustion processes and the conversion of CO_2. In the first part, mechanisms of rhenium-mediated CO_2 conversion to CO are reported. The second part presents data for two key combustion intermediates: the reaction energies for vinyl radical + molecular hydrogen and the infrared signature of methyl peroxy radical.

INDEX WORDS: carbon dioxide conversion, rhenium catalysts, density functional theory, combustion, soot formation, coupled cluster theory, vibrational perturbation theory, alkyl peroxy radicals

Computational Studies of Environmentally-Related Topics: Part I. Elucidating Mechanisms of Rhenium-Mediated Carbon Dioxide Conversion Part II. Investigating Vinyl Radical and Methyl Peroxy Radical Combustion Intermediates

by

Jay Agarwal

B.S., University of New Hampshire, 2010

A Dissertation Submitted to the Graduate Faculty
of The University of Georgia in Partial Fulfillment
of the
Requirements for the Degree

Doctor of Philosophy

Athens, Georgia

2013

Computational Studies of Environmentally-Related Topics: Part I. Elucidating Mechanisms of Rhenium-Mediated Carbon Dioxide Conversion Part II. Investigating Vinyl Radical and Methyl Peroxy Radical Combustion Intermediates

by

Jay Agarwal

Approved:

Major Professors: Henry F. Schaefer III

Committee: Geoffrey D. Smith
Johnathan L. Stickney

Electronic Version Approved:

Dr. Maureen Grasso
Dean of the Graduate School
The University of Georgia
May 2013

Acknowledgments

For their wonderful support and genuine interest in my success, I thank my parents, my brother, family friends Edgar and Suzanne, and the Birchard family. I also wish to acknowledge two grade-school teachers I found particularly inspirational: my fourth-grade math teacher Mrs. Gamache and my high-school English teacher Mr. Cole. I also thank the Mueller family for their hospitality and kindness.

For academic advice and assistance at the University of New Hampshire, I thank Mr. Cary Kilner, Dr. Gonghu Li, Dr. Richard Johnson, Dr. Ed Wong, and Mr. Tom Towle. Additionally, I acknowledge many faculty members at the University of Georgia who provided laboratory use and helpful collaboration. They are: Dr. Gary Douberly, Dr. George Majetich, Dr. Todd Harrop, and Dr. Jason Locklin. I also thank Drs. Etsuko Fujita and Jim Muckerman at Brookhaven National Laboratory and Dr. Andy Bocarsly at Princeton University for their summer support and assistance. To my committee members, Drs. Geoff Smith and John Stickney, thank you for your time and patience.

To my advisor, Dr. Schaefer, I am very grateful for your trust and thankful for your support as I pursued experimental and theoretical research at UGA and elsewhere. I also acknowledge the CCQC members for their help and support. In particular, Dr. Andy Simmonett, Stefan Vogt, Shane McNew, Mrs. Linda Rowe, Dr. Justin Turney, Alex Sokolov, David Hollman, and Brandon Magers.

Table of Contents

Part I

Elucidating Mechanisms of Rhenium-Mediated Carbon Dioxide Conversion

Chapter 1

Introduction and Literature Review

Carbon dioxide is a simple, linear, three-atom molecule that was first prepared by van Helmont[1] and later studied by many famous scientists, including Cavendish,[2] Priestley,[3] Lavoisier,[4] and Faraday.[5] In present times, CO_2 is commonly employed as a refrigerant, chemical feedstock, or inert gas.[6–10] Yet, despite these uses, only half of the CO_2 generated (e.g., from the combustion of fossil-fuels) is recovered[11] due, in part, to the difficulty in separating it from other components of flue gas. Additionally, the financial cost of isolating CO_2 and transporting it after production is much greater than its economic value. Still, there is an impetus to develop uses for CO_2 to mitigate its release into the atmosphere where it functions as a greenhouse gas.[12–23]

In this context, the 'greenhouse effect' describes the absorption of scattered light energy, and subsequent increase in temperature within the inner atmosphere. Carbon dioxide exhibits infrared absorption at wavelengths longer than 1.5 μm, and is generally considered to be the main cause of this effect.[24] As such, it is termed a greenhouse gas. CO_2 is not alone, however; CO, N_2O and CH_4 are all greenhouse gases that are present in the inner atmosphere and exhibit infrared absorption. Their presence is key to sustaining life on Earth, much like the important layer of ozone in the stratosphere that prevents ultraviolet light from reaching the Earth's surface. But, CO_2 is a much stronger absorber than the others,[25] which makes

its utilization a primary environmental objective.

A recent study published in *Nature* estimates that the warming of the inner atmosphere occurs at a rate of 2.2-4.8 K per doubling of atmospheric CO_2.[26] This result, combined with the increase in CO_2 concentration from 295 to 371 parts per million volume (ppmv) in just the last 100 years (and the continued rise), suggests serious implications for terrestrial systems.[27] It is worth noting, however, that there is controversy surrounding the exact impact of CO_2 on climate change. Notwithstanding, CO_2 is also an attractive feedstock for building carbon products because of its abundance and low cost.[28]

Simply increasing CO_2 utilization through existing processes is unlikely to address the issue of rising concentration because, among other reasons, another feedstock would be consumed on the same order of magnitude as the CO_2 converted. Few species exist that have a negligible cost and the abundance to be employed on this scale, and most of them are very thermodynamically stable like CO_2. One potential solution is to mimic nature and utilize water as a feedstock. In this motif, an oxidation-reduction reaction could be designed to include the oxidation of water to two protons, two electrons and oxygen at an anode, liberating O_2. The cathode would then mediate the reduction of CO_2 using the two electrons and two protons garnered from water to yield CO or HCO_2H. If multiple equivalents of protons and electrons could be stored and utilized per molecule of CO_2, additional products may be envisioned.[29] One prohibiting factor, however, is the preference of proton reduction (to H_2) rather than CO_2 reduction at the surface of common metal cathodes.

Current research in CO_2 conversion is directed towards identifying suitable cathodic materials; species that prefer to form bonds with carbon, to reduce CO_2, rather than hydrogen, to reduce protons. Many heterogenous catalysts have been successfully employed in this context as shown in Figure 1.1.[30] Most, however, display little selectivity between methane, carbon monoxide, formic acid, and hydrogen, among other products not shown. Coinage metals exhibit a modest preference for CO_2 reduction and copper produces a significant

amount of methane. In practice however, these metals are either too expensive or have limited lifetimes, but recent work to electrochemically control surface oxide formation shows promise.[31–33]

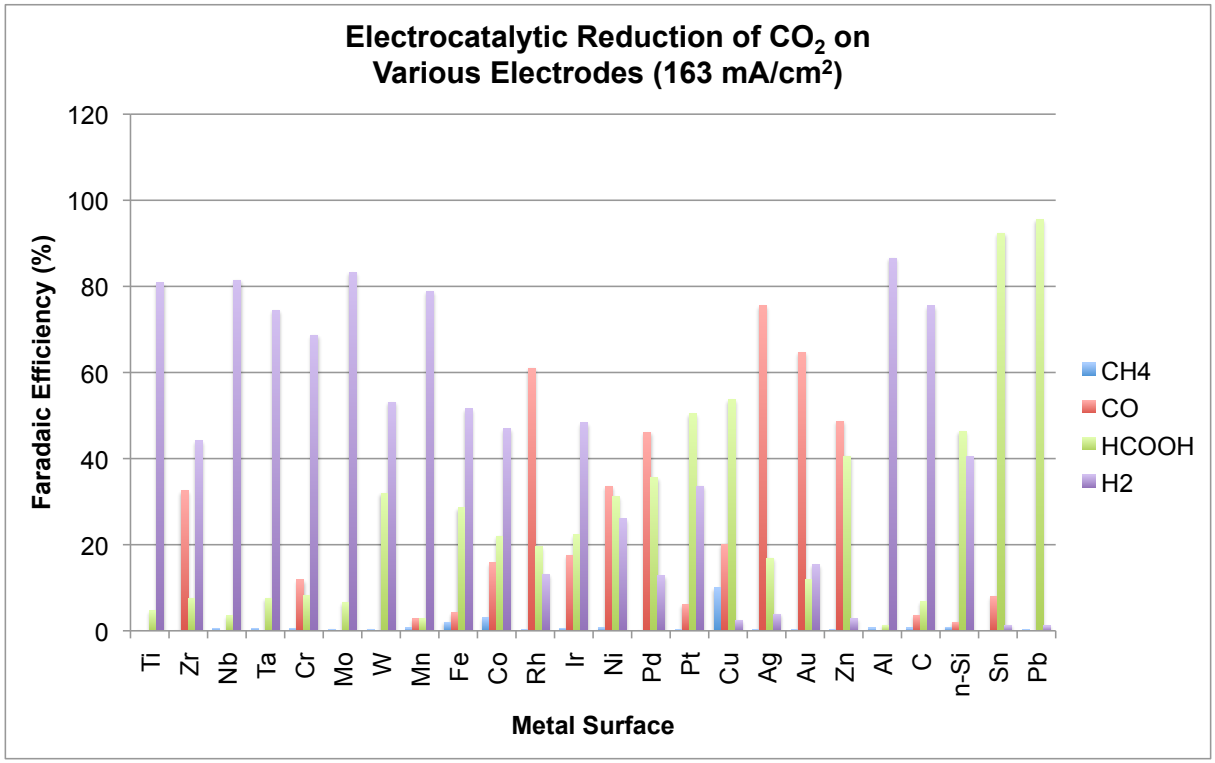

Figure 1.1: Products Formed as a Result of CO_2 Reduction at Selected Metal Cathodes. Adapted from Hara, Kudo and Sakata. [30]

Alternatively, homogenous organometallic complexes may be employed as catalysts. These species may be tethered or adsorbed onto the surface of electrodes or, instead, coupled to a photosensitizer to harness light energy. Homogenous catalysts benefit from increased selectivity, both in terms of reactants and products. Conversely, they are generally more expensive to synthesize than their heterogeneous counterparts and are often subject to scale-up issues. Nonetheless, the possibility of designing a molecular catalyst to selectively yield products like methanol or butanol has led to the development of iron,[34–36] ruthenium,[37–44] rhenium,[45–50] cobalt,[36,51–58] iridium,[59,60] and nickel[52,61–67] centered complexes.

Regardless of the metal center, promising molecular catalysts must be able to i) store redox equivalents; ii) coordinate and reduce CO_2; and, iii) dissociate the reduced product. Many known species already achieve this. Grignard species, for instance, are well known for their reactivity towards carbonyl containing compounds, including CO_2. In order for Grignard reagents to be catalytic, however, the metal, often magnesium, must be reduced after reaction. For magnesium, that requires a large electromotive force of -2.12 V versus the saturated calomel electrode (SCE).[68] Electrical consumption at this voltage on the scale required for CO_2 utilization would likely be cost prohibitive. For reference, many of the aforementioned catalysts operate at voltages less than -1.8 V versus SCE,[69,70] while the theoretical voltage required for the two-electron reduction of CO_2 is only -0.36 V versus SCE for formic acid production.[29] Clearly, the continued optimization of catalysts for CO_2 reduction is needed.

The subject of Chapters 2 and 3 is on rhenium tricarbonyl catalysts of the form Re(N-N)$(CO)_3$X where N-N is a pyridyl ligand, such as bipyridine, and X is generally a halogen, such as Br or Cl. Rhenium catalysts of this type exhibit some of the highest efficiencies for CO_2 reduction to CO.[71,72] This activity, combined with the relative ease of working with rhenium compared to first-row transition metals, has made them an attractive prototype for studying the underlying mechanisms of CO_2 reduction. Ultimately, cheaper first-row metals are envisioned for industrial use. In fact, isoelectronic manganese tricarbonyl complexes have recently been studied and show promise toward CO_2 reduction,[73,74] Development of these catalysts has been guided in part by the mechanistic understanding garnered from rhenium analogues.

Chapters 2 and 3 focus on the elucidation of the CO_2 reduction mechanism involving two related, but electronically disparate, pathways. Chapter 2 presents mechanisms for the one-electron reduction (OER) pathway, while Chapter 3 focuses on intermediates of the two-electron reduction (TER) pathway. The distinction between OER and TER often leads to confusion in the literature, especially since many variations of either route have been investigated.[29,45,46,69,70,75–77]

In Chapter 2, a complete pathway for rhenium-mediated reduction is proposed from a density functional theory (DFT) investigation. This pathway begins with the OER of $Re(bpy)(CO)_3Cl$ to give the neutral radical $Re(bpy)(CO)_3^{\bullet}$. Chapter 3 concentrates on intermediates of the TER pathway beginning from $Re(bpy)(CO)_3^{-}$. This reduced anion is thought to coordinate CO_2 via η^1, Re-COO bonding. In a protic environment, this could yield a myriad of species, but CO production is the major product. One suggested intermediate is $Re(bpy)(CO)_3COOH$. A pathway for CO formation from this intermediate is presented from a joint theoretical and experimental investigation using DFT and isotopically labeled ^{13} CO_2, respectively.

Chapter 2

Mechanisms for CO Production from CO_2 Using Reduced Rhenium Tricarbonyl Catalysts [1]

[1] J. Agarwal, E. Fujita, H. F. Schaefer, and J. T. Muckerman *J. Am. Chem. Soc.*, **2012**, 134, 5180-5186. Reproduced by permission of The American Chemical Society.

2.1 Abstract

The chemical conversion of CO_2 has been studied by numerous experimental groups. Particularly the use of rhenium tricarbonyl based molecular catalysts has attracted interest owing to their ability to absorb light, store redox equivalents, and convert CO_2 into higher-energy products. The mechanism by which these catalysts mediate reduction, particularly to CO and $HCOO^-$, is poorly understood, and studies aimed at elucidating the reaction pathway have likely been hindered by the large number of species present in solution. Herein the mechanism for carbon monoxide production using rhenium tricarbonyl catalysts has been investigated using density functional theory (DFT). The investigation presented proceeds from the experimental work of Meyer's group (*J. Chem. Soc. Chem. Commun.* **1985**, 1414-1416) in DMSO and Fujita's group (*J. Am. Chem. Soc.* **2003**, 125, 11976-11987) in dry DMF. The latter's work with a simplified reaction mixture, one that removes the photo-induced reduction step with a sacrificial donor, is used for validation of the proposed mechanism, which involves formation of a rhenium carboxylate dimer, $[Re(dmb)(CO)_3]_2(OCO)$ where dmb = 4,4'-dimethyl-2,2'-bipyridine. CO_2 insertion into this species, and subsequent rearrangement, is proposed to yield CO and the carbonate bridged $[Re(dmb)(CO)_3]_2(OCO_2)$. Structures and energies for the proposed reaction path are presented and compared to previously published experimental observations.

2.2 Introduction

The utilization of carbon dioxide is a primary environmental objective due to its role as a greenhouse gas (GHG).[13–15,17,18,20,22,23] The abundance of CO_2 also makes it an attractive feedstock, similar to H_2O and N_2, but the thermodynamic stability of these species makes chemical conversion an energy intensive process.[78] With regard to CO_2, several metal-centered catalysts are capable of mediating chemical conversion to higher-energy products,

including nickel,[52,61–66] cobalt,[36,51–58] ruthenium,[37–44] rhenium,[45–49,79] and iron[34–36,80] complexes. The work herein is focused on rhenium tricarbonyl photocatalysts. In particular [*fac*-Re(2,2'-bipyridine)$(CO)_3X]^n$, where the bipyridine may be bare or functionalized and X is an axial ligand such as a halide (n = 0) or a solvent molecule (n = +1). Herein we use 'axial' to describe ligands perpendicular to the 'equatorial' plane formed by bipyridine, the metal, and two carbonyl ligands. Prior work has shown that this catalyst, once irradiated in a CO_2 saturated solvent, yields two products: CO (major) and $OCHO^-$.[45,48,69,71,81,82] The mechanisms for product formation, however, are not well understood.

Mechanistic studies are hindered in part by the large number of species present in solution, especially in the case of photochemical reduction with a sacrificial electron donor, which makes spectroscopic analysis difficult. Since catalytic CO_2 reduction is preceded by reduction of the metal center, sacrificial donors must be included in solution to quench the excited metal center after irradiation. These sacrificial species, often tertiary amines, are added in excess, and the oxidized, open-shell products participate in several decomposition pathways.[83,84] Subsequent by-products continue to react with species in solution, which makes elucidation of the specific reaction path difficult. Previously, amines have been proposed as both a proton and electron source for reduction,[50,85,86] but CO_2 can also be reduced in the absence of such species.[45,87]

We note that in published mechanistic studies several steps have been observed after the metal center has been reduced.[45,53,87] First the axial ligand (X) dissociates, leaving a 5-coordinate (17 e^-) complex. This neutral radical is trapped by coordinating solvents such as acetonitrile (MeCN) and dimethylformamide (DMF) to form a 6-coordinate ("19 e^-") species with the unpaired electron on the bipyridine ligand. An equilibrium between the 5- and 6-coordinate species allows for potential CO_2 coordination at the axial position.[88] Further steps have been postulated in previous experimental publications to include dimer formation,[45] carboxylic acid formation,[77] and/or outer-sphere electron transfer.[69]

One way to simplify the reaction is to remove the photoexcitation step. This can be achieved by monitoring CO_2 reduction on an electrode-immobilized catalyst, or a catalyst in a solution with supporting electrolyte using an electrochemical method.[89?] Alternatively, the one-electron-reduced (OER) center can be prepared by photo-cleavage of a Re-Re dimer in a CO_2 saturated solvent.[45] We have focused on studies using the latter, which mitigates the inclusion of excess electrolyte, but forgoes the catalytic cycle. Thus, the reactants are simply the OER rhenium catalyst [where the active species is $Re(bpy)(CO)_3^{\bullet}$], CO_2, and solvent.

Of special interest to us is the experimental work of Hayashi, Kita, Brunschwig, and Fujita, who prepared the OER rhenium catalyst by photo-cleaving the Re-Re bond of $[Re(dmb)(CO)_3]_2$ where dmb = 4,4'-dimethyl-bpy, which was prepared using Na-Hg reduction.[45] Briefly, they observed that in CO_2 saturated DMF several products formed: carbon monoxide, a rhenium carbonate dimer, $[Re(dmb)(CO)_3]_2(OCO_2)$, and $Re(dmb)(CO)_3(OCO_2H)$. They were also able to observe a long-lived intermediate, $[Re(dmb)(CO)_3]_2(C(O)O)$, using NMR. This species decomposes with a rate that is first-order in $[CO_2]$ and produces CO with a 25-50% yield based on [Re]. From this work we propose a mechanistic pathway for CO production that begins with the formation of a rhenium carboxylate dimer, as observed, and proceeds with CO_2 insertion into the rhenium-oxygen bond. We present energies and structures from our density-functional theory (DFT) investigation in the following sections.

2.3 Theoretical Methods

All computations were performed using density-functional theory (DFT) as implemented in Gaussian 09.[90] Geometry optimization and vibrational analysis were computed in the gas-phase. Molecular size precluded geometry optimization with implicit solvent, but solvation was included in subsequent single-point energy computations using the polarizable continuum model (CPCM) with default parameters for DMF.[91,92] Stationary points were verified using vibrational analysis, and transition-state structures were connected to minima using intrinsic reaction coordinate (IRC) computations.[93–95]

We chose to employ the popular B3LYP functional, which includes Becke's three-parameter hybrid functional with the Lee-Yang-Parr correction for correlation.[96–98] Additionally, we have included energy values computed with M06-L, a local density functional recently developed by Zhao and Truhlar.[99] Prior work has shown that these functionals are appropriate for studying complexes containing transition metals,[100–103] and for rhenium specifically.[104,105]

To parameterize the rhenium center we chose the LANL08F basis set with Hay-Wadt relativistic effective core potential (ECP). In prior work, this uncontracted triple-ζ quality basis set has been shown to provide an appropriate description of rhenium's core and valence shells.[105–107] For light atoms (H, C, N, and O), the 6-31++G(d,p) Pople basis set was used.[108,109] Where appropriate, a correction was applied to account for the standard-state of 1 molar for non-gases in solution.

2.4 Results and Discussion

Our proposed mechanism for CO production is outlined in Scheme 2.1. We first discuss the pathways that are depicted in this figure before relating them to experiment. Relative standard enthalpies for the reaction steps shown in Scheme 2.1 are listed in Table 2.1, with a depiction of the energy profile shown in Figure 2.2. Geometries for the transition states

are shown in Figure 2.3. We reference the solvent-phase M06-L enthalpies in our discussion, but provide additional results from computations using B3LYP and M06-L functionals for later comparison.

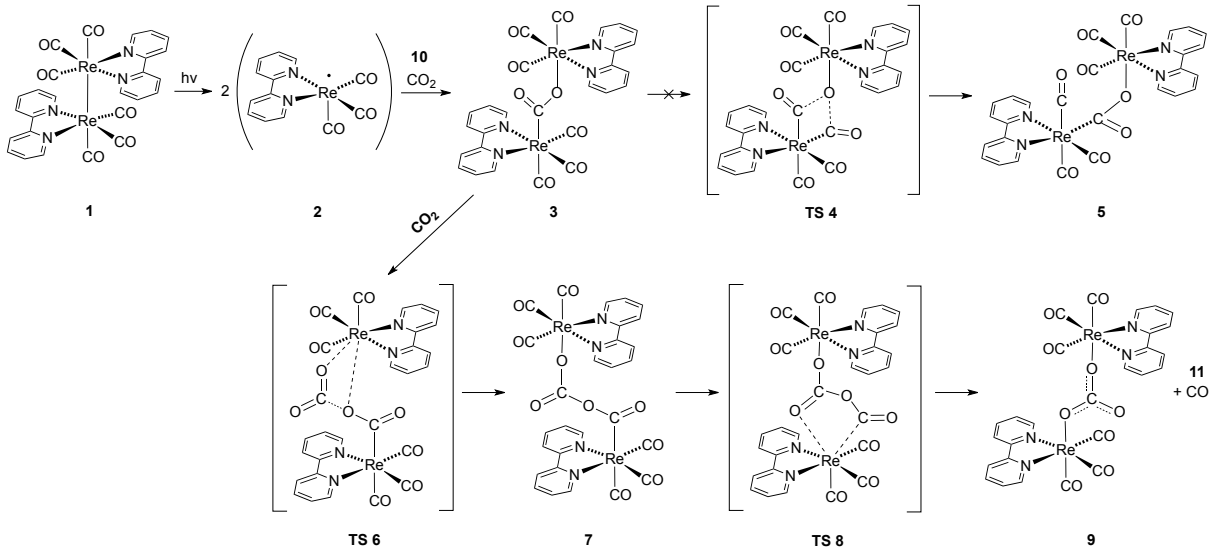

Figure 2.1: Proposed Reduction Pathway

A. Mechanism

Our investigation begins with the OER rhenium catalyst, **2**, which is formed regardless of the reduction mechanism. That is, $Re(bpy)(CO)_3^{\bullet}$ may be formed from photocleavage of the Re-Re bond in **1**, the one-electron reduction of $Re(bpy)(CO)_3X$ using an electrical bias, or the photochemical reduction of $Re(bpy)(CO)_3X$ using tertiary amines. This OER species exists in an equilibrium between the 5- and 6-coordinate configurations, the latter having been solvated by a coordinating solvent. In the 5-coordinate arrangement there is a vacant coordination site at an axial position that allows for CO_2 coordination. In the event that two OER centers are in the proximity of CO_2, a carboxylate dimer, **3**, may form. This process is not favored entropically, however, as three bodies must converge to one, but we find that it is a significantly exothermic step (-36.0 kcal mol^{-1}).

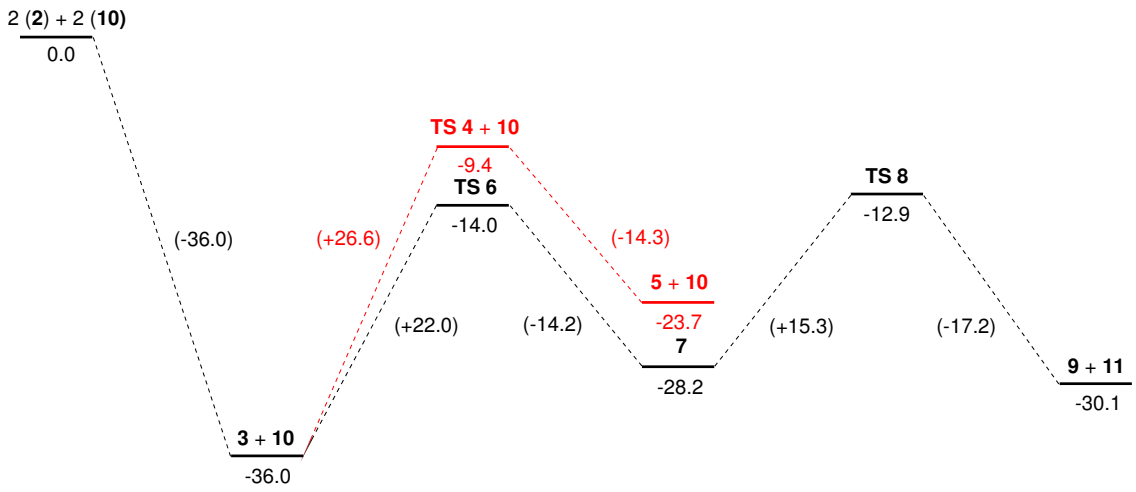

Figure 2.2: Standard Enthalpy Profile. ΔH^*(DMF) energies shown in kcal mol^{-1}. The isomerization of **3** is indicated in red.

The geometry of **3** is a skewed 'trans' configuration with respect to the bipyridine rings; the bipyridine ligands oppose each other, but are not parallel so no symmetry plane exists. In our investigation we considered the rotation of the monomer units around the bridging carbon dioxide moiety while searching for the lowest energy structure by considering 'cis', 'trans', and skewed arrangements, but in each case optimization yields a skewed 'trans' minimum. From further analysis we found that the dimer may then follow two potential pathways: one leading to isomerization and the other to CO_2 insertion. We are primarily concerned with the latter, but briefly discuss the former.

Isomerization of **3** proceeds through **TS 4**. The original dimer, **3**, contains a bridged CO_2 species, with a carbon atom bound at the axial position of one rhenium center and an oxygen atom bound at the axial position of the other. The first step of isomerization is formation of a bond between the rhenium bound oxygen of CO_2 and an equatorial carbonyl ligand coordinated to the opposing rhenium center. This yields the transition state **TS 4**.

Table 2.1: Relative Enthalpies for Steps of the Present Mechanism for Given DFT Functionals [a]

	B3LYP		M06-L	
Reaction Step	ΔH^o(Gas)	ΔH^o(DMF) [b]	ΔH^*(Gas) [c]	ΔH^*(DMF) [d]
2 (**2**) + **10** → **3**	-30.7	-34.8	-32.9	-36.0
3 → **TS 4**	24.8	25.8	25.6	26.6
3 → **5**	10.0	12.4	10.1	12.3
3 + **10** → **TS 6**	25.4	22.0	25.5	22.0
3 + **10** → **7**	7.7	8.6	7.1	7.8
7 → **TS 8**	22.8	14.5	23.6	15.3
7 → **9** + **11**	-4.7	-0.6	-6.0	-1.9

[a] Energies shown in kcal mol^{-1}. Thermal correction to the enthalpy (H_{corr}) computed with B3LYP in the gas-phase. Energy values include ZPVE correction. [b] H = E[M06-L(Gas)] + H_{corr}. [c] H = E[B3LYP(DMF)] + H_{corr}. [d] H = E[M06-L(DMF)] + H_{corr}.

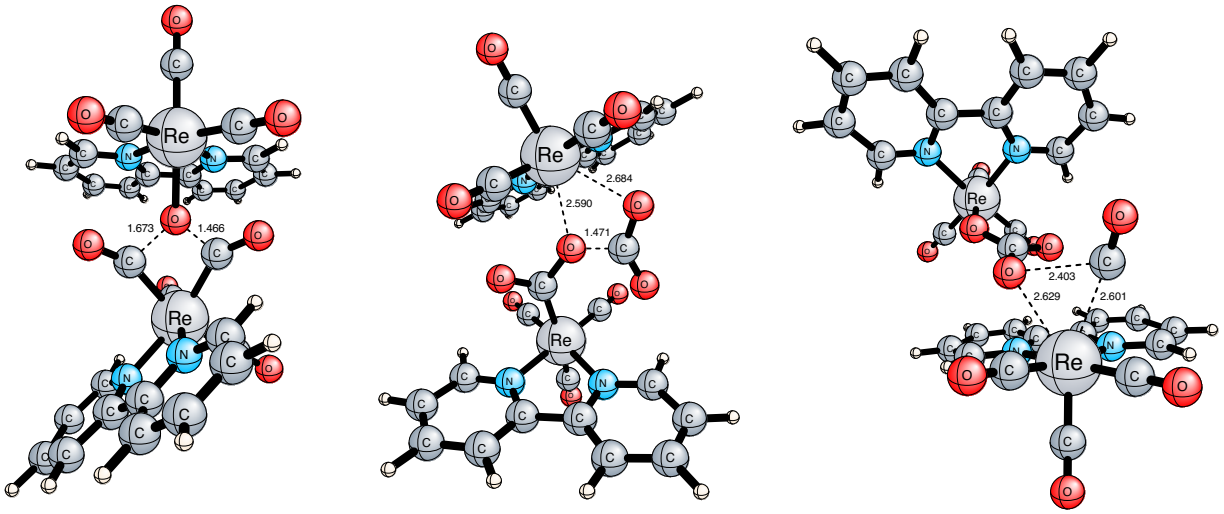

TS 4 **TS 6** **TS 8**

Figure 2.3: Optimized geometries for the isomerization, CO_2 insertion, and rearrangement transition state structures. Bond lengths shown in Angstroms. Geometries were optimized at the B3LYP/LANL08F (Re), 6-31++G(d,p) (H,N,C,O,Cl) level of theory.

Next, the original oxygen-carbon bond in the bridging CO_2 species is cleaved, leaving a carbonyl ligand at the axial position of one rhenium center. After cleavage, the rhenium centers are still bridged by CO_2, but with an oxygen atom bound at the axial position of one rhenium center and a carbon atom bound at the equatorial position of the other. There exists a high activation barrier to this process (26.6 kcal mol^{-1}), and the isomerization is overall endothermic by 12.3 kcal mol^{-1}. Thus the original dimer, **3**, is favored.

If an additional CO_2 molecule is available in solution, it may insert into the carboxylate dimer, **3**, at the rhenium-oxygen bond. CO_2 insertion is a step-wise process beginning with the insertion transition-state **TS 6**, leading to **7**, a local minimum. Then, the complex rearranges through **TS 8** to yield **9**. It is important to note that the initial insertion step mirrors that of CO_2 insertion into a rhenium-hydride bond.[50,110] In both cases the carbon atom of the attacking CO_2 molecule acts as a Lewis acid, and forms a covalent bond with the electron-rich axial ligand bound to rhenium. At the same time, an oxygen atom of CO_2 donates a lone pair of electrons to form a rhenium-oxygen dative bond. In the case of the dimer, the electron-rich ligand is an oxygen atom that belongs to the bridging CO_2 species. This first step yields **7**, a dimer with an elongated bridging ligand consisting of two CO_2 monomers. Insertion, therefore, may be viewed as the oligomerization of CO_2. Importantly, the activation barrier to forming **TS 6** (22.0 kcal mol^{-1}) is lower than that of isomerization. Overall, this step is endothermic by 7.8 kcal mol^{-1}.

Following insertion, the new dimer complex, **7**, undergoes rearrangement. This is a critical step that yields carbon monoxide. The rearrangement step involves migration of one rhenium center from the carbon atom of the original CO_2 to the oxygen atom of the attacking CO_2. The result of this process is cleavage of a carbon-oxygen bond within the original CO_2 to yield CO, **11**, in addition to CO_3, which has a formal -2 charge (i.e., carbonate) and bridges the two Re(I) centers to yield **9**. The activation barrier for this step, through **TS**

8, is 15.3 kcal mol^{-1}. This process, **3** + **10** → **9** + **11**, is endothermic by 5.9 kcal mol^{-1}. Overall the two steps of the insertion process can be viewed as disproportionation of two CO_2 molecules with two electrons (one from each of the two Re centers) to yield carbonate and carbon monoxide.

Tryk and co-workers previously investigated electrochemical CO_2 reduction using metal-supported nanoporous activated carbon fiber electrodes in aqueous $KHCO_3$.[111] They proposed the involvement of $(CO_2)_2^{\bullet-}$ formed by the reaction of CO_2 with $CO_2^{\bullet-}$. Subsequent reduction of this species forms $(CO_2)_2^{2-}$, which produces CO and CO_3^{2-} by disproportionation. Our system also produces $(CO_2)_2^{2-}$ [in the form of Re^{I}-$(CO_2)_2^{2-}$-Re^{I}], but from the direct two-electron reduction of CO_2 rather than through a radical intermediate.

Another way to describe the insertion process is through the movement of electrons. The initial metal-metal dimer, **1**, is a neutral complex with a 34-electron dinuclear core. Homolytic cleavage of the weak Re-Re bond in this dimer yields two 5-coordinate, 17-electron monomers that are neutral radicals. As mentioned, the monomer exists in an equilibrium between the 5-coordinate 17-electron species and the solvated, 6-coordinate "19-electron" species with the unpaired electron on the bipyridine ligand.

The carboxylate dimer, **3**, forms through the addition of the two radical Re metal centers across a CO double bond to form CO_2^{2-} with a bent structure. Thus each metal center is oxidized by one electron, leaving each rhenium with a +1 formal charge. Overall, the carboxylate dimer is a neutral singlet.

Insertion of an additional CO_2 into **3** of course has no effect on the overall charge. The two electrons that form a dative bond between the oxygen atom of CO_2 and the rhenium center are used to form a covalent bond with the carbon atom of the inserting CO_2 molecule. Subsequently a double bond in the attacking CO_2 breaks heterolytically, which allows for a dative bond to form between a new oxygen atom and rhenium. Therefore, the two electrons that originated from the reduced metal centers are still contained within the bridging moiety,

which has a formal -2 charge. Disproportionation of this moiety through rearrangement yields neutral CO and the dianion $CO_3{}^{2-}$, which bridges the two cationic metal centers to yield the neutral dimer **9**. It is important to note that the first equivalent of CO_2, the one used to form **3**, contains the carbon atom that is part of the CO product. The second equivalent of CO_2, on the other hand, contains the carbon atom that becomes part of the $CO_3{}^{2-}$ moiety in **9**.

B. Comparison to Experimental Work

Sullivan and co-workers[87] and Hayashi and co-workers[45] have both studied the reduction of CO_2 using a reduced Re-Re dimer. Homolytic cleavage of the weak metal-metal bond in this species yields two neutral radical monomers, which react with CO_2. The same monomer is produced in photocatalytic reduction, but requires the presence of sacrificial donors in solution. As mentioned, removing the photo-reduction step has the consequence of eliminating the catalytic cycle, but the benefit of greatly simplifying the reaction mixture.

To produce the reduced rhenium dimer, Sullivan and co-workers began with $Re_2(CO)_{10}$. In a reflux of xylenes and bpy (2,2'-bipyridine), they exchanged four CO ligands for the bidentate bpy to produce **1**. Conversely, Hayashi and co-workers started with two rhenium monomers, $Re(dmb)(CO)_3OTf$, and reduced them with Na-Hg amalgam to produce $[Re(dmb)(CO)_3]_2$. In either case, the neutral radical monomer can be produced from the metal-metal dimer and a CO product is observed when using a CO_2 saturated solvent. It is important to note that for our investigation we have used bpy, like Sullivan and co-workers, instead of dmb, like Hayashi and co-workers, in an effort to reduce the size of our computations. Therefore in the following discussion we refer to our structures in Figure 2.1 for simplicity, in spite of the fact that they contain bare rather than functionalized bpy ligands.

Sullivan and co-workers carried out experiments with the reduced dimer in CO_2 saturated dimethylsulfoxide (DMSO). They observed CO and Re(bpy)$(CO)_3$(OC(O)OH) as products, but were unable to observe intermediates. They conjectured that it was possible the radical monomers, **2**, reacted directly with CO_2. Hayashi and co-workers began with a similar experiment, employing the Re-Re dimer in a $^{13}CO_2$ saturated solution of dimethylformamide (DMF) with incident irradiation. By monitoring the reaction with ^{1}H NMR, ^{13}C NMR, FTIR, and GC, they were able to identify ^{13}CO, [Re(dmb)$(CO)_3]_2(O^{13}CO_2)$, and Re(dmb)$(CO)_3(O^{13}$C(O)OH) as products. They note that the Re(dmb)$(CO)_3$(OC(O)OH) product, left to stand, converts to [Re(dmb)$(CO)_3]_2(OCO_2)$. Importantly, they did not observe H_2, ^{12}CO, or $HCOO^-$ production, but identified the carboxylate dimer [Re(dmb)$(CO)_3]_2(O^{13}$CO) as a long-lived intermediate.

Our proposed insertion pathway agrees well with the experimental observations. To begin, we find the first equivalent of CO_2 bridges two reduced monomers, **2**, to form **3**. While a carboxylate bridge could conceivably be formed through other routes, the observation of [Re(dmb)$(CO)_3]_2(O^{13}$CO) using $^{13}CO_2$ indicates that the first equivalent of CO_2 becomes the bridging species. From **3**, we predict the activation barrier for isomerization or insertion to be relatively high ($>$ 20 kcal mol^{-1}), adding to the stability of the carboxylate dimer as a long-lived intermediate. The high barrier to insertion (21.5 kcal mol^{-1}), which is the energetically favored route, also agrees with the relatively slow reaction rate of 0.003 s^{-1}.[45] Similarly, the decay of [Re(dmb)$(CO)_3]_2(O^{13}$CO) is first-order in [$^{13}CO_2$],[45] therefore formation of the products, ^{13}CO and [Re(dmb)$(CO)_3]_2(O^{13}CO_2)$ agrees with our proposed insertion step, **3** + **10** $\rightarrow$ **TS 6**, which is required for CO production.

Subsequent rearrangement of the dimer with an -O(CO)O(CO)- bridge, **7**, may be difficult to observe experimentally. The activation barrier for this step, **7** $\rightarrow$ **TS 8**, is modest (16.5 kcal mol^{-1}), and rearrangement is overall slightly exothermic (-0.3 kcal mol^{-1}). Again, this step is supported by experimental observations. We find that both of the products, **9**

and **11**, contain carbon atoms from added CO_2 equivalents. Therefore, if $^{13}CO_2$ is employed, the carbonate moiety of **9** and the CO product, **11**, should be ^{13}C labeled. This aligns with the observations of Hayashi and co-workers, who observed $[Re(dmb)(CO)_3]_2(O^{13}CO_2)$ and ^{13}CO using $^{13}CO_2$.[45]

More importantly, Hayashi and co-workers[45] did not observe ^{12}CO when employing $^{13}CO_2$. This eliminates the possibility that CO production is the result of ligand dissociation. Initially we had considered the possibility of a tetracarbonyl intermediate, $Re(bpy)(CO)_4^+$, but the presence of both isotope labeled and unlabeled axial carbonyl ligands should produce both labeled and unlabeled CO products. This is an important argument against the isomerization pathway, which we predict to be energetically unfavorable. The isomerization product **5** contains axial CO ligands that could dissociate to yield CO, but would yield both labeled and unlabeled products when employing $^{13}CO_2$. Furthermore, isomerization would form a dimer with an unlabeled carboxylate bridge, which does not match experimental observations. We did, however, "probe" the isomerized dimer for reaction with an additional equivalent of CO_2 at the carbon and oxygen atoms of the carboxylate bridge, but observed dissociation of the added CO_2 (i.e., no reaction) in each case. Conversely, we cannot account for the small amount of $Re(dmb)(CO)_3(OC(O)OH)$ that is observed. The formation of this species requires a proton source, likely trace water in solution.

C. Energetics

Standard enthalpies of reaction computed with the B3LYP and M06-L functionals are presented in Table 1. As the M06-L functional was designed for use with transition metals,[99,112] we chose to utilize it for comparison to our B3LYP values. Overall we find that enthalpies computed in solvent with the M06-L functional yield a description of the potential energy surface that is more consistent with experiment, but both functionals yield roughly the same trend in enthalpies across the reaction coordinate. Using both functionals we also

find that the change in energy as a result of including an implicit solvent model (CPCM) is small for each reaction step (< 1.5 kcal mol^{-1}), which is in part a consequence of all species being charge-neutral. For comparison, we briefly discuss the reaction pathways with regard to results from solvated enthalpies computed with B3LYP and M06-L.

For the formation of carboxylate dimer, step 2 (**2**) + **10** $\rightarrow$ **3**, B3LYP yields an enthalpy that is roughly 3 kcal mol^{-1} higher than M06-L (-32.9 kcal mol^{-1} vs. -36.0 kcal mol^{-1}). This trend persists in the activation barrier for insertion, with B3LYP returning a value 3.5 kcal mol^{-1} higher than M06-L (25.5 kcal mol^{-1} vs. 22.0 kcal mol^{-1}). For the barrier to isomerization, however, both functionals yield a relatively similar value, deviating by only 1 kcal mol^{-1}. As a result, B3LYP predicts a 0.1 kcal mol^{-1} preference for the insertion route rather than isomerization. On the other hand M06-L gives a larger difference of 4.7 kcal mol^{-1}. There is little experimental evidence for the formation of the axial-equatorial dimer, **5**, and the high barrier to isomerization, especially with respect to the insertion pathway, is aligned with the M06-L results.

Following the insertion pathway, we find that for the activation barrier to rearrangement, step **7** $\rightarrow$ **TS 8**, B3LYP and M06-L values deviate substantially, at 23.6 kcal mol^{-1} vs. 15.3 kcal mol^{-1} respectively. Given that with B3LYP the barrier to isomerization is roughly equal to the activation barrier for both insertion and isomerization steps, those processes would likely be slow if not prohibited under the reaction conditions. On the other hand, the decreased barrier for rearrangement using M06-L generally agrees with the experimental observation that rearrangement is not a rate limiting step, and **7** is not a long-lived intermediate. Both functionals predict rearrangement to be overall exothermic, but B3LYP returns a value roughly 4 kcal mol^{-1} lower than M06-L (-6.0 kcal mol^{-1} vs. -1.9 kcal mol^{-1}).

2.5 Summary

We have investigated the production of CO from a CO_2 saturated solution containing reduced rhenium complexes. Using density functional theory (DFT), we have proposed a pathway involving CO_2 insertion into a long-lived carboxylate dimer intermediate. This pathway generally agrees with the experimentally observed products described by Sullivan and co-workers and Hayashi and co-workers. Furthermore, our mechanism aligns with labeling studies performed by the latter. From our investigation, we propose the formation of a stable $[Re(dmb)(CO)_3]_2(OCO)$ intermediate via the two electron reduction of CO_2. The high barrier to isomerization of this dimer and the significant exothermicity of the formation step assists the long-lived nature of this species. In the presence of CO_2, $[Re(dmb)(CO)_3]_2(OCO)$ undergoes attack via the insertion of CO_2 into the rhenium-oxygen bond. Subsequent rearrangement produces CO and $[Re(dmb)(CO)_3]_2(OCO_2)$, both experimentally observed products. The insertion step also agrees with the kinetic dependence on the concentration of $[Re(dmb)(CO)_3]_2(OCO)$ and CO_2 for the production of CO. We find that from the reduced monomer, $Re(dmb)(CO)_3^{\bullet}$, and two equivalents of CO_2, the overall reaction is exothermic by -30.2 kcal mol^{-1} with the largest barrier being that of insertion at 21.9 kcal mol^{-1}.

2.6 Acknowledgments

The work at Brookhaven National Laboratory is funded under contract DE-AC02-98CH10886 with the U.S. Department of Energy (DOE) and supported by its Division of Chemical Sciences, Geosciences, & Biosciences, Office of Basic Energy Sciences. EF and JTM also thank the DOE for funding under the BES Solar Energy Utilization Initiative. Research at Georgia was supported by the National Science Foundation, Grant CHE-1054286.

2.7 Supporting Information

A. Complete Citations

Gurney, K. R.; Law, R. M.; Denning, A. S.; Rayner, P. J; Baker, D.; Bousquet, P.; Bruhwiler, L.; Chen, Y-H.; Ciais, P.; Fan, S.; Fung, I. Y.; Gloor, M.; Heimann, M.; Higuchi, K.; John, J.; Maki, T.; Maksyutov, S.; Masarie, K.; Peylin, P.; Prather, M.; Pak, B. C.; Randerson, J.; Sarmiento, J.; Taguchi, S.; Takahashi, T.; Yuen, C-W. *Nature* **2002**, *415*, 626-630.

Gaussian 09, Revision B.01, Frisch, M. J.; Trucks, G. W.; Schlegel, H. B.; Scuseria, G. E.; Robb, M. A.; Cheeseman, J. R.; Scalmani, G.; Barone, V.; Mennucci, B.; Petersson, G. A.; Nakatsuji, H.; Caricato, M.; Li, X.; Hratchian, H. P.; Izmaylov, A. F.; Bloino, J.; Zheng, G.; Sonnenberg, J. L.; Hada, M.; Ehara, M.; Toyota, K.; Fukuda, R.; Hasegawa, J.; Ishida, M.; Nakajima, T.; Honda, Y.; Kitao, O.; Nakai, H.; Vreven, T.; Montgomery, Jr., J. A.; Peralta, J. E.; Ogliaro, F.; Bearpark, M.; Heyd, J. J.; Brothers, E.; Kudin, K. N.; Staroverov, V. N.; Kobayashi, R.; Normand, J.; Raghavachari, K.; Rendell, A.; Burant, J. C.; Iyengar, S. S.; Tomasi, J.; Cossi, M.; Rega, N.; Millam, N. J.; Klene, M.; Knox, J. E.; Cross, J. B.; Bakken, V.; Adamo, C.; Jaramillo, J.; Gomperts, R.; Stratmann, R. E.; Yazyev, O.; Austin, A. J.; Cammi, R.; Pomelli, C.; Ochterski, J. W.; Martin, R. L.; Morokuma, K.; Zakrzewski, V. G.; Voth, G. A.; Salvador, P.; Dannenberg, J. J.; Dapprich, S.; Daniels, A. D.; Farkas, .; Foresman, J. B.; Ortiz, J. V.; Cioslowski, J.; Fox, D. J. Gaussian, Inc., Wallingford CT, 2009.

B. Data for Computed Stationary Points

2

Charge = 0 Multiplicity = 2

Atom	X	Y	Z	Atom	X	Y	Z
Re	0.881945	-0.000136	-0.103453	N	-0.809751	1.306120	-0.081095
N	-0.810088	-1.306030	-0.080989	C	-2.064489	0.720850	-0.038094
C	-2.064669	-0.720440	-0.038038	C	-0.741252	-2.671416	-0.085850
C	-3.227995	-1.517598	-0.009568	C	-3.133491	-2.895328	-0.019296
C	-1.850353	-3.486478	-0.057055	C	-0.740588	2.671501	-0.086080
C	-1.849487	3.486831	-0.057349	C	-3.132776	2.896003	-0.019539
C	-3.227615	1.518297	-0.009695	C	2.171382	1.359823	-0.561360
C	2.171038	-1.360475	-0.561267	O	2.916130	2.203988	-0.865263
O	2.915513	-2.204904	-0.865101	C	1.515221	0.000088	1.671387
O	1.872071	0.000617	2.783302	H	0.257135	-3.090381	-0.110942
H	-4.201369	-1.042412	0.021639	H	-4.027771	-3.509473	0.003558
H	-1.722652	-4.563131	-0.063276	H	0.257904	3.090212	-0.111215
H	-1.721520	4.563453	-0.063661	H	-4.026902	3.510373	0.003262
H	-4.201103	1.043349	0.021542				

Zero-point correction = 0.184972 (Hartree/Particle)
Thermal correction to Energy = 0.201604
Thermal correction to Enthalpy = 0.202548
Thermal correction to Gibbs Free Energy = 0.137831
Sum of electronic and zero-point Energies = -914.465638
Sum of electronic and thermal Energies = -914.449006
Sum of electronic and thermal Enthalpies = -914.448062
Sum of electronic and thermal Free Energies = -914.512779

3

Charge = 0 Multiplicity = 1

Atom	X	Y	Z	Atom	X	Y	Z
Re	-2.276016	1.048410	0.310446	N	-3.301934	-0.344682	-1.022962
N	-2.408319	-0.840366	1.404106	C	-2.999982	-1.893638	0.776691
C	-3.496074	-1.617027	-0.582743	C	-3.089697	-3.147450	1.393705
H	-3.559674	-3.976641	0.879593	C	-2.560686	-3.330564	2.666448
H	-2.617836	-4.300012	3.150772	C	-1.947200	-2.247461	3.298630
H	-1.509938	-2.340260	4.286576	C	-1.890874	-1.028383	2.635790
H	-1.415244	-0.166725	3.086446	C	-4.098631	-2.582114	-1.397983
H	-4.248322	-3.590476	-1.032625	C	-3.665608	-0.032184	-2.282470
H	-3.463158	0.982990	-2.598025	C	-4.263937	-0.945757	-3.141636
H	-4.535785	-0.637102	-4.144973	C	-4.491502	-2.245980	-2.689398
H	-4.955259	-2.987495	-3.332053	C	-3.924552	1.789186	1.085443
O	-4.888803	2.251201	1.549296	C	-2.112654	2.518440	-0.916799
O	-2.008900	3.384200	-1.693047	C	-1.178456	2.002695	1.563308
O	-0.489840	2.549832	2.332867	C	-0.462656	0.125794	-0.591198
O	0.490518	-0.199218	0.262615	O	-0.360398	-0.099460	-1.810486
O	1.278999	-2.795073	-2.636763	O	1.981698	-3.425809	1.646524
C	1.650568	-2.133023	-1.756547	C	2.122846	-2.552853	0.882185
O	5.217630	-2.019690	-0.996230	C	4.135857	-1.667907	-0.727456
Re	2.359608	-1.067559	-0.304140	H	2.040658	0.088661	-3.231645
H	3.200675	-0.971737	2.739902	C	2.297214	0.989779	-2.691463
N	2.555227	0.839668	-1.378844	C	3.277803	0.076793	2.479033
N	3.026671	0.384467	1.191617	C	2.325720	2.227761	-3.323462
H	2.106152	2.292791	-4.383085	C	2.837011	1.937546	-0.630809
C	3.617355	1.031360	3.430004	C	3.108411	1.683083	0.798526
H	3.807361	0.726303	4.453132	C	2.608438	3.362384	-2.563397
C	2.865184	3.214746	-1.204072	C	3.699952	2.367941	3.036747
C	3.445918	2.692192	1.708840	H	2.620051	4.348092	-3.017632
H	3.075492	4.085857	-0.596509	H	3.955339	3.144492	3.750606
H	3.502755	3.723816	1.385466				

Zero-point correction = 0.385784 (Hartree/Particle)
Thermal correction to Energy = 0.423931
Thermal correction to Enthalpy = 0.424875
Thermal correction to Gibbs Free Energy = 0.308979
Sum of electronic and zero-point Energies = -2017.556384
Sum of electronic and thermal Energies = -2017.518236
Sum of electronic and thermal Enthalpies = -2017.517292
Sum of electronic and thermal Free Energies = -2017.633188

TS 4 Isomerization Transition State

Charge = 0 Multiplicity = 1

Atom	X	Y	Z	Atom	X	Y	Z
Re	2.020513	-0.538582	0.652985	N	3.777317	-0.875064	-0.548882
N	2.954007	1.427429	0.406255	C	4.051316	1.498563	-0.399081
C	4.491339	0.218184	-0.964384	C	4.700209	2.722063	-0.624233
H	5.570495	2.767700	-1.267596	C	4.228825	3.876792	-0.012182
H	4.723806	4.827834	-0.181699	C	3.113479	3.788602	0.827477
H	2.711886	4.659968	1.332891	C	2.507718	2.552964	1.007773
H	1.638257	2.434035	1.644327	C	5.569597	0.094865	-1.853000
H	6.107370	0.977929	-2.176895	C	4.162009	-2.092648	-1.012121
H	3.580156	-2.932358	-0.653099	C	5.224463	-2.273695	-1.881792
H	5.478408	-3.276253	-2.209311	C	5.946446	-1.156121	-2.321308
H	6.779192	-1.261444	-3.008944	C	2.751886	-0.730844	2.446446
O	3.103513	-0.826587	3.556169	C	1.379116	-2.327494	0.728129
O	1.008121	-3.445114	0.742897	C	0.185549	0.253539	1.282069
O	-0.396762	0.689764	2.255464	C	0.719401	-0.132340	-0.998624
O	-0.527612	0.353588	0.004619	O	0.446478	-0.083791	-2.150764
O	-1.811487	2.818969	-2.723847	O	-2.422689	3.409382	1.557165
C	-2.085900	2.137680	-1.821032	C	-2.458669	2.497731	0.837411
O	-5.553362	1.582069	-0.855772	C	-4.422537	1.362404	-0.669517
Re	-2.570641	0.983138	-0.356486	H	-2.357973	-0.068901	-3.334529
H	-3.182605	0.729598	2.740903	C	-2.461890	-1.003621	-2.799116
N	-2.614877	-0.908650	-1.464267	C	-3.175723	-0.312625	2.452043
N	-2.980174	-0.565818	1.144311	C	-2.420573	-2.222504	-3.465376
H	-2.292409	-2.240014	-4.541777	C	-2.730916	-2.047083	-0.730110
C	-3.335522	-1.321559	3.395123	C	-2.926590	-1.856460	0.722204
H	-3.484939	-1.060733	4.436644	C	-2.524764	-3.396463	-2.719642
C	-2.681952	-3.305699	-1.340253	C	-3.267643	-2.648746	2.974192
C	-3.061356	-2.917234	1.624370	H	-2.481644	-4.368103	-3.201435
H	-2.758316	-4.206314	-0.744689	H	-3.365721	-3.463933	3.683981
H	-2.993788	-3.941738	1.281667				

Imaginary Frequency = 201.48i
Zero-point correction = 0.384568 (Hartree/Particle)
Thermal correction to Energy = 0.421964
Thermal correction to Enthalpy = 0.422908
Thermal correction to Gibbs Free Energy = 0.310335
Sum of electronic and zero-point Energies = -2017.516101
Sum of electronic and thermal Energies = -2017.478705

Sum of electronic and thermal Enthalpies = -2017.477761
Sum of electronic and thermal Free Energies = -2017.590334

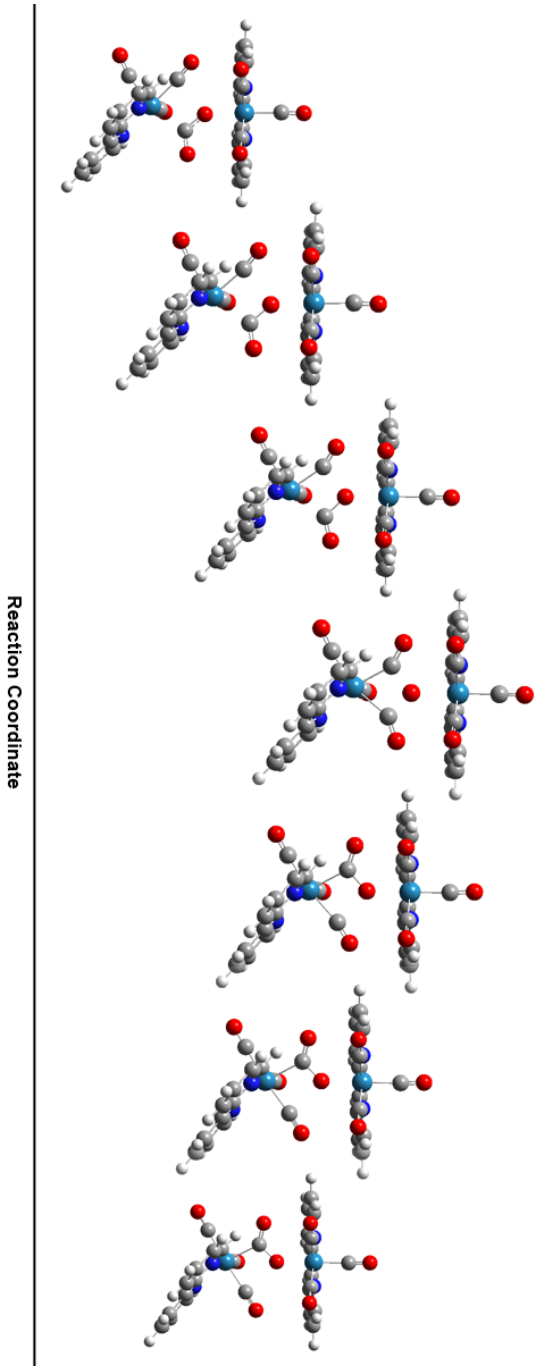

Figure SI-1. Structural Images from IRC Computations of **TS 4**. [Rotated]

5 $[Re(bpy)(CO)_3]_2(C(O)O)$

Charge = 0 Multiplicity = 1

Atom	X	Y	Z	Atom	X	Y	Z
Re	-2.065920	0.422638	-0.080139	N	-4.188553	0.997709	-0.224384
N	-3.261755	-1.435947	0.247379	C	-4.614747	-1.333483	0.139689
C	-5.133103	0.021505	-0.119935	C	-5.438545	-2.457199	0.284620
H	-6.513847	-2.365079	0.194181	C	-4.868760	-3.699465	0.547102
H	-5.498123	-4.577485	0.656168	C	-3.482373	-3.788802	0.671233
H	-2.990432	-4.732369	0.881492	C	-2.712336	-2.638639	0.518773
H	-1.626925	-2.625738	0.625016	C	-6.499297	0.313532	-0.243173
H	-7.235165	-0.477196	-0.163585	C	-4.601113	2.267706	-0.440861
H	-3.815023	3.008669	-0.519748	C	-5.938029	2.620187	-0.563721
H	-6.203281	3.657602	-0.736678	C	-6.911640	1.621463	-0.467047
H	-7.966616	1.857112	-0.563993	C	-1.809137	0.749741	1.853409
O	-1.545992	0.951658	2.966853	C	-1.305054	2.131845	-0.394514
O	-0.888678	3.214875	-0.581870	C	-0.129626	-0.570286	0.083768
O	0.025093	-1.626777	0.740773	C	-1.838274	0.031455	-2.017526
O	0.877293	-0.013280	-0.547487	O	-1.619240	-0.184091	-3.133464
O	2.967325	-0.961770	-3.631949	O	2.221832	-3.766840	-0.339645
C	2.925134	-0.908768	-2.467860	C	2.433691	-2.626643	-0.425502
O	5.884686	-1.455206	-0.396779	C	4.747980	-1.190789	-0.470230
Re	2.880230	-0.749794	-0.553596	H	3.531046	1.690819	-2.454540
H	2.433570	-2.190931	2.222374	C	3.426559	2.199071	-1.503810
N	3.201977	1.412919	-0.433960	C	2.515007	-1.162206	2.546971
N	2.742161	-0.254158	1.579620	C	3.515211	3.583541	-1.415981
H	3.690779	4.167608	-2.312475	C	3.052187	1.990626	0.786854
C	2.368619	-0.811454	3.884219	C	2.810309	1.061351	1.910013
H	2.185341	-1.583214	4.623300	C	3.361818	4.185939	-0.167248
C	3.131002	3.379520	0.942274	C	2.441192	0.536379	4.235436
C	2.662023	1.480294	3.237734	H	3.414475	5.264516	-0.058520
H	3.001546	3.829431	1.918527	H	2.319459	0.850436	5.267268
H	2.712386	2.531728	3.491159				

Zero-point correction = 0.385665 (Hartree/Particle)
Thermal correction to Energy = 0.423793
Thermal correction to Enthalpy = 0.424738
Thermal correction to Gibbs Free Energy = 0.309438
Sum of electronic and zero-point Energies = -2017.540420
Sum of electronic and thermal Energies = -2017.502292
Sum of electronic and thermal Enthalpies = -2017.501348
Sum of electronic and thermal Free Energies = -2017.616647

TS 6 Insertion Transition State

Charge = 0 Multiplicity = 1

Atom	X	Y	Z	Atom	X	Y	Z
Re	-2.594813	1.021543	0.142751	N	-3.469468	-0.442991	-1.241212
N	-3.308456	-0.664592	1.386566	C	-3.905904	-1.705358	0.748833
C	-3.953769	-1.601780	-0.722269	C	-4.439475	-2.785591	1.460791
H	-4.911452	-3.607935	0.937768	C	-4.367273	-2.794195	2.850628
H	-4.777261	-3.625728	3.415215	C	-3.761818	-1.717795	3.496921
H	-3.675645	-1.677113	4.576865	C	-3.241379	-0.679076	2.731942
H	-2.736820	0.156657	3.193409	C	-4.446267	-2.616164	-1.551626
H	-4.818143	-3.539096	-1.124646	C	-3.452588	-0.287162	-2.579304
H	-3.033787	0.640323	-2.945618	C	-3.934369	-1.252639	-3.455775
H	-3.897695	-1.071470	-4.524191	C	-4.440772	-2.441678	-2.931986
H	-4.816696	-3.223376	-3.584464	C	-4.286879	1.952764	0.452303
O	-5.285899	2.526228	0.620207	C	-2.102265	2.339450	-1.155580
O	-1.818837	3.118915	-1.978747	C	-1.733031	2.097840	1.498448
O	-1.233612	2.780105	2.295726	C	-0.729640	-0.042920	-0.454188
O	0.403078	-0.373086	0.331193	O	-0.546320	-0.305773	-1.637978
O	1.368329	-2.841106	-2.389727	O	3.421437	-3.604447	1.342285
C	1.876352	-2.166260	-1.593027	C	3.168548	-2.659734	0.716796
O	5.383287	-1.509008	-1.887529	C	4.393129	-1.348483	-1.283834
Re	2.814272	-1.066560	-0.310874	H	1.499523	0.191708	-2.899495
H	4.349272	-0.970631	2.438848	C	1.910290	1.081945	-2.444771
N	2.525101	0.911945	-1.257945	C	4.348272	0.082257	2.190712
N	3.772424	0.415379	1.020627	C	1.770740	2.329432	-3.044785
H	1.253383	2.410197	-3.993816	C	3.033971	1.998571	-0.619555
C	4.895484	1.025651	3.052582	C	3.700768	1.723359	0.670016
H	5.348139	0.701891	3.983018	C	2.284959	3.449373	-2.394813
C	2.925780	3.279538	-1.170576	C	4.828204	2.373466	2.700482
C	4.221100	2.724487	1.498781	H	2.186140	4.439445	-2.828281
H	3.334674	4.136758	-0.650696	H	5.232874	3.140615	3.353089
H	4.143301	3.766749	1.216094	C	0.457387	-0.518592	1.794450
O	-0.545388	-0.292065	2.459876	O	1.617204	-0.884150	2.084732

Imaginary Frequency = 109.56i
Zero-point correction = 0.399506 (Hartree/Particle)
Thermal correction to Energy = 0.439806
Thermal correction to Enthalpy = 0.440751
Thermal correction to Gibbs Free Energy = 0.320969
Sum of electronic and zero-point Energies = -2206.090394

Sum of electronic and thermal Energies = -2206.050094
Sum of electronic and thermal Enthalpies = -2206.049150
Sum of electronic and thermal Free Energies = -2206.168932

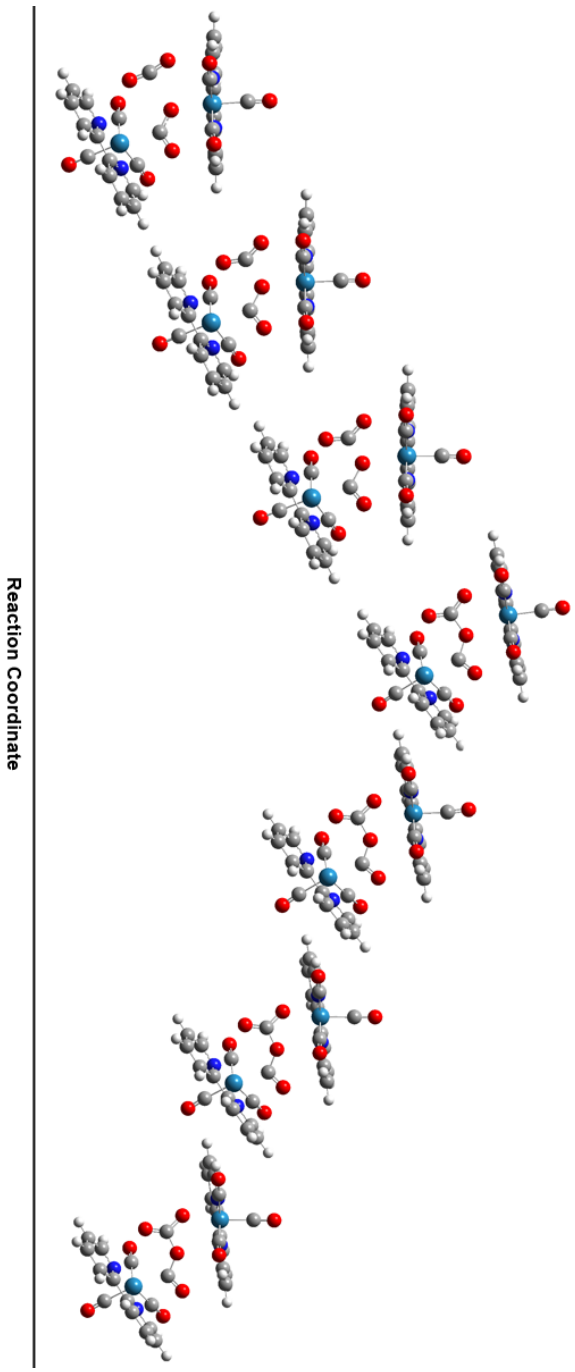

Figure SI-2. Structural Images from IRC Computations of **TS 6**. [Rotated]

7

Charge = 0 Multiplicity = 1

Atom	X	Y	Z	Atom	X	Y	Z
Re	-2.734982	0.896485	0.140148	N	-4.084687	-0.405401	-1.004035
N	-3.340645	-0.727904	1.510116	C	-4.198128	-1.666660	1.030693
C	-4.580241	-1.508936	-0.385894	C	-4.673976	-2.699839	1.845478
H	-5.356074	-3.441606	1.449085	C	-4.268550	-2.767661	3.175254
H	-4.630020	-3.564310	3.817892	C	-3.393465	-1.797109	3.659700
H	-3.041261	-1.808067	4.684967	C	-2.949209	-0.800956	2.796479
H	-2.244954	-0.050661	3.124065	C	-5.381320	-2.426146	-1.075881
H	-5.761691	-3.306619	-0.573434	C	-4.355330	-0.213355	-2.309216
H	-3.913039	0.662740	-2.764131	C	-5.149859	-1.082366	-3.048263
H	-5.337048	-0.876183	-4.096134	C	-5.673988	-2.211088	-2.419157
H	-6.291599	-2.917437	-2.964852	C	-4.186854	2.012557	0.834919
O	-5.041113	2.696122	1.231545	C	-2.389314	2.184968	-1.233101
O	-2.203851	2.956285	-2.091681	C	-1.465143	1.822001	1.259029
O	-0.710414	2.412394	1.920662	C	-1.212961	-0.388403	-0.862072
O	0.066806	-0.789307	-0.375320	O	-1.357996	-0.712091	-2.030294
O	2.136480	-3.164066	-2.077033	O	4.684091	-3.161648	1.476677
C	2.590306	-2.347944	-1.387215	C	4.174832	-2.358521	0.804612
O	5.858348	-0.916513	-2.092951	C	4.920182	-0.953189	-1.398537
Re	3.372692	-0.979002	-0.270768	H	1.633290	-0.254560	-2.814688
H	5.160680	-0.348275	2.261899	C	1.764303	0.724805	-2.374213
N	2.493800	0.779604	-1.243932	C	4.771686	0.637980	2.040384
N	4.002419	0.738401	0.940284	C	1.171337	1.849123	-2.938023
H	0.575181	1.743610	-3.836740	C	2.655565	1.975229	-0.619020
C	5.057164	1.723834	2.860617	C	3.475498	1.946737	0.610782
H	5.682090	1.585917	3.735874	C	1.328251	3.079689	-2.303274
C	2.080263	3.141928	-1.133090	C	4.515764	2.967372	2.534602
C	3.719246	3.077204	1.399181	H	0.859392	3.973296	-2.701674
H	2.206011	4.088366	-0.622513	H	4.705728	3.837523	3.154937
H	3.282417	4.032152	1.136116	C	0.452157	-0.803584	0.960121
O	-0.369219	-0.829594	1.870601	O	1.731512	-0.812341	1.097713

Zero-point correction = 0.400363 (Hartree/Particle)
Thermal correction to Energy = 0.441203
Thermal correction to Enthalpy = 0.442148
Thermal correction to Gibbs Free Energy = 0.320589
Sum of electronic and zero-point Energies = -2206.119071
Sum of electronic and thermal Energies = -2206.078231
Sum of electronic and thermal Enthalpies = -2206.077286

Sum of electronic and thermal Free Energies = -2206.198845

TS 8 Rearrangement Transition State

Charge = 0 Multiplicity = 1

Atom	X	Y	Z	Atom	X	Y	Z
Re	3.321250	0.685541	-0.476864	N	3.344639	-0.801307	1.159020
N	2.170535	-1.078199	-1.196970	C	1.993291	-2.106230	-0.334553
C	2.604461	-1.926854	0.996726	C	1.291834	-3.257102	-0.712079
H	1.146701	-4.068203	-0.010596	C	0.756546	-3.341240	-1.992746
H	0.195729	-4.219718	-2.295158	C	0.936082	-2.272506	-2.871187
H	0.521658	-2.285079	-3.872769	C	1.643130	-1.159836	-2.432176
H	1.780429	-0.294900	-3.068065	C	2.462648	-2.854292	2.035893
H	1.836882	-3.727301	1.904669	C	3.972663	-0.596947	2.333573
H	4.556559	0.312369	2.410205	C	3.886343	-1.484745	3.398084
H	4.414015	-1.270144	4.320794	C	3.105385	-2.632476	3.247870
H	2.996716	-3.342215	4.061992	C	4.841766	-0.032664	-1.323473
O	5.783576	-0.489207	-1.845135	C	4.479664	1.993787	0.313739
O	5.225647	2.738040	0.813829	C	3.042330	1.872912	-1.979994
O	2.876663	2.556610	-2.900333	C	1.845705	1.791081	1.358150
O	0.125588	-0.132041	0.999204	O	1.250159	2.587335	1.926127
O	-1.285463	-2.938985	1.622613	O	-2.979201	-2.751117	-2.371591
C	-1.858079	-2.123505	1.018221	C	-2.938885	-2.036535	-1.447523
O	-5.499859	-2.039321	1.159325	C	-4.511407	-1.590359	0.726200
Re	-2.886993	-0.823217	0.034170	H	-1.883524	-0.267662	2.982120
H	-4.457266	-0.161745	-2.633211	C	-2.258817	0.710701	2.714516
N	-2.826394	0.815090	1.499702	C	-4.460549	0.809507	-2.153576
N	-3.910055	0.864320	-0.926768	C	-2.134110	1.794365	3.577868
H	-1.665205	1.657276	4.545655	C	-3.275401	2.025573	1.079864
C	-5.001970	1.922744	-2.786708	C	-3.878741	2.052365	-0.269888
H	-5.429732	1.822305	-3.778015	C	-2.595285	3.040846	3.158836
C	-3.171043	3.156744	1.896800	C	-4.970475	3.149204	-2.122663
C	-4.406858	3.210755	-0.852174	H	-2.501815	3.912720	3.798531
H	-3.524861	4.120083	1.551902	H	-5.376839	4.043389	-2.584640
H	-4.373633	4.154301	-0.322327	C	-0.103354	0.437146	-0.113606
O	0.754533	1.207148	-0.702025	O	-1.256320	0.264823	-0.744245

Imaginary Frequency = 198.86i
Zero-point correction = 0.397665 (Hartree/Particle)
Thermal correction to Energy = 0.439052
Thermal correction to Enthalpy = 0.439996
Thermal correction to Gibbs Free Energy = 0.317708

Sum of electronic and zero-point Energies = -2206.083332
Sum of electronic and thermal Energies = -2206.041945
Sum of electronic and thermal Enthalpies = -2206.041001
Sum of electronic and thermal Free Energies = -2206.163288

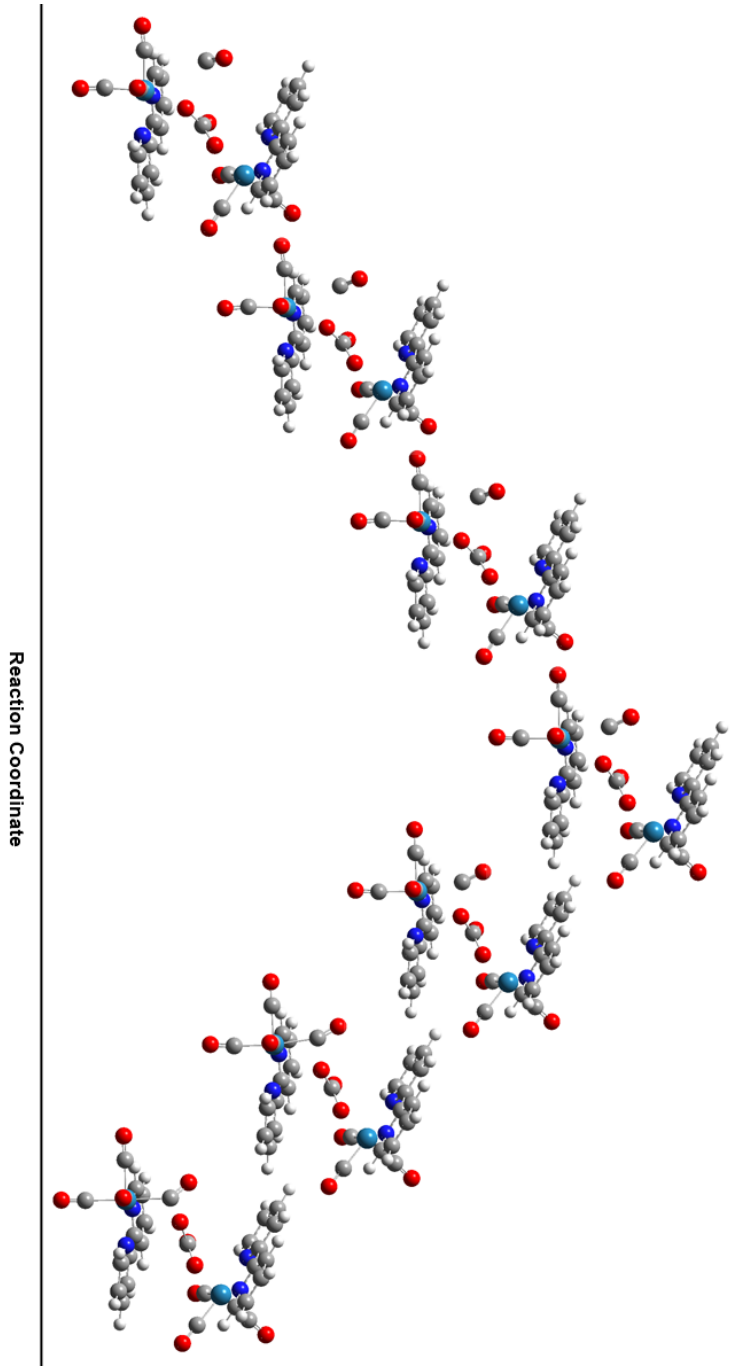

Figure SI-3. Structural Images from IRC Computations of **TS 8**. [Rotated]

9

Charge = 0 Multiplicity = 1

Atom	X	Y	Z	Atom	X	Y	Z
Re	2.476191	0.967895	-0.389959	N	3.950760	-0.069634	0.867721
N	2.373166	-1.144498	-0.983219	C	3.054486	-2.025168	-0.204345
C	3.934671	-1.426326	0.822006	C	2.929512	-3.404588	-0.399417
H	3.466884	-4.100015	0.232828	C	2.095450	-3.885243	-1.405216
H	1.980969	-4.954014	-1.555641	C	1.405813	-2.973907	-2.203110
H	0.730482	-3.293633	-2.988326	C	1.571306	-1.614935	-1.955560
H	1.037877	-0.873524	-2.535835	C	4.734519	-2.184498	1.685214
H	4.711060	-3.266186	1.646518	C	4.752558	0.547027	1.754109
H	4.722006	1.629932	1.750364	C	5.572816	-0.147220	2.636727
H	6.197645	0.399859	3.333884	C	5.558417	-1.541682	2.603699
H	6.177673	-2.120902	3.281375	C	3.763891	1.450697	-1.733779
O	4.549159	1.723078	-2.555569	C	2.630141	2.710831	0.403186
O	2.746329	3.755637	0.908119	C	1.071337	1.639389	-1.518501
O	0.254247	2.044746	-2.243729	C	0.098695	-0.346964	1.154250
O	-0.629251	-0.112751	0.069044	O	-0.303082	-1.049649	2.101642
O	-1.959560	-3.706957	0.980119	O	-1.882976	-1.988375	-3.018343
C	-2.163855	-2.650229	0.542454	C	-2.149387	-1.605441	-1.944319
O	-5.523821	-1.770283	-0.572756	C	-4.406021	-1.454350	-0.447424
Re	-2.574035	-0.917512	-0.212880	H	-2.747477	-1.456969	2.897432
H	-2.788705	0.827962	-2.843507	C	-2.958345	-0.397489	2.872435
N	-2.989817	0.173406	1.654647	C	-2.971419	1.582909	-2.089190
N	-2.974421	1.156704	-0.812561	C	-3.159373	0.327635	4.042893
H	-3.124772	-0.181656	4.999230	C	-3.189131	1.511872	1.555131
C	-3.181855	2.910968	-2.441714	C	-3.187049	2.058423	0.181597
H	-3.159061	3.197985	-3.486875	C	-3.373502	1.701602	3.951791
C	-3.384690	2.300188	2.694984	C	-3.399398	3.844171	-1.429261
C	-3.402673	3.410969	-0.106807	H	-3.521543	2.302469	4.843708
H	-3.536013	3.368604	2.606670	H	-3.560697	4.891927	-1.662207
H	-3.569187	4.121265	0.693166	O	1.289187	0.215123	1.179355

Zero-point correction = 0.391534 (Hartree/Particle)
Thermal correction to Energy = 0.430306
Thermal correction to Enthalpy = 0.431250
Thermal correction to Gibbs Free Energy = 0.314742
Sum of electronic and zero-point Energies = -2092.817560
Sum of electronic and thermal Energies = -2092.778789
Sum of electronic and thermal Enthalpies = -2092.777845
Sum of electronic and thermal Free Energies = -2092.894353

10

Charge = 0 Multiplicity = 1

Atom	X	Y	Z	Atom	X	Y	Z
C	0.000000	0.000000	0.000000	O	0.000000	0.000000	1.169762
O	0.000000	0.000000	-1.169762				

Zero-point correction = 0.011586 (Hartree/Particle)
Thermal correction to Energy = 0.014219
Thermal correction to Enthalpy = 0.015163
Thermal correction to Gibbs Free Energy = -0.009128
Sum of electronic and zero-point Energies = -188.575852
Sum of electronic and thermal Energies = -188.573219
Sum of electronic and thermal Enthalpies = -188.572275
Sum of electronic and thermal Free Energies = -188.596566

11

Charge = 0 Multiplicity = 1

Atom	X	Y	Z	Atom	X	Y	Z
C	0.000000	0.000000	-0.649884	O	0.000000	0.000000	0.487413

Zero-point correction = 0.005019 (Hartree/Particle)
Thermal correction to Energy = 0.007380
Thermal correction to Enthalpy = 0.008324
Thermal correction to Gibbs Free Energy = -0.014118
Sum of electronic and zero-point Energies = -113.310206
Sum of electronic and thermal Energies = -113.307845
Sum of electronic and thermal Enthalpies = -113.306901
Sum of electronic and thermal Free Energies = -113.329344

Chapter 3

Exploring the Intermediates of Photochemical CO_2 Reduction: Reaction of $Re(dmb)(CO)_3COOH$ with CO_2 [1]

[1] J. Agarwal, B. C. Sanders, E. Fujita, H. F. Schaefer, T. C. Harrop, and J. T. Muckerman *Chem. Commun.*, **2012**, 48, 6797-6799. Reproduced by permission of The Royal Society of Chemistry.

3.1 Abstract

We have investigated the reaction of Re(dmb)$(CO)_3$COOH with CO_2 using density functional theory, and propose a mechanism for the production of CO. This mechanism supports the role of Re(dmb)$(CO)_3$COOH as a key intermediate in the formation of CO. Our new experimental work supports the proposed scheme.

3.2 Literature Review, Results and Discussion

Carbon dioxide is a principal product of combustion and, as such, it is emitted in high concentrations in the flue gas of fossil-fuel burning power plants.[27] Utilization of this available CO_2 is limited, but it is an attractive feedstock for use in producing other, higher-energy products such as carbon monoxide, formic acid, or methanol.[113] CO_2 utilization is also a primary environmental objective due to its role as a greenhouse gas. Although the chemical conversion of CO_2 occurs naturally in plants, there exist no robust artificial solutions. Several promising organic- and metal-based systems have been explored, but a limited understanding of the underlying mechanisms has hindered optimization.[114]

One widely studied catalyst for photochemical CO_2 reduction to CO is rhenium tricarbonyl, $[fac\text{-Re(N-N)}(CO)_3X]^n$, where N-N is a bidentate pyridyl ligand such as 2,2'-bipyridine and X is a labile ligand such as Cl^- or Br^- (n=0), or solvent (n=1).[47,48,53,69,71,81,82,115?] Several groups, including ours, have tried to elucidate the mechanism for reduction, but the complex reaction mixture makes determination of the exact pathway difficult and it is likely that several pathways contribute to overall CO production. To simplify the problem, some experimental groups have synthesized proposed intermediates and examined their reactivity with CO_2.[45,46,76,77] We have focused on one such intermediate, Re(dmb)$(CO)_3$COOH (dmb = 4,4'-dimethyl-2,2'-bipyridine). Herein, we describe our proposed mechanism for the re-

duction of CO_2 with Re(dmb)$(CO)_3$COOH (**1**) from a theoretical analysis. We also describe our subsequent experimental analysis using isotope labeled $^{13}CO_2$.

Gibson and Yin were the first to synthesize and isolate Re(dmb)$(CO)_3$COOH.[75] In two separate studies they monitored the reaction of Re(dmb)$(CO)_3$COOH with CO_2 in DMSO-d_6 using ^{1}H NMR.[77,116] In the first study, they reported the conversion of Re(dmb)$(CO)_3$COOH to Re(dmb)$(CO)_3OCO_2H$ (97%) after standing for 3 hours.[116] In the second study, Gibson and co-workers reported 42% conversion of Re(dmb)$(CO)_3$COOH after 10 min and 70% conversion after just 20 min.[77] Importantly, the conversion of Re(dmb)$(CO)_3$COOH to Re(dmb)$(CO)_3OCO_2H$ yields CO.

Our predicted mechanism for this process is shown in Figure 3.1. All structures were optimized in solvent (DMSO) using the polarizable continuum model (CPCM). Stationary points were verified by frequency analysis and transition states were connected to minima using intrinsic reaction coordinate computations. For this work we employed the M06-L functional[99] as implemented in Gaussian 09[90] with LANL08F (Re) and 6-31++G** (H,N,C, and O) basis sets. The pyridyl ligand, dmb, was simplified to 2,2'-bipyridine (bpy) to reduce computation time.

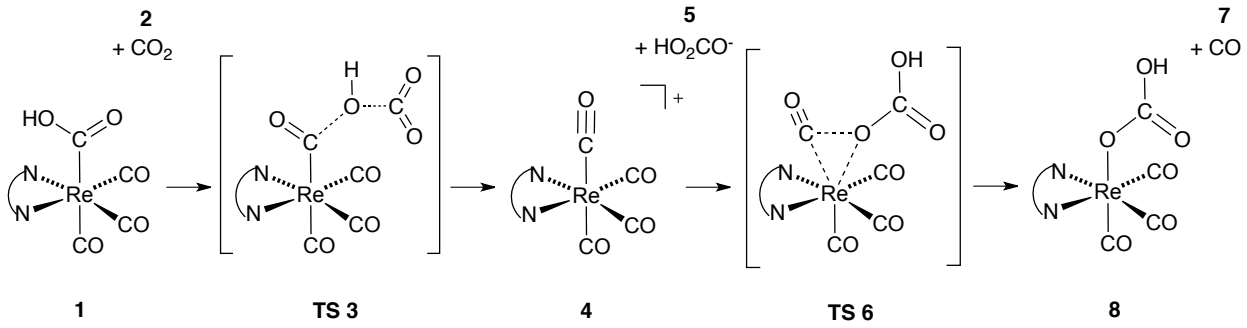

Figure 3.1: Proposed Mechanism for the Conversion of Re(bpy)$(CO)_3$COOH + CO_2 to Re(bpy)$(CO)_3OCO_2H$ + CO. N-N = 2,2'-bipyridine

Table 3.1: Standard Reaction Enthalpies for the Conversion of $Re(bpy)(CO)_3COOH + CO_2$ to $Re(bpy)(CO)_3OCO_2H + CO$ [a]

Reaction Step	ΔH^*(DMSO) [b]
1 + **2** → **TS 3**	23.9 (23.9)
1 + **2** → **4** + **5**	13.1 (13.1)
4 + **5** → **TS 6**	12.6 (26.0)
4 + **5** → **7** + **8**	-6.9 (6.2)

[a] Energies are shown in kcal mol^{-1} and include ZPVE corrections as well as thermal corrections to the enthalpy. Energies were computed in solvent (DMSO) at the M06-L/LANL08F (Re), 6-31++G**(H,N,C, and O) level of theory. [b] Overall enthalpies referenced to **1** + **2** shown in parenthesis.

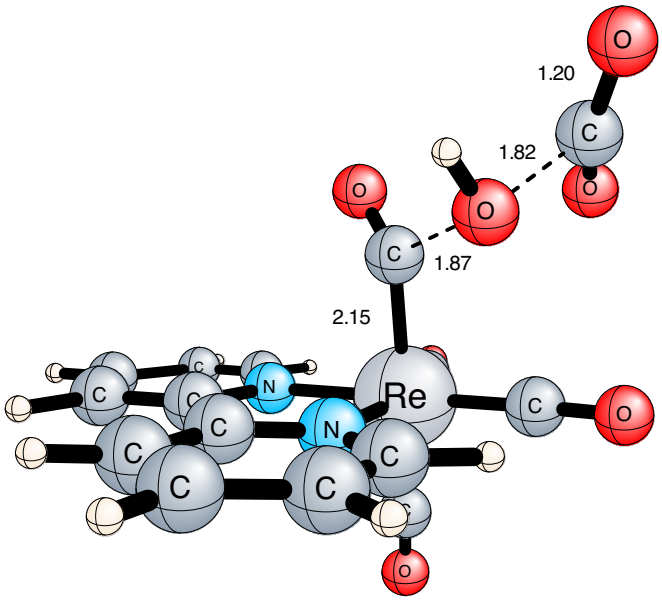

TS 3

Figure 3.2: Optimized geometry for the CO_2 addition transition-state structure. Bond lengths shown in Angstroms.

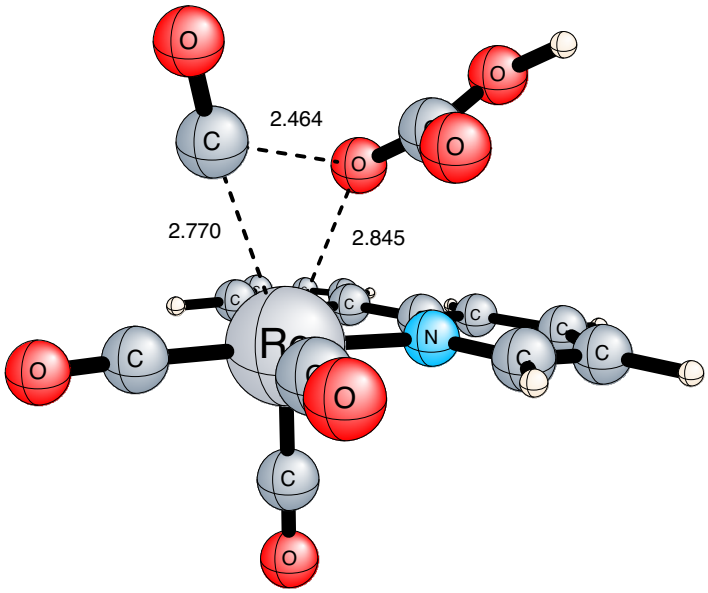

Figure 3.3: Optimized geometry for the heptacoordinate transition-state structure. Bond lengths shown in Angstroms.

From our analysis, we predict that in the presence of CO_2, **2**, the acid, **1**, reduces CO_2 and yields the addition transition state **TS 3**. The newly formed carbon-oxygen bond between the carboxylic acid and the attacking CO_2 in **TS 3** forms the carbonate moiety present in the product, **8**. Cleavage of the carbon-oxygen single bond in the original COOH group yields bicarbonate, **5**, and the widely discussed rhenium tetracarbonyl, **4**.[76,117] The newly formed ion pair, **4**-**5**, is in close proximity and combine to form the heptacoordinate **TS 6**. This transition state allows for CO production through associative ligand exchange, resulting in two neutral species, **7** and **8**.

Standard enthalpies for the mechanism in Figure 3.1 are shown in Table 3.1. We find that the barrier to the reduction of CO_2 by $Re(bpy)(CO)_3COOH$ is significant at 24 kcal mol^{-1}, which contributes to its stability. Overall the addition step, through **TS 3**, is endothermic by 13 kcal mol^{-1}. From the ion pair (**4** + **5**), formation of the heptacoordinate transition state **TS 6** has a modest barrier of 13 kcal mol^{-1}. Realization of the bicarbonate-containing

product (**8**) and carbon monoxide is exothermic from the ion pair (-7 kcal mol^{-1}), but endothermic from the starting species, **1** and **2**, by 6 kcal mol^{-1}. To our knowledge, **TS 6** is the first explicit example of bicarbonate promoting the production of CO. We note that an ion pair similar to **4** and **5**, namely $Re(dmb)(CO)_4^+$ and $HCOO^-$, has been observed as an intermediate in the reaction of $Re(dmb)(CO)_3CHO$ and CO_2.[76]

Given Figure 3.1, we identified two outstanding issues that could be addressed by experiment to further support the proposed mechanism. First, Gibson and co-workers observed the reaction of $Re(dmb)(CO)_3COOH$ and CO_2 under fluorescent light, which contains ultraviolet radiation. Therefore rhenium tetracarbonyl, **4**, which is known to eject an axial CO at wavelengths < 400 nm,[117] could cleave CO without forming **TS 6**. Secondly, we predict the carbon atom of the final bicarbonate ligand originates from the attacking CO_2 species. However, it is possible that the carbon atom could originate from the carboxylic acid moiety of $Re(dmb)(CO)_3COOH$ through a CO_2 insertion mechanism, or from an adjacent carbonyl ligand through an isomerization pathway. To address these points, we have synthesized $Re(dmb)(CO)_3COOH$ and monitored its conversion to $Re(dmb)(CO)_3OCO_2H$ in the dark and with isotopically labeled $^{13}CO_2$.

The acid (**1**) was synthesized by treating $Re(dmb)(CO)_3OTf$,[117] with KOH in the dark as previously reported.[75] Complex **1** was characterized using IR and ^1H NMR[118] and compared to previously reported values.[45,75] Two solutions of the acid (35 mg, 0.07 mmol) in DMSO-d_6 were purged with CO_2 and $^{13}CO_2$, respectively. After standing for 2 h, both solutions were analyzed in DMSO with ^1H and ^{13}C NMR[119] and compared to previously reported values from Fujita's and Gibson's groups.[45,116]

Analysis of the results shows near quantitative conversion of $Re(dmb)(CO)_3COOH$ to $Re(dmb)(CO)_3OCO_2H$ based on NMR. Given that this conversion occurred in the dark (a red lamp was used during preparation), no light-promoted CO ejection should have occurred from the rhenium tetracarbonyl, **4**. Furthermore, overlay of the ^{13}C NMR spectra for the

CO_2 and $^{13}CO_2$ solutions shows that the bicarbonate product contains a carbon atom from the added CO_2, as evidenced by a large intensity change for the same concentration at 158.62 ppm (OCO_2H). Infrared analysis of the products is also aligned with the NMR results.

It is important to note that the bicarbonate product, **8**, has been observed as a product in related reactions with the carboxylate dimer, $[Re(dmb)(CO)_3]_2(OCO)$, which is known to be a long-lived intermediate.[45,120] Since the dimer may form as a result of the combination of $Re(dmb)(CO)_3COOH$ molecules in solution[77] it could potentially participate in the reaction mechanism. However, we did not observe the dimer in our IR, ^1H NMR, and ^{13}C NMR analyses. That is, we find dimerization does not occur on the same time scale as the reaction of **1** with CO_2 in DMSO, which is consistent with prior results.[116]

Furthermore while the ion-pair, **4-5**, is likely in close proximity due to electrostatics, the bicarbonate ion is free to orbit the molecule and dissociate away from the coordination sphere. Therefore while we predict that the bicarbonate ion mediates dissociation of the axial carbonyl ligand formed in the previous step, the original carbonyl ligand on the opposite side could dissociate since **4** is symmetric with respect to the equatorial plane. We also investigated the possibility that the bicarbonate ion could mediate the dissociation of an equatorial carbonyl ligand. The transition state for that process, however, is roughly 26 kcal mol^{-1} higher than **TS 6** (39 kcal mol^{-1} barrier from the reactants), which precludes its involvement in the pathway for CO formation.

In this work we have utilized density functional theory (DFT) to propose a pathway for CO_2 reduction to CO using $Re(dmb)(CO)_3COOH$. We find that CO_2 may add directly to the carboxylate moiety of $Re(dmb)(CO)_3COOH$, yielding $Re(dmb)(CO)_4^+$ and $HOCO_2^-$. This ion pair may combine to yield CO and $Re(dmb)(CO)_3OCO_2H$ through a heptacoordinate transition state. The largest barrier in this pathway is the initial CO_2 addition to $Re(dmb)(CO)_3COOH$ at 24 kcal mol^{-1}, and from the starting species CO production is overall endothermic at 6 kcal mol^{-1}. The present experimental work supports CO production

through an associative ligand exchange rather than light-promoted CO dissociation from $Re(dmb)(CO)_4^+$. Additionally, isotope labeling using $^{13}CO_2$ has identified that the carbon atom in the bicarbonate moiety of $Re(dmb)(CO)_3OCO_2H$ originates from the attacking CO_2.

3.3 Acknowledgments

The work at Brookhaven National Laboratory is funded under contract DE-AC02-98CH10886 with the U.S. Department of Energy (DOE) and supported by its Division of Chemical Sciences, Geosciences, & Biosciences, Office of Basic Energy Sciences. Research at Georgia was supported by the National Science Foundation, Grants CHE-1054286 and CHE-0953102. J. A. acknowledges assitance from Dr. C. A. Barrett, a post-doc in the laboratory of Dr. T. T. Salguero.

3.4 Supporting Information

A. Complete Citation

Gaussian 09, Revision B.01, Frisch, M. J.; Trucks, G. W.; Schlegel, H. B.; Scuseria, G. E.; Robb, M. A.; Cheeseman, J. R.; Scalmani, G.; Barone, V.; Mennucci, B.; Petersson, G. A.; Nakatsuji, H.; Caricato, M.; Li, X.; Hratchian, H. P.; Izmaylov, A. F.; Bloino, J.; Zheng, G.; Sonnenberg, J. L.; Hada, M.; Ehara, M.; Toyota, K.; Fukuda, R.; Hasegawa, J.; Ishida, M.; Nakajima, T.; Honda, Y.; Kitao, O.; Nakai, H.; Vreven, T.; Montgomery, Jr., J. A.; Peralta, J. E.; Ogliaro, F.; Bearpark, M.; Heyd, J. J.; Brothers, E.; Kudin, K. N.; Staroverov, V. N.; Kobayashi, R.; Normand, J.; Raghavachari, K.; Rendell, A.; Burant, J. C.; Iyengar, S. S.; Tomasi, J.; Cossi, M.; Rega, N.; Millam, N. J.; Klene, M.; Knox, J. E.; Cross, J. B.; Bakken, V.; Adamo, C.; Jaramillo, J.; Gomperts, R.; Stratmann, R. E.; Yazyev, O.; Austin, A. J.; Cammi, R.; Pomelli, C.; Ochterski, J. W.; Martin, R. L.; Morokuma, K.; Zakrzewski, V. G.; Voth, G. A.; Salvador, P.; Dannenberg, J. J.; Dapprich, S.; Daniels, A. D.; Farkas, .; Foresman, J. B.; Ortiz, J. V.; Cioslowski, J.; Fox, D. J. Gaussian, Inc., Wallingford CT, 2009.

B. Data for Computed Stationary Points

1

Charge = 0 Multiplicity = 1

Atom	X	Y	Z	Atom	X	Y	Z
Re	-0.870789	-0.000049	-0.168570	N	0.885861	1.321933	-0.216571
N	0.885951	-1.321894	-0.216544	C	2.103548	0.732916	-0.096104
C	2.103602	-0.732794	-0.096116	C	0.815454	-2.664728	-0.261977
C	3.268667	-1.497867	-0.015595	C	3.186132	-2.881597	-0.057186
C	1.934580	-3.478142	-0.187454	C	0.815275	2.664763	-0.261990
C	1.934344	3.478251	-0.187405	C	3.185930	2.881787	-0.057079
C	3.268555	1.498063	-0.015507	C	-2.212603	1.341350	0.060429
C	-2.212497	-1.341556	0.060466	O	-3.011111	2.183232	0.226030
O	-3.010941	-2.183515	0.225985	C	-1.108530	0.000064	-2.111054
O	-1.294616	0.000198	-3.264314	H	-0.179685	-3.085271	-0.362014
H	4.233641	-1.014067	0.077972	H	4.085370	-3.485002	0.006111
H	1.819265	-4.554813	-0.229407	H	-0.179889	3.085242	-0.362056
H	1.818958	4.554915	-0.229348	H	4.085123	3.485253	0.006273
H	4.233550	1.014322	0.078113	C	-0.450029	0.000028	1.997186
O	-1.546081	0.000166	2.830941	O	0.663049	-0.000151	2.521452
H	-1.206822	0.000188	3.744467				

Zero-point correction = 0.210078 (Hartree/Particle)
Thermal correction to Energy = 0.230377
Thermal correction to Enthalpy = 0.231321
Thermal correction to Gibbs Free Energy = 0.159254
Sum of electronic and zero-point Energies = -1103.570744
Sum of electronic and thermal Energies = -1103.550445
Sum of electronic and thermal Enthalpies = -1103.549501
Sum of electronic and thermal Free Energies = -1103.621569

2

Charge = 0 Multiplicity = 1

Atom	X	Y	Z	Atom	X	Y	Z
C	0.000000	0.000000	0.000000	O	0.000000	0.000000	1.168469
O	0.000000	0.000000	-1.168469				

Zero-point correction = 0.011748 (Hartree/Particle)
Thermal correction to Energy = 0.014375
Thermal correction to Enthalpy = 0.015319

Thermal correction to Gibbs Free Energy = -0.008961
Sum of electronic and zero-point Energies = -188.571170
Sum of electronic and thermal Energies = -188.568543
Sum of electronic and thermal Enthalpies = -188.567598
Sum of electronic and thermal Free Energies = -188.591878

TS 3

Charge = 0 Multiplicity = 1

Atom	X	Y	Z	Atom	X	Y	Z
Re	-0.209337	-0.626366	0.486335	N	1.737200	-0.699012	-0.556850
N	0.630534	1.412895	0.582929	C	2.454897	0.453363	-0.630643
C	1.843536	1.623937	0.008013	C	-0.004861	2.444267	1.165988
C	2.439747	2.884682	0.032331	C	1.784114	3.941449	0.648835
C	0.536787	3.718934	1.223538	C	2.231554	-1.812477	-1.126974
C	3.449520	-1.837362	-1.787988	C	4.190719	-0.662530	-1.867347
C	3.686903	0.491410	-1.283602	C	-0.771202	-2.432314	0.176380
C	-1.869537	-0.251189	1.376589	O	-1.090438	-3.535385	-0.039529
O	-2.852178	0.023048	1.941464	C	0.595580	-1.159862	2.186851
O	1.068267	-1.501048	3.193582	H	-0.978398	2.225254	1.590369
H	3.408821	3.039500	-0.426204	H	2.240927	4.925031	0.676216
H	-0.014745	4.513998	1.710971	H	1.619115	-2.703828	-1.042386
H	3.801231	-2.762901	-2.228220	H	5.147673	-0.642365	-2.377841
H	4.248103	1.416660	-1.336283	C	-0.953546	-0.022759	-1.432917
O	-2.148449	1.363203	-1.062790	O	-0.887645	-0.171637	-2.593375
H	-1.959052	2.056198	-1.713724	O	-3.910455	-0.320733	-1.144577
C	-3.811040	0.809930	-1.536950	O	-4.329919	1.739530	-2.097674

Imaginary Frequency = 482.94i
Zero-point correction = 0.220213 (Hartree/Particle)
Thermal correction to Energy = 0.244371
Thermal correction to Enthalpy = 0.245315
Thermal correction to Gibbs Free Energy = 0.163018
Sum of electronic and zero-point Energies = -1292.104132
Sum of electronic and thermal Energies = -1292.079974
Sum of electronic and thermal Enthalpies = -1292.079029
Sum of electronic and thermal Free Energies = -1292.161327

4

Charge = 1 Multiplicity = 1

Atom	X	Y	Z	Atom	X	Y	Z
Re	-0.883109	-0.000001	0.000173	N	0.878637	1.325293	-0.000214
N	0.878636	-1.325295	-0.000022	C	2.102574	0.732852	-0.000337
C	2.102574	-0.732855	-0.000313	C	0.801766	-2.668504	0.000040
C	3.268029	-1.498174	-0.000591	C	3.181215	-2.883023	-0.000524
C	1.925153	-3.480378	-0.000192	C	0.801770	2.668503	-0.000254
C	1.925158	3.480375	-0.000411	C	3.181219	2.883019	-0.000507
C	3.268031	1.498169	-0.000468	C	-2.253429	1.364853	0.000282
C	-2.253450	-1.364835	0.000622	O	-3.053034	2.207074	-0.000168
O	-3.053086	-2.207025	0.000525	C	-0.886117	-0.000117	-2.012822
O	-0.922620	-0.000918	-3.162901	H	-0.196405	-3.091966	0.000277
H	4.237251	-1.014171	-0.000879	H	4.082542	-3.485888	-0.000733
H	1.806338	-4.557136	-0.000125	H	-0.196401	3.091967	-0.000155
H	1.806344	4.557133	-0.000441	H	4.082547	3.485882	-0.000610
H	4.237252	1.014164	-0.000520	C	-0.885384	0.000130	2.013166
O	-0.921490	0.000870	3.163257				

Zero-point correction = 0.195284 (Hartree/Particle)
Thermal correction to Energy = 0.214361
Thermal correction to Enthalpy = 0.215305
Thermal correction to Gibbs Free Energy = 0.145781
Sum of electronic and zero-point Energies = -1027.603539
Sum of electronic and thermal Energies = -1027.584461
Sum of electronic and thermal Enthalpies = -1027.583517
Sum of electronic and thermal Free Energies = -1027.653042

5

Charge = -1 Multiplicity = 1

Atom	X	Y	Z	Atom	X	Y	Z
O	-1.188587	-0.615036	-0.000094	C	-0.139464	0.059107	0.000003
O	0.032379	1.300804	-0.000009	O	1.039754	-0.719341	0.000084
H	1.768411	-0.086054	0.000129				

Zero-point correction = 0.026349 (Hartree/Particle)
Thermal correction to Energy = 0.029866
Thermal correction to Enthalpy = 0.030810
Thermal correction to Gibbs Free Energy = 0.000590
Sum of electronic and zero-point Energies = -264.517108

Sum of electronic and thermal Energies = -264.513591
Sum of electronic and thermal Enthalpies = -264.512647
Sum of electronic and thermal Free Energies = -264.542867

TS 6

Charge = 0 Multiplicity = 1

Atom	X	Y	Z	Atom	X	Y	Z
C	-0.853149	-1.804361	1.853021	O	-0.722896	-0.549059	1.885655
O	-0.091844	-2.649244	1.337479	O	2.406773	-2.573057	-0.970575
O	3.584998	1.551720	0.136377	C	1.872403	-1.566229	-0.730031
C	2.586555	0.965720	-0.018206	O	1.184462	0.922747	-3.252085
C	1.079906	0.589214	-2.133218	Re	0.926796	0.065768	-0.349246
H	-0.502546	-2.530093	-1.508712	H	1.023025	3.003658	0.806828
C	-1.362721	-1.892078	-1.338031	N	-1.105826	-0.685429	-0.809199
C	-0.047798	2.866617	0.700828	N	-0.444667	1.690282	0.183426
C	-2.648979	-2.318679	-1.638198	H	-2.801992	-3.304686	-2.060886
C	-2.137857	0.160753	-0.559099	C	-0.938405	3.857855	1.083280
C	-1.774201	1.458704	0.018545	H	-0.562109	4.786088	1.496432
C	-3.712166	-1.459798	-1.383774	C	-3.452285	-0.207108	-0.842404
C	-2.300424	3.627231	0.921868	C	-2.717932	2.418079	0.382744
H	-4.731897	-1.757062	-1.604552	H	-4.268145	0.476954	-0.641662
H	-3.029744	4.376621	1.210705	H	-3.774637	2.219210	0.251101
O	-2.010128	-2.259491	2.464696	C	1.717739	-0.645602	2.208750
O	1.914279	-0.983208	3.284203	H	-1.997456	-3.222456	2.382128

Imaginary Frequency = 175.64i
Zero-point correction = 0.221923 (Hartree/Particle)
Thermal correction to Energy = 0.245663
Thermal correction to Enthalpy = 0.246607
Thermal correction to Gibbs Free Energy = 0.166904
Sum of electronic and zero-point Energies = -1292.100347
Sum of electronic and thermal Energies = -1292.076607
Sum of electronic and thermal Enthalpies = -1292.075663
Sum of electronic and thermal Free Energies = -1292.155366

7

Charge = 0 Multiplicity = 1

Atom	X	Y	Z	Atom	X	Y	Z
C	0.000000	0.000000	-0.651588	O	0.000000	0.000000	0.488691

Zero-point correction = 0.005011 (Hartree/Particle)
Thermal correction to Energy = 0.007372
Thermal correction to Enthalpy = 0.008316
Thermal correction to Gibbs Free Energy = -0.014131
Sum of electronic and zero-point Energies = -113.296325
Sum of electronic and thermal Energies = -113.293964
Sum of electronic and thermal Enthalpies = -113.293020
Sum of electronic and thermal Free Energies = -113.315467

8

Charge = 0 Multiplicity = 1

Atom	X	Y	Z	Atom	X	Y	Z
C	-1.528793	0.000470	2.510149	O	-0.511613	0.000214	1.727248
O	-2.728023	0.000617	2.221558	O	-2.893698	2.164239	-0.512977
O	-2.893420	-2.164851	-0.512299	C	-2.073712	1.331202	-0.482995
C	-2.073559	-1.331682	-0.482552	O	-0.592748	-0.000699	-3.506408
C	-0.630157	-0.000473	-2.334644	Re	-0.701634	-0.000148	-0.432718
H	0.001570	3.082866	-0.461685	H	0.002014	-3.083076	-0.460722
C	0.972488	2.664310	-0.217918	N	1.042285	1.322793	-0.175087
C	0.972874	-2.664303	-0.217095	N	1.042473	-1.322762	-0.174666
C	2.065291	3.480251	0.032866	H	1.953790	4.556983	-0.014532
C	2.230120	0.734092	0.120061	C	2.065806	-3.480005	0.033901
C	2.230229	-0.733796	0.120269	H	1.954462	-4.556768	-0.013166
C	3.283828	2.885273	0.343101	C	3.365680	1.500181	0.384369
C	3.284270	-2.884753	0.343899	C	3.365918	-1.499636	0.384743
H	4.160835	3.489392	0.549308	H	4.307647	1.018985	0.619254
H	4.161378	-3.488678	0.550241	H	4.307829	-1.018226	0.619410
O	-1.137047	0.000692	3.825018	H	-1.949610	0.000921	4.347968

Zero-point correction = 0.215658 (Hartree/Particle)
Thermal correction to Energy = 0.236990
Thermal correction to Enthalpy = 0.237935
Thermal correction to Gibbs Free Energy = 0.161476
Sum of electronic and zero-point Energies = -1178.836413
Sum of electronic and thermal Energies = -1178.815080
Sum of electronic and thermal Enthalpies = -1178.814136
Sum of electronic and thermal Free Energies = -1178.890595

Transition state for equatorial CO ligand loss.

Charge = 0 Multiplicity = 1

Atom	X	Y	Z	Atom	X	Y	Z
C	-3.767412	0.211289	0.204109	O	-2.772012	0.706368	0.818145
O	-3.802634	-0.377857	-0.887703	O	-2.335341	2.198414	-1.767464
O	-1.951600	-2.746083	0.503334	C	-1.596070	1.748489	-1.014311
C	-1.357614	-1.750931	0.301185	O	-0.626422	-0.919312	-3.000132
C	-0.472377	-0.600066	-1.895805	Re	-0.319390	-0.202075	0.045771
H	-0.041153	3.076996	0.184579	H	0.742446	-3.082749	0.038897
C	0.999528	2.777621	0.130906	N	1.227651	1.458379	0.020241
C	1.669794	-2.525824	-0.012738	N	1.551223	-1.178764	0.013722
C	2.014968	3.719572	0.183501	H	1.767047	4.770636	0.274709
C	2.513625	1.023060	-0.005469	C	2.889505	-3.172358	-0.097317
C	2.691220	-0.427567	-0.043704	H	2.911862	-4.255663	-0.113803
C	3.333849	3.282126	0.117440	C	3.583504	1.920728	0.030791
C	4.055047	-2.413855	-0.155853	C	3.945970	-1.033383	-0.127786
H	4.157689	3.987309	0.146952	H	4.604031	1.559220	0.002227
H	5.028484	-2.886989	-0.223178	H	4.836099	-0.418559	-0.175827
O	-4.961266	0.397415	0.889584	C	-0.339461	-0.021878	2.033724
O	-0.405880	-0.005333	3.189673	H	-5.647612	-0.002911	0.339355

Imaginary Frequency = 213.75i
Zero-point correction = 0.220473 (Hartree/Particle)
Thermal correction to Energy = 0.244858
Thermal correction to Enthalpy = 0.245802
Thermal correction to Gibbs Free Energy = 0.162563
Sum of electronic and zero-point Energies = -1292.060251
Sum of electronic and thermal Energies = -1292.035866
Sum of electronic and thermal Enthalpies = -1292.034922
Sum of electronic and thermal Free Energies = -1292.118161

C. Experimental Methods

General Information. All reagents were procured from commercial suppliers and used as received unless otherwise noted. $^{13}CO_{2(g)}$ (^{13}C, 99%) and DMSO-d_6 were purchased from Cambridge Isotope Laboratories and used without further purification. Dichloromethane (CH_2Cl_2) was purified using activated alumina columns in an MBraun MB-SPS solvent purification system and stored over 4 Å molecular sieves under a nitrogen (N_2) atmosphere. All reactions were performed using standard Schlenk-line and glovebox techniques under an atmosphere of purified N_2 with minimal exposure to light.

Physical Methods. FTIR spectra were collected with a ThermoNicolet 6700 spectrophotometer running OMNIC software. Samples were run in a KBr matrix under a stream of dry N_2. All FTIR samples were prepared under N_2 with minimal light exposure. ^{1}H NMR and ^{13}C NMR spectra were recorded in DMSO-d_6 on a Bruker BZH 400/52 400 MHz NMR spectrometer or a Varian Unity Inova 500 MHz NMR spectrometer at 298 K. Chemical shifts were referenced to TMS or residual protio signal of the deuterated solvent.

***fac*-Re(4,4'-dimethyl-2,2'-bipyridine)$(CO)_3$COOH (1)**. Silver triflate (0.229 g, 1.16 mmol) was dissolved in 20 mL of degassed CH_2Cl_2 and added to a flask containing $Re(CO)_5Cl$ (0.401 g, 1.11 mmol) dissolved in 80 mL of CH_2Cl_2. This clear solution was allowed to stir at room temperature for 18 hrs. The white AgCl precipitate was removed by filtration and washed with CH_2Cl_2. An aliquot of 4,4'-dimethyl-2,2'-bipyridine (0.221 g, 1.20 mmol) was added to the filtrate, and the solution was stirred for 8 hrs. The resulting yellow-green solution was reduced to 20 mL under vacuum. The addition of hexanes afforded a yellow precipitate, which was collected by filtration and dried under vacuum to yield 0.456 g (0.72 mmol, 65 %) of a light yellow solid. This intermediate, *fac*-Re(4,4'-dimethyl-2,2'-bipyridine)$(CO)_4(CF_3SO_3)$, was confirmed by IR spectroscopy and used without further purification. The intermediate (0.456 g, 0.72 mmol) was dissolved in 60 mL of deionized water. Potassium hydroxide (0.040 g, 0.71 mmol) was added to the rhenium solution, which was allowed to stir for 1 hr. A yellow precipitate formed almost immediately after the addition of KOH. The precipitate was collected by filtration and dried under vacuum, yielding 0.266 g (0.56 mmol, 78 %) of product. IR ν_{CO} (KBr, cm^{-1}): 2008 (s), 1916 (sh), 1880 (s). ^{1}H NMR (DMSO-d_6, 25 °C): δ 9.02 (1H, s), 8.79 (2H, d, J=4Hz), 8.58 (2H, s), 7.50 (2H, d, J=4Hz), 2.53 (6H, s).

Reaction of *fac*-Re(dmb)$(CO)_3$COOH (1) with CO_2. Complex **1** (0.035g, 0.07 mmol) was dissolved in approximately 2.25 mL of DMSO-d_6, yielding a dark yellow mixture. The solution was purged with either unlabeled or ^{13}C labeled CO_2 then allowed to stand for 2 hrs in the dark. Reaction of Re(dmb)CO_3COOH and CO_2 in dark after 2 h. ^{1}H NMR (DMSO-d_6, 25 °C): δ 9.11 (1H, br), 8.86 (2H, d, J=5Hz), 8.59 (2H, s), 7.58 (2H, d, J=5Hz), 2.53 (6H, s). ^{13}C NMR (DMSO-d_6, 25 °C): δ 198.33, 194.61, 158.61 (OCO_2H), 154.95, 152.68, 152.46, 128.09, 124.56, 20.97. IR ν_{CO} (KBr, cm^{-1}): 2028 (s), 1905 (s), 1857 (s), 1621 (m), 1416 (m), 1346 (m) Reaction of Re(dmb)CO_3COOH and $^{13}CO_2$ in dark after 2 h. ^{1}H NMR (DMSO-d_6, 25 °C): δ 9.10 (1H, br), 8.86 (2H, d, J=8Hz), 8.61 (2H, s), 7.58 (2H, d, J=8Hz), 2.54 (6H, s). ^{13}C NMR (DMSO-d_6, 25 °C): δ 198.33, 194.62, 158.62 (O^{13}COOH), 154.94, 152.66, 152.46, 128.08, 124.57, 20.96. IR ν_{CO} (KBr, cm^{-1}): 2027 (s), 1904 (s), 1858 (s), 1574 (m), 1393 (w), 1330 (m)

D. Data from Experiment

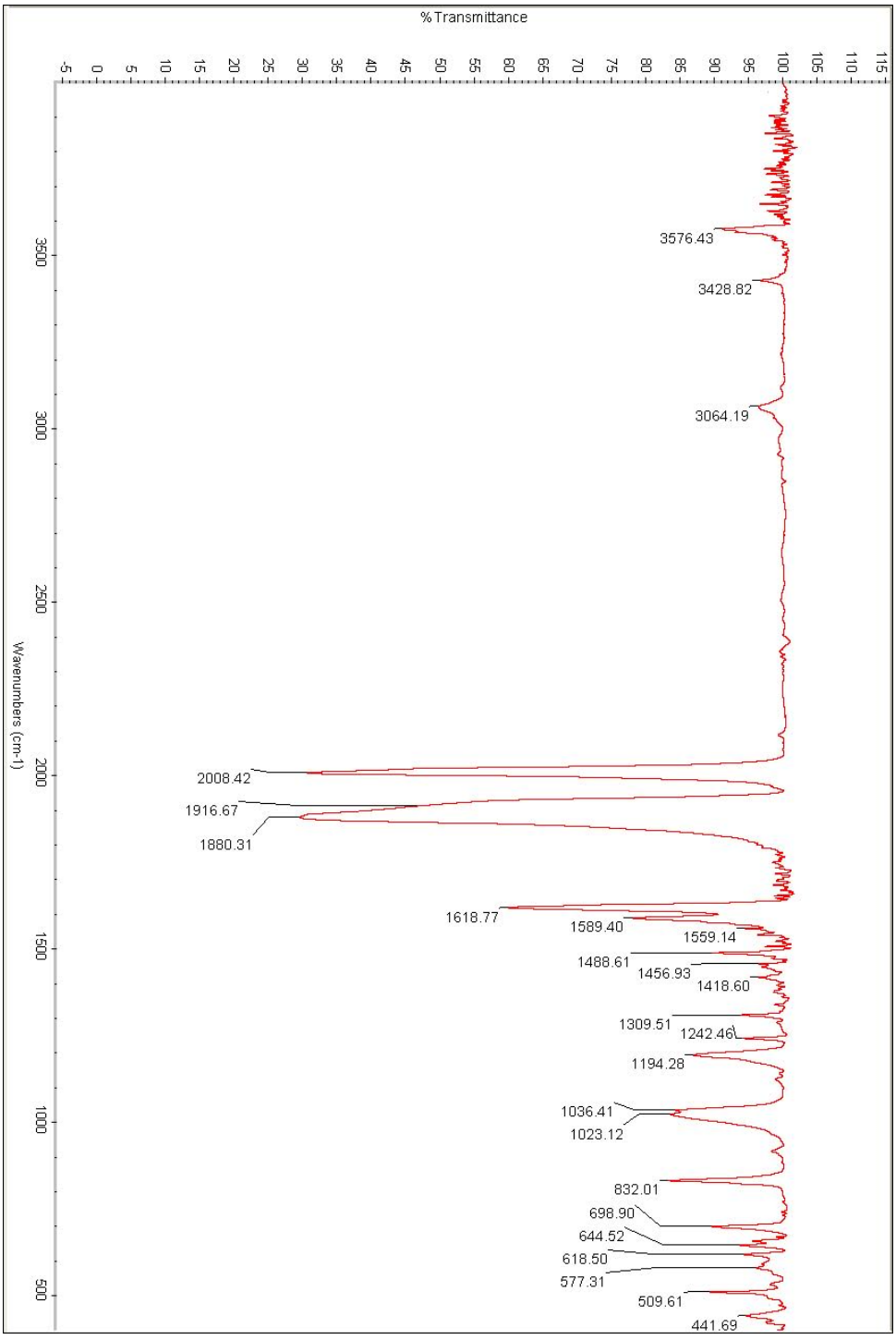

Figure SI-3: FTIR Spectrum of Re(dmb)$(CO)_3$COOH (**1**) (KBr matrix).

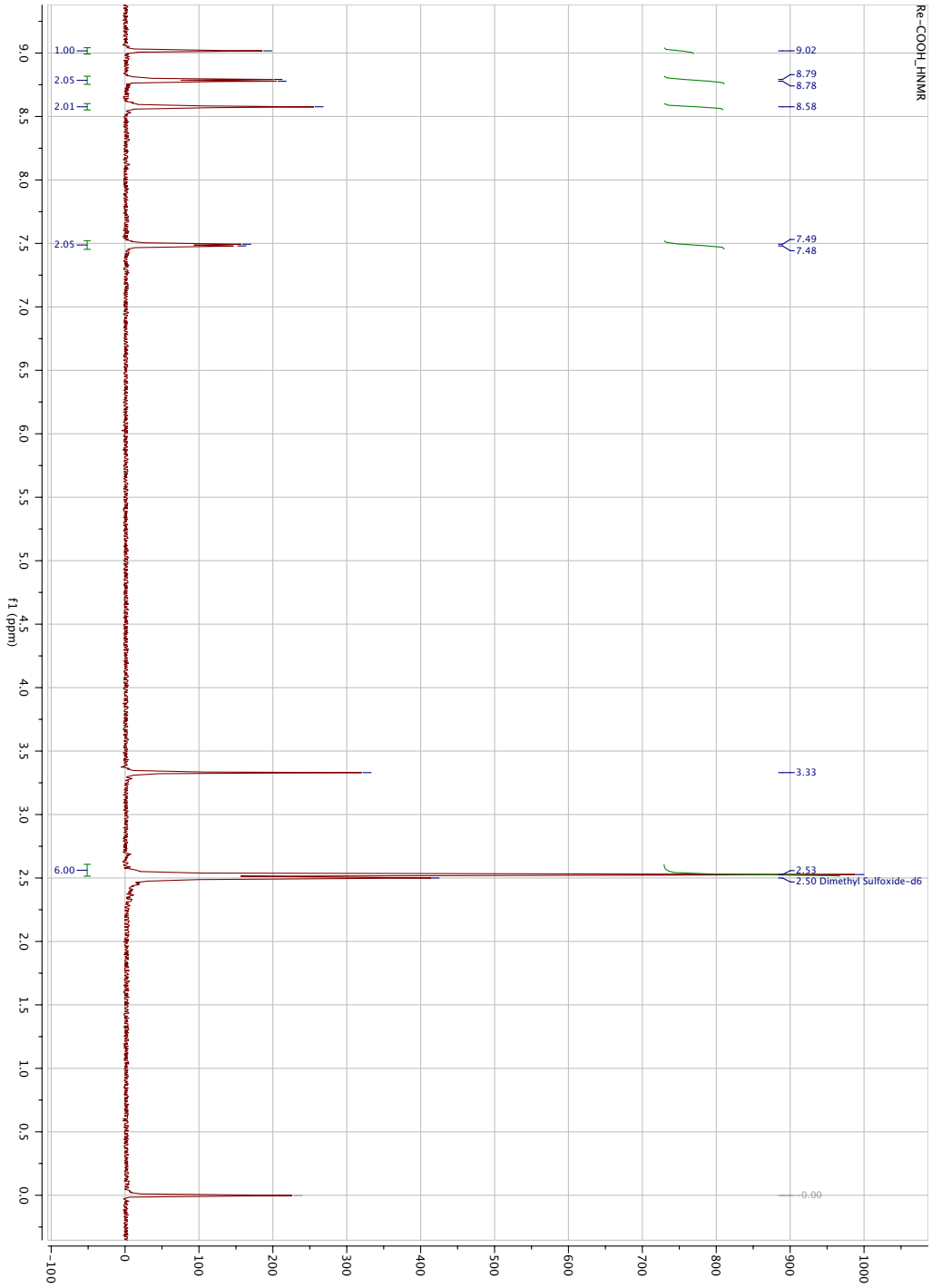

Figure SI-4: ^{1}H NMR Spectrum of Re(dmb)(CO)$_3$COOH (**1**) in DMSO-d_6.

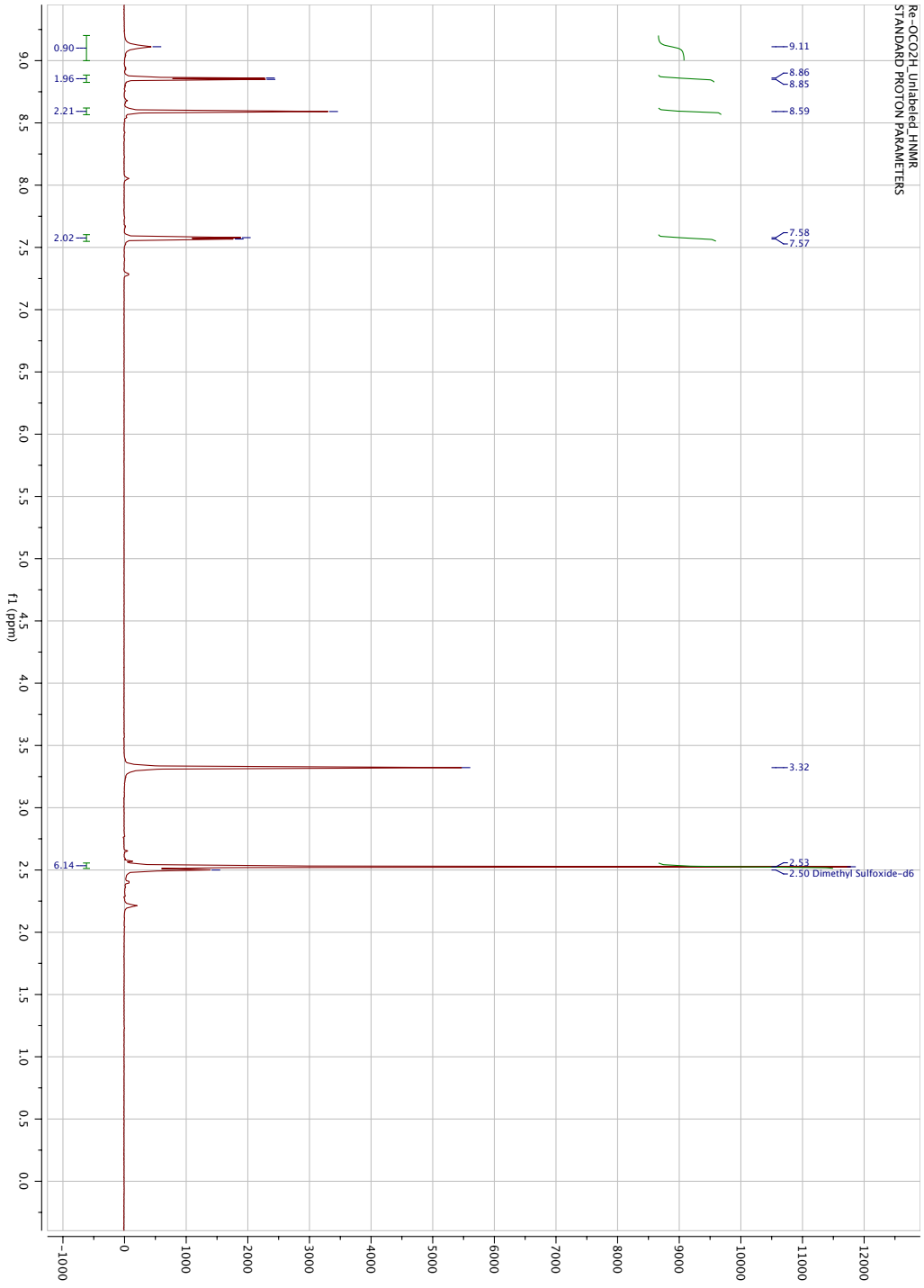

Figure SI-5: ^{1}H NMR Spectrum of Re(dmb)(CO)$_3$OCO$_2$H (**8**), from the reaction of Re(dmb)(CO)$_3$COOH (**1**) with CO_2, in DMSO-d_6.

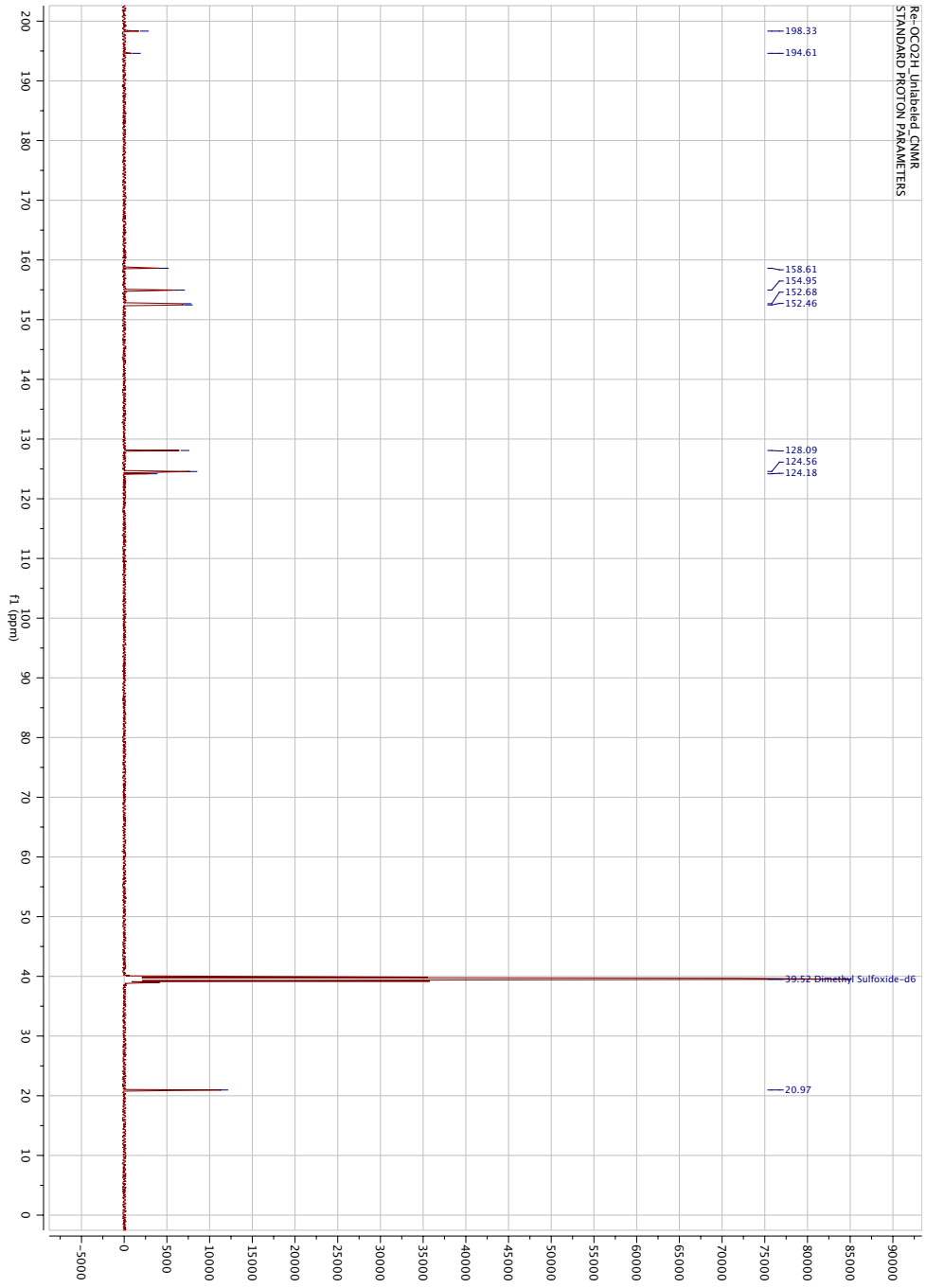

Figure SI-6: ^{13}C NMR Spectrum of Re(dmb)(CO)$_3$OCO$_2$H (**8**), from the reaction of Re(dmb)(CO)$_3$COOH (**1**) with CO_2, in DMSO-d_6. The peak at 124.18 ppm is assigned to the carbon atom of CO_2.

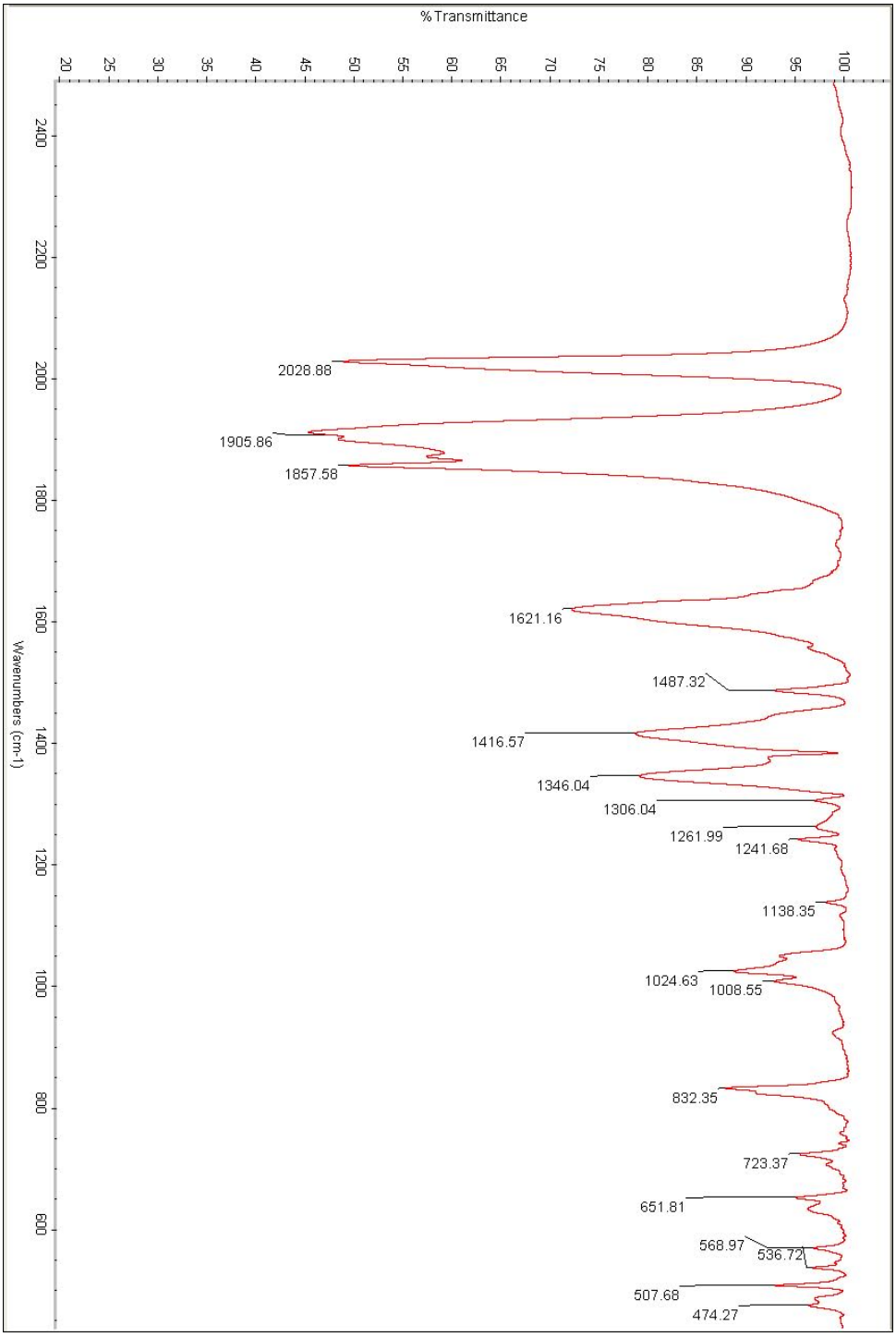

Figure SI-7: FTIR Spectrum of Re(dmb)$(CO)_3OCO_2H$ (**8**), from the reaction of Re(dmb)$(CO)_3COOH$ (**1**) with CO_2 (KBr Matrix).

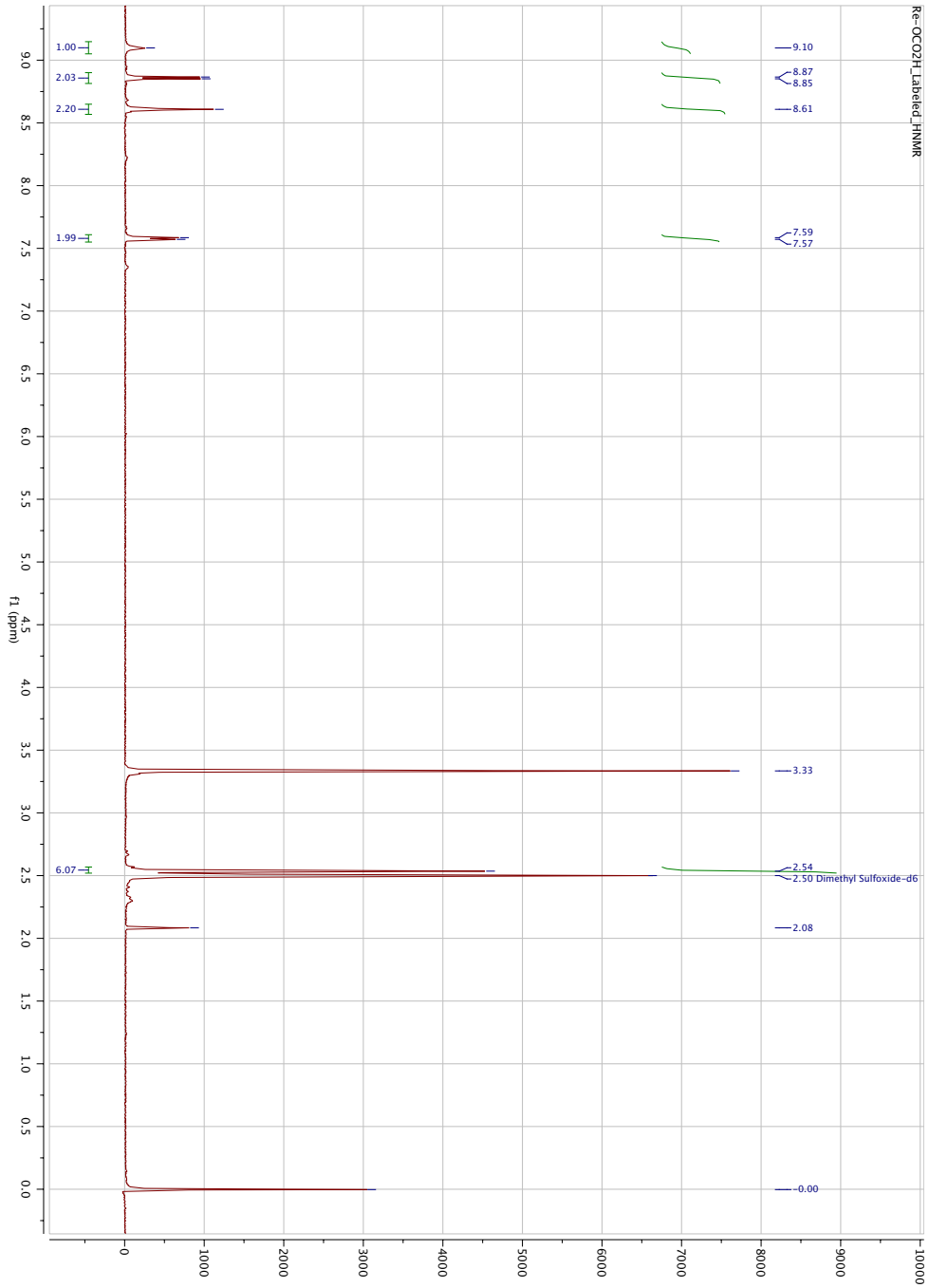

Figure SI-8: ^{1}H NMR Spectrum of Re(dmb)(CO)$_3$OCO$_2$H (**8**), from the reaction of Re(dmb)(CO)$_3$COOH (**1**) with $^{13}CO_2$, in DMSO-d_6. The peak at 2.08 ppm is assigned to acetone.

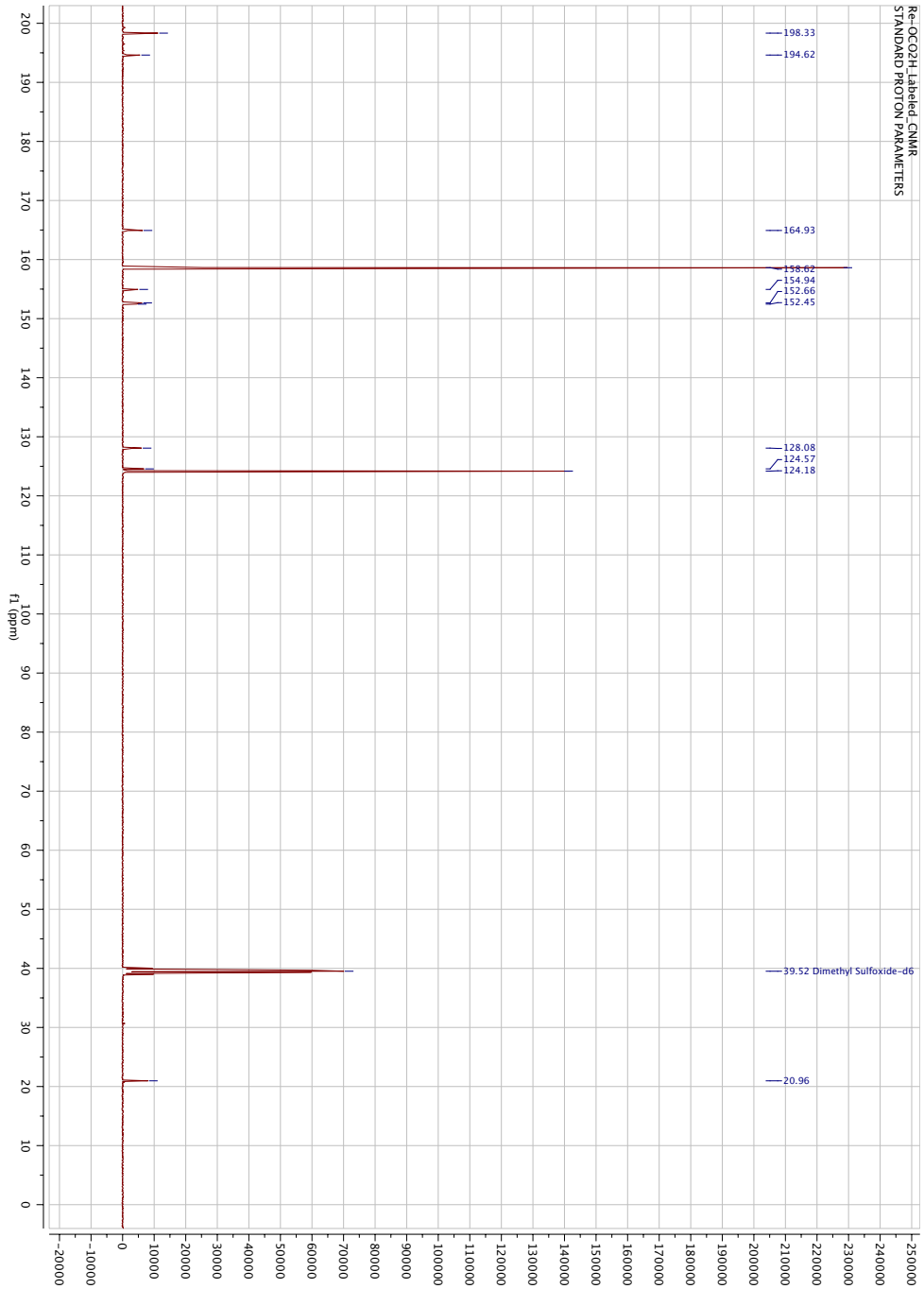

Figure SI-9: ^{13}C NMR Spectrum of Re(dmb)(CO)$_3$OCO$_2$H (**8**), from the reaction of Re(dmb)(CO)$_3$COOH (**1**) with $^{13}CO_2$, in DMSO-d_6. The peak at 124.18 ppm is assigned to the carbon atom of CO_2. The peak at 158.62 ppm is assigned to the carbon atom of $HOCO_2^-$.

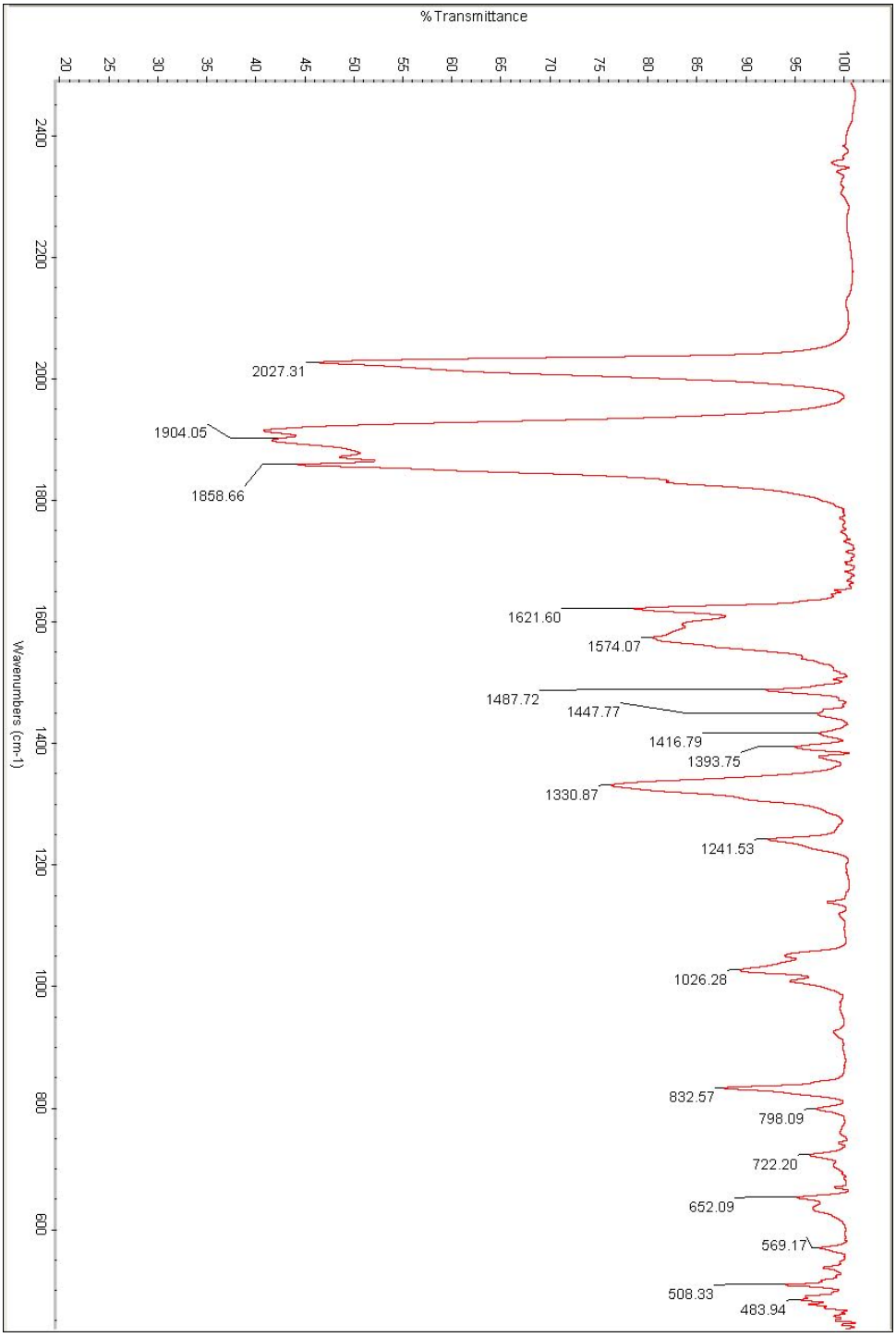

Figure SI-10: FTIR Spectrum of $Re(dmb)(CO)_3OCO_2H$ (**8**), from the reaction of $Re(dmb)(CO)_3COOH$ (**1**) with $^{13}CO_2$ (KBr Matrix).

Chapter 4

Conclusions

Rhenium molecular catalysts have been employed since the 1980's as mediators of CO_2 reduction to carbon monoxide and formic acid, which makes it curious that their mechanisms have remained so elusive. Only recently have large molecular systems become tractable with theoretical methods (especially using solvent models) as computational power has increased and become more affordable. Chapter 2 reports, for the first time, a complete mechanism for carbon monoxide reduction from one-electron reduced rhenium tricarbonyl catalysts. This is an important result that could only be achieved by working closely with experimentalists in order to deduce plausible intermediates.

The mechanism presented in Chapter 2 begins from a reduced monomer, $Re(bpy)(CO)_3^{\bullet}$, which is directly comparable to the $Re(dmb)(CO)_3^{\bullet}$ analogue employed by Hayashi and co-workers. In the presence of CO_2, a dimer forms with CO_2 bridging two reduced monomers. This allows for the requisite overall two-electron reduction. An additional equivalent of CO_2 reacts with the bridged dimer to form a carbonate bridged dimer and carbon monoxide. Thus, overall CO production occurs from the reaction of two reduced monomers with two equivalents of CO_2. Aspects of the proposed mechanism, including positions of the carbon atoms from CO_2 and barrier heights, agree with experimentally observed kinetic rates and structures from isotope labeling experiments.

Chapter 3 presents a mechanism for carbon monoxide formation from a proposed intermediate Re(dmb)$(CO)_3$COOH, which could form after the reaction of the two-electron reduced monomer, Re(dmb)$(CO)_3^-$, and CO_2 in a protic environment. Previously, Gibson and co-workers had observed CO production from Re(dmb)$(CO)_3$COOH, but the mechanism was unknown. In Chapter 3, experimental and theoretical work is presented to support a mechanism that involves the reaction of Re(dmb)$(CO)_3$COOH with CO_2 to form Re(dmb)$(CO)_4^+$ and $HOCO_2^-$, an ion-pair. Subsequently, the ions combine to form CO and Re(dmb)$(CO)_3OCO_2H$ through a heptacoordinate transition state. This is the first example of bicarbonate promoting the production of CO. The results of isotope labeling are presented to confirm the presence of the carbon atom from $^{13}CO_2$ within the bicarbonate moiety of the product.

The mechanisms presented in Chapters 2 and 3 uncover underlying components of the one-electron and two-electron reduction pathways. This work should greatly aid experimentalists in the design of new catalysts, such as in the recent development of manganese tricarbonyl analogues. Moreover, the energies reported should provide a useful benchmark for further work that aims to improve the efficiency of rhenium catalysts for CO_2 reduction.

Part II

Investigating Vinyl Radical and Methyl Peroxy Radical Combustion Intermediates

Chapter 5

Introduction and Literature Review

The energy density of hydrocarbon fuels like gasoline are among the highest known, which has, for centuries, made them attractive energy sources.[121,122] Their abundance and ease of transport will likely ensure their use for the foreseeable future. In fact, the ability to store energy in carbon-hydrogen bonds is an appealing storage medium for renewable fuels like hydrogen as a method to convert a gas into a dense and easily transportable liquid. Even as the availability of easily-accessed crude oil deposits diminishes, the abundance of natural gas and the availability of methods for fixing combustion products like CO_2 into hydrocarbon fuels[11] highlights the importance of combustion research.

The combustion of hydrocarbons, such as in the cylinder of an Otto-cycle engine, yields purely CO_2 and H_2O if enough oxygen is present. The stoichiometric amount of molecular oxygen required for complete combustion may be determined using the formula

$$C_mH_n + (m + n/4)O_2 = mCO_2 + (n/2)H_2O \tag{5.1}$$

for any hydrocarbon fuel. In practice, however, an excess is usually required due to inhomogeneous regions within the fuel mixture and the presence of side reactions that also consume O_2.[123]

In a typical gasoline engine, air and fuel is premixed before combustion. This nearly homogenous mixture is injected into the engine cylinder where it is compressed through piston movement then ignited by a spark from a spark plug. Two actions are at play here: ignition and compression. The ignition of the vaporized fuel closest to the spark source rapidly triggers combustion across the cylinder. Additionally, as the piston movement continues to compress the fuel the volatile gas may spontaneously ignite before the entire fuel has been consumed from spark ignition. As a result, there may be two ignition sources; the intended spark ignition and unintended compression ignition. The latter is generally termed 'engine knock' from the audible noise that results.[123]

Several additional features exist within the flame, namely the conditions that cause soot and NO_x species to form. Although a lean fuel mixture (i.e., excess oxygen) is often employed, which should provide more than the required stoichiometric amount of oxygen, there are areas of reduced oxygen concentration. Here, the high heat allows for reaction between the carbon components of the fuel; dimerization and isomerization normally precluded by high reaction barriers may be accessed. The formation of radical species as a result of available hydroxyl radical also contributes to the reactivity of the unoxidized fuel. A complex reaction pathway ensues, yielding larger carbon fragments, then aromatic rings, and finally polycyclic aromatic structures, or soot.[124,125]

NO_x formation follows from the composition of air, which contains relatively little oxygen (21%).[126] Molecular nitrogen is instead the principle component of air and is therefore in abundance within the engine cylinder. While N_2 is thermodynamically stable, increasing temperatures within the cylinder may allow for its reaction to form nitric oxide (NO) and nitrogen dioxide (NO_2). These species that are environmentally harmful because they lead to the production of ozone within the inner atmosphere, among other things.[127]

Fundamental combustion research encompasses the development of soot formation models in order to understand the overall rate of production and, perhaps, limit it.[128] Since soot formation is the result of a network of many elementary reactions, tens or hundreds of rate constants are assembled in a larger model to predict the overall rate. Uncertainties in the underlying kinetic rates can significantly distort the predicted overall soot production, and in many elementary reactions the rate has never been solved in experiment. For radical and charged species, in particular, the kinetic rate is difficult to measure directly in the laboratory due to their fleeting nature. Instead, concentrations of the stable, closed-shell precursors and products are often the species that are monitored.[128] Quantum mechanical (QM) tools are particularly valuable for the study of fundamental combustion reactions since they involve relatively small molecules that occur in the gas-phase. And, careful treatment with QM methods can yield sub-chemical accuracy for such systems.[129]

Chapter 6 deals with one such fundamental reaction: hydrogen abstraction by vinyl radical to form ethylene and a hydrogen atom. This reaction is central to terrestrial combustion, such as in the engine of a vehicle, and in planetary systems where an excess of methane and abundant incident light allows for the formation of the requisite precursors.[130] Specifically, the reaction barriers of $C_2H_3 + H_2$ are predicted from a series of single point energies that are extrapolated to the basis-set limit using the focal point approach.[129,131–133] Computations include the recently developed and rigorous CCSDT(Q) method, which includes single, double, triple, and perturbative quadruple excitations.[134–136] The result, which was corrected for the

zero-point vibrational energy, relativistic effects, and the Born-Oppenheimer approximation, has an estimated accuracy of within 0.1 kcal mol^{-1}. Analysis of the reaction coordinate using natural bonding orbitals (NBO) is also presented.

While Chapter 6 deals with the result of the first of the aforementioned features preventing complete combustion, soot formation, Chapter 7 deals with an aspect of the second: NO_x formation. The oxidation of molecular nitrogen (e.g., to NO or NO_2) is preferred over N_2 as temperatures rise within the flame. Obviously, reducing of the temperature would lead to decreased NO_x production. And, in practice, this may be achieved by recycling flue gas into the combustion chamber to i) reduce the temperature, and ii) burn any remaining fuel.[137] An attractive alternative to this methodology is to design a fuel mixture that inherently maintains low temperature combustion. One such engine has been proposed that utilizes components of both gasoline- and diesel-type engines.

In a gasoline engine, as discussed, a homogenous air and fuel mixture enters a cylinder where it combusts after spark ignition or, unfavorably, as a result of compression. In a diesel engine, compression is the only ignition source. This has the advantage of eliminating engine knock and providing additional torque. In a diesel engine, the fuel is simply injected directly into a cylinder where it mixes with the hot air present. The result is a relatively fuel-rich environment. The lack of available oxygen, however, usually leads to higher soot formation. On the other hand, the high fuel compression affords greater fuel efficiency.

The homogenous charge compression ignition (HCCI) engine has been proposed as a high-efficiency, low-pollutant solution. HCCI engines rely on the compression ignition of diesel engines, which yields high fuel efficiency, and the homogenous air/fuel mixture of gasoline engines, which produces less soot.[123] Furthermore, they can operate with very lean fuel mixtures ([air] >> [fuel]), which results in a lower temperatures and therefore decreased NO_x formation. Unfortunately, the maintenance of low temperatures throughout the combustion event cannot be guaranteed by design, but must be a property of the fuel mixture. Determin-

ing suitable fuel types depends on a thorough understanding of the underlying kinetics. In particular, the formation and reactivity of alkyl peroxy radicals that result from the reaction of available radical species in solution and oxygen, which is present in high concentrations.

Experimental and theoretical cooperation is central to understanding the reactivity of alkyl peroxy radicals.[138] In Chapter 7 the infrared signature of methyl peroxy radical, a fundamental alkyl peroxy molecule, is predicted with second-order vibrational perturbation theory (VPT2) for the parent isotopologue and three related isotopologues. Reliable spectroscopic data is essential for monitoring the presence of alkyl peroxy species for kinetic-rate determination. Previously, the complete gas-phase spectrum of CH_3O_2 had never been observed in the laboratory. While many traditional quantum mechanical predictions rely on the determination of relative energies, and the inherit cancellation of errors, VPT2 is unique in that experimental comparison can be made directly from the absolute values garnered from computation.

In most frequency computations, second-derivatives of the energy with respect to nuclear coordinates yields frequencies within the double harmonic approximation. These values are not comparable to experiment, but may be scaled and used as a predictive tool for spectral assignment. Computing the anharmonic frequencies, which are directly comparable to experiment, involves correcting the harmonic frequencies for the anharmonic nature of the potential energy surface (PES). Unfortunately, this requires a rigorous description of the PES, which is usually determined from many second derivative computations at displaced geometries from equilibrium. For methyl peroxyl radical, only one second-derivative computation is required to determine the harmonic frequencies, but 21 are required to determine the anharmonic frequencies; a significant computational effort. But, for modes that are difficult to assign, have never been observed, or have no symmetry information, the data garnered from VPT2 analysis is invaluable.

Methyl peroxy radical is particularly suitable for VPT2 treatment, as opposed to variational approaches like variational self-consistent field (VSCF) or variational configuration interaction (VCI), because of the relatively large system size and the relatively rigid nature of the molecule. VPT2 analysis breaks down for systems with large amplitude motions, weak bonding (e.g., van der Waals interactions), or second- or third-rank resonances,[139,140] which necessitates a variational or variational-like approach, but methyl peroxy radical exhibits none of these characteristics.

VPT2 theory starts from the vibration-rotation Hamiltonian in normal coordinates ($\mathbf{Q}$), which is expanded using a power series expansion.[141] Rayleigh-Schrödinger treatment or contact transformation of the expanded Hamiltonian yields the first- and second- order contributions of the potential energy term and the first-order kinetic energy terms required to determine the anharmonic constants (x_{rr}) and (x_{rs}) that are appended to the harmonic frequencies.[142,143]

$$x_{rr} = \frac{1}{16}\phi_{rrrr} - \frac{1}{16}\sum_{s}\phi_{rrs}^2(8\omega_r^2 - 3\omega_s^2)/\omega_s(4\omega_r^2 - \omega_s^2) \tag{5.2}$$

$$x_{rs} = \frac{1}{4}\phi_{rrss} - \frac{1}{4}\sum_{t}\phi_{rrt}\phi_{tss}/\omega_t - \frac{1}{2}\sum_{t}\phi_{rst}^2\omega_t(\omega_t^2 - \omega_r^2 - \omega_s^2)/\Delta_{rst} + \Gamma_{rs} \tag{5.3}$$

$$\Delta_{rst} = (\omega_r + \omega_s + \omega_t)(\omega_r + \omega_s - \omega_t)(\omega_r - \omega_s + \omega_t)(\omega_r - \omega_s - \omega_t) \tag{5.4}$$

$$\Gamma_{rs} = \left[A_e(\zeta_{r,s}^{(a)})^2 + B_e(\zeta_{r,s}^{(b)})^2 + C_e(\zeta_{r,s}^{(c)})^2\right](\omega_r/\omega_s + \omega_s/\omega_r) \tag{5.5}$$

Equations 5.2-5.5 involve the quadratic force constants (ω), the cubic force constants (ϕ_{rst}), and semi-diagonal quartic force constants (ϕ_{rrss}). Vibration-rotation coupling is included with the Coriolis zeta terms ($\zeta_{r,s}^{a}$). A_e, B_e, and C_e are rotational constants determined at the equilibrium geometry. Anharmonic corrections for the intensities of each mode may be determined using the same quantities.[144,145] In addition to anharmonic frequencies for CH_3O_2, $^{13}CH_3OO$, and $CH_3{}^{18}O{}^{18}O$, Chapter 7 also includes vibrational zero-point corrections to the rotational constants and structural parameters.

Chapter 6

Reaction Energetics for the Abstraction Process

$C_2H_3 + H_2 \rightarrow C_2H_4 + H$ [1]

[1] J. Agarwal, J. M. Turney, and H. F. Schaefer *J. Phys. Chem. Lett.*, **2011**, 2, 2587-2592. Reproduced by permission of The American Chemical Society.

6.1 Abstract

The fundamentally important combustion reaction of vinyl radical with hydrogen has been studied in the laboratory by at least five experimental groups. Herein, the reaction $C_2H_3 + H_2 \rightarrow C_2H_4 + H$ has been examined using focal-point analysis. Molecular energies were determined from extrapolations to the complete basis-set limit using correlation-consistent basis sets (cc-pVTZ, cc-pVQZ, and cc-pV5Z) and coupled-cluster theory with single and double excitations (CCSD), perturbative triples [CCSD(T)], full triples [CCSDT], and perturbative quadruples [CCSDT(Q)]. Reference geometries were optimized at the all-electron CCSD(T)/cc-pCVQZ level. Computed energies were also corrected for relativistic effects and the Born-Oppenheimer approximation. The activation energy for hydrogen abstraction is predicted to be 9.65 kcal mol^{-1} and the overall reaction is predicted to be exothermic by 5.65 kcal mol^{-1}. Natural resonance theory (NRT) analysis was performed to verify the reaction pathway and describe bond-breaking and bond-forming events along the reaction coordinate.

6.2 Introduction

Small hydrocarbons are ubiquitous in the chemistries of combustion processes and planetary atmospheres.[125,130,146–148] Their reactivity, which can lead to the formation of aromatic compounds or soot, is a central topic of research in both fields. In flames, soot production results from incomplete combustion, which yields fragments that combine to form larger hydrocarbon species. Similarly, many planetary atmospheres contain high concentrations of molecular hydrogen and methane.[149–151] The photolysis of these species, usually from incident UV radiation, results in photofragments, which also combine to produce larger hydrocarbons as in combustion.

Soot does not form directly from initial hydrocarbon fragments, but rather as a result of a complex network of reactions that may be modeled with kinetic data. Prior work has elucidated the reaction rates and absorption spectra of many neutral hydrocarbons,[152–156] but the analogous radical and charged species are much more difficult to study. While neutral species can be produced in large quantity, isolated, and observed, radical and charged species are often produced through photolysis, which yields a myriad of highly-reactive products. Subsequent isolation of the desired species, usually though mass-selection, significantly reduces the concentration, which makes spectroscopic analysis difficult. The time-independent nature of a theoretical investigation is ideal for the study of these species, and high-accuracy computational methods have been shown to yield subchemical accuracy for the reaction enthalpies of such systems.[129,131–133]

The vinyl radical is among the most important species in combustion chemistry. Herein we have investigated, using computational methods, a single pathway involving the reaction of the vinyl radical with hydrogen. Although vinyl radical readily reacts with other hydrocarbons (CH_3, C_2H_3, C_2H_5, etc.) and diatomics (O_2, Cl_2, etc.),[128] prior work has shown that in an atmosphere of H_2 vinyl radical abstracts a hydrogen atom from molecular hydrogen to yield C_2H_4 and H.[128,157–163] Subsequently the two products combine in a propagation step to form ethyl radical, C_2H_5. Callear and Smith first indirectly measured the kinetic rate for the hydrogen abstraction step in the mid 1980s. They reported a small activation energy of 5.5 kcal mol^{-1} and a rate of 2.6×10^{-17} cm^3 molecule $^{-1}$ s^{-1} at 298 K.[157]

Since their work, several groups have reported kinetic rates for the hydrogen abstraction process using data from experimental and theoretical investigations. In 1986, Tsang and Hampson reported a data base of kinetic rates for combustion processes, which included vinyl radical.[158] Two years later, Weissman and Benson reported results from transition-state theory analysis, which estimated the rate at 5.0×10^{-17} cm^3 molecule $^{-1}$ s^{-1} at 298 K.[164]

In 1995, two groups reported reaction rates for this process. In a theoretical investigation using QCISD(T) and CCSD(T) theories with a 6-311+G(3*df*,2*p*) basis for single-point energies, Mebel, Morokuma, and Lin reported a rate of 2.98×10^{-19} cm^3 molecule $^{-1}$ s^{-1} at 298 K. They found the activation barrier for the forward reaction to be 10.4 kcal mol^{-1} and the overall reaction to be exothermic by 7.1 kcal mol^{-1} [using CCSD(T)].[159] Then, Fahr, Monks, Steif, and Laufer reported a comparable rate by employing kinetic absorption spectroscopy and gas chromatographic product analysis.[160] In 1996, Knyazev, Bencsura, Stoliarov, and Slagle reported the first direct experimental measurement of the abstraction process using photoionization mass spectroscopy. They found the rate to be 7.1×10^{-18} cm^3 molecule $^{-1}$ s^{-1} at 298 K.[161] Much of this past work is summarized in a review by Laufer and Fahr, which discusses the kinetics for many small hydrocarbon reactions.[128]

More recently, there have been two theoretical studies concerning the abstraction step. In 2004, Li, Lü, and Wang employed MP4(SDQ) theory with a 6-311++G(d,p) Pople basis set to fit a rate constant using improved canonical variational transition-state theory with a small-curvature tunneling correction. They reported a rate of 5.22×10^{-17} cm^3 molecule $^{-1}$ s^{-1} at 298K using an activation barrier of 9.95 kcal mol^{-1} and an exothermicity of 6.12 kcal mol^{-1}.[162] And in 2006, Tautermann, Wellenzohn, and Clary found a similar rate constant of 2.1×10^{-18} cm ^{3} molecule $^{-1}$ s^{-1} at 298K using an activation barrier of 10.34 kcal mol^{-1} and an exothermicity of 4.84 kcal mol^{-1}. They employed time-independent scattering theory with a 2D potential energy surface using B3LYP/6-31G* geometries and G3GB scheme for single-point energies.[163]

The reported reaction rates vary from 10^{-17} to 10^{-20} cm^3 molecule $^{-1}$ s^{-1} and represent relatively small changes in the activation energy or exothermicity. In fact, Knyazev and co-workers note that a reduction of only 1.3 kcal mol^{-1} in the activation barrier obtained by Mebel and co-workers would account for the discrepancy between their rate constants, which differ by one unit of magnitude.[161] Given that variances in the reaction energies are of the

same magnitude as the energies themselves, particular care must be taken to obtain values with an accuracy of less than a kcal mol^{-1}. Prior work has relied on explicitly correlated methods paired with uncorrelated valence basis sets that do not yield the required accuracy. Herein we improve upon previous theoretical studies by pairing correlated methods with the appropriate correlation consistent basis sets[165] followed by focal-point analysis[129,131–133] to obtain molecular energies extrapolated to the complete basis-set limit. Furthermore we have included corrections for relativistic effects and the Born-Oppenheimer approximation. We also compare the vibrational frequencies obtained in our study for species in the reaction to experimentally obtained spectra.[156,166,167]

6.3 Theoretical Methods

Reference geometries were optimized by all-electron (AE) coupled cluster theory incorporating single, double, and perturbative triple excitations [CCSD(T)][168–173] using a core-valence correlation-consistent quadruple-ζ basis-set (cc-pCVQZ).[174] The large core-valence cc-pCVQZ basis-set provides 288 contracted Gaussian functions for ethylene and 258 for vinyl radical. This AE-CCSD(T)/cc-pCVQZ level of theory has been shown to be highly accurate for equilibrium geometric parameters of single-reference molecules.[175]

The relative energies of the species involved in the reaction were obtained by the focal point approach,[129,131–133] a convergent scheme in which both electron correlation and basis set limits are systematically approached. The correlation treatment was extended as far as the recently developed CCSDT(Q) method,[134–136] which includes contributions from quadruple excitations analogous to the triples term in the popular CCSD(T) theory. The CCSD(T) and CCSDT(Q) methods using the cc-pVXZ (X=D,T,Q,5) family of basis-sets[176] were used for computation. The resulting single-point energies were extrapolated to the complete basis-set limits (CBS) using a three-parameter exponential function[177] for the Hartree-Fock energy

extrapolation and a two-term X^{-3} form[178] for the correlation energy extrapolation. In the focal point extrapolations, only valence electrons were correlated; thus, an auxiliary core correlation correction (Δ_{core}) was determined by differencing all-electron (AE) and frozen-core CCSD(T)/cc-pCVQZ energetics.

Because the hydrogen atoms rearrange in the reaction, high accuracy was ensured by including diagonal Born-Oppenheimer corrections[179,180] (Δ_{DBOC}) evaluated at the HF level using the cc-pVTZ basis set.[176] Relativistic effects (Δ_{rel}) were also accounted for by appending mass-velocity and Darwin one-electron terms[181,182] computed with the AE-CCSD/cc-pCVTZ method.

All geometric structures were optimized using the MOLPRO[183] suite of electronic structure codes. The CCSDT(Q) correction employed in the focal point analysis was obtained using the string-based quantum chemistry code (MRCC) of Kállay, as interfaced with CFOUR.[135,184,185] DBOC energies and relativistic corrections were also evaluated using CFOUR.[185] Natural resonance theory analysis was performed using NBO 5.0[186]

6.4 Results and Discussion

A. Structures

We have considered the reaction $C_2H_3 + H_2$, which has been shown to proceed through a hydrogen abstraction mechanism.[159] The abstraction process involves a single transition state, **TS 1**, which is the result of C-H bond formation between the least saturated carbon of the vinyl radical, $\mathbf{C_2H_3}$, and a hydrogen atom of molecular hydrogen, $\mathbf{H_2}$. The transition state structure retains the C_s symmetry of vinyl radical, but with a slightly elongated C=C bond distance (1.318 Å vs. 1.310 Å). Similarly, the H-H bond distance of the $\mathbf{H_2}$ moiety increases from 0.742 Å to 0.865 Å. Optimized structures of the reactants, transition state, and products are shown in 6.1. We note reasonable agreement in bond angle, bond length, and symmetry between our structures and those found in prior theoretical work.[159,162]

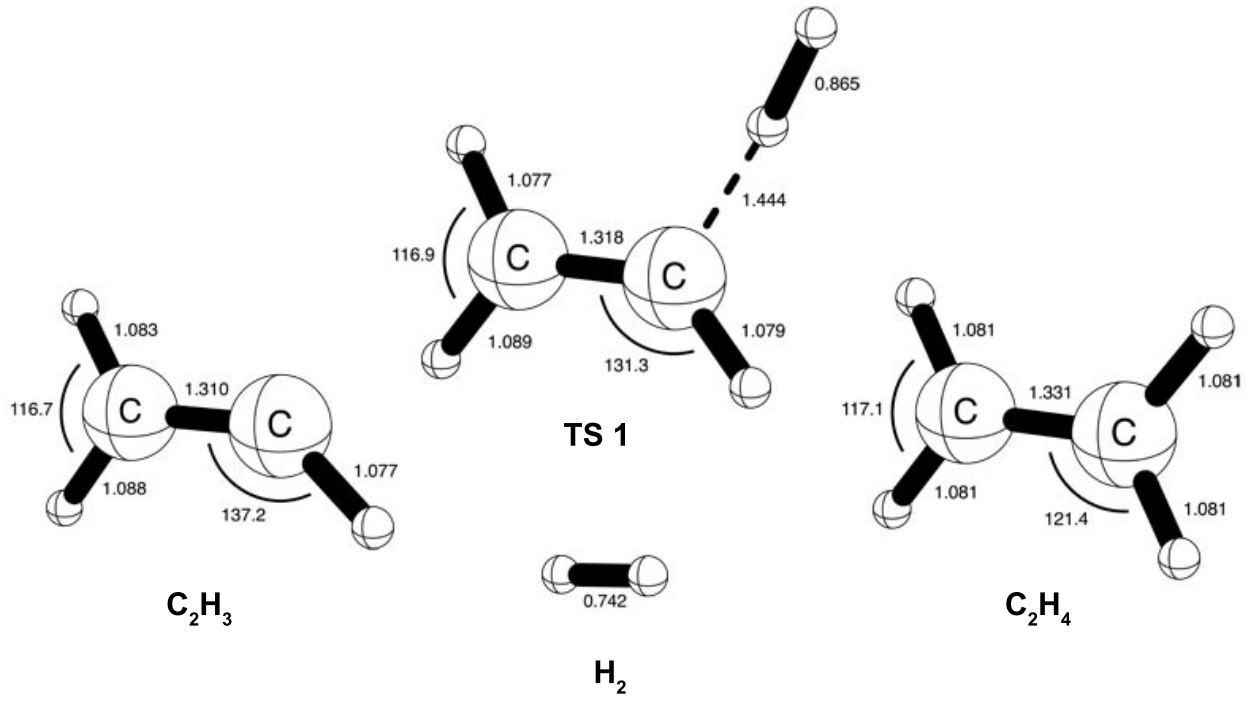

Figure 6.1: Optimized geometries of the reactants, products, and transition state for the abstraction of a hydrogen atom by vinyl radical, $C_2H_3 + H_2 \rightarrow C_2H_4 + H$. Bond lengths are shown in Angstroms, and bond angles in degrees. Geometries were optimized at the AE-CCSD(T)/cc-pCVQZ level of theory.

B. Natural Resonance Theory

Additionally, we have analyzed changes in the bond-order across the intrinsic reaction coordinate (IRC) using natural resonance theory (NRT). This ensures that the transition state connects to the correct minima on the potential energy surface, and quantitatively describes bond-breaking and bond-forming events. These results are shown graphically in 6.2. The red (square) line shows C-H bond formation between vinyl radical and molecular hydrogen and the blue (diamond) line shows H-H bond cleavage in molecular hydrogen. Additionally, The green (triangle) line shows the pairing of a lone electron on the carbon radical of vinyl radical and the purple (x) line shows the cleavage of molecular hydrogen, which leaves a lone electron on a hydrogen atom. The pairs of lines are coupled events whose intersections fall at the same point along the reaction coordinate, indicating concerted steps. That is, C-H bond formation and H-H bond cleavage occurs at the same step as electron pairing of the carbon radical and formation of the hydrogen atom product after homolytic cleavage. These events occur at steps > 0 indicating they are after the energetic maximum is reached. Therefore the transition state resembles the reactants and the overall process should be exothermic by Hammond's postulate.[187]

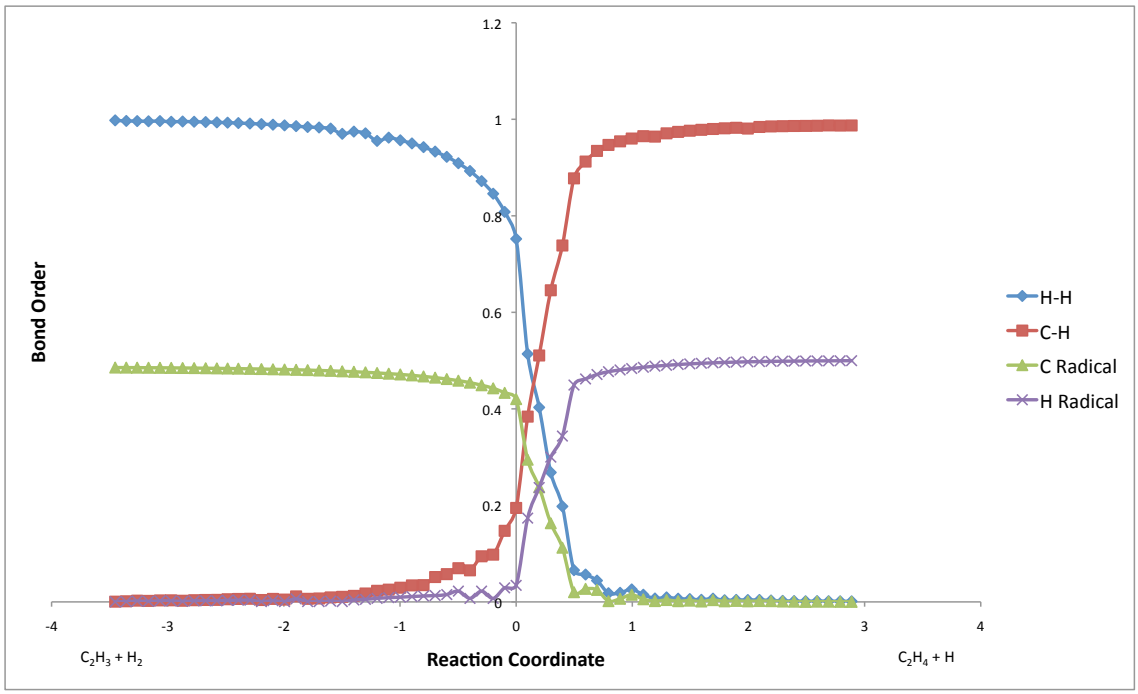

Figure 6.2: Natural Resonance Theory (NRT) analysis of the Intrinsic Reaction Coordinate (IRC). The x-axis is demarcated to indicate mass-weighted IRC steps in units of amu$^{-1/2}$ bohr. The H-H plot shows the bond order between the atoms in H_2. The C-H plot shows the change in bond order in the formation of the C-H bond between C_2H_3 + H_2. The C Radical and H Radical plots show the pairing of a lone electron on the C atom of C_2H_3 and the presence of a lone electron on the H atom product after abstraction, respectively. Although omitted from the figure, it should be noted that the C-C bond order remains relatively unchanged across the reaction coordinate, ranging from a bond order of 2.035 in C_2H_3 to 2.021 in C_2H_4

C. Vibrational Frequencies

Normal vibrational frequencies for the optimized structures are shown in 6.1. Frequencies were computed at the same level of theory as optimization, AE-CCSD(T)/cc-pCVQZ. Experimental frequencies are also shown for vinyl radical and ethylene. We have included the complete spectral assignment for ground state vinyl radical obtained by Letendre and co-workers[166] in addition to a revised set of frequencies obtained by Nikow and co-workers.[167] Similarly, 6.1 includes comparative general harmonic force-field data for ethylene obtained by Duncan and co-workers.[156]

With regard to vinyl radical, obtaining resolved experimental spectra is difficult owing to the low concentrations in which vinyl radical is produced and the inherent instability of a reactive radical intermediate. While much of the prior work has resolved vibrationally hot bands for vinyl radical,[188–195] only recently have ground state frequencies been obtained. The first ground-state assignment for the entire vibrational spectra was obtained by Letendre and co-workers.[166] Previously, Sattelmeyer and Schaefer identified a discrepancy in the assignment of the v_5 band using equation of motion coupled cluster methods.[196] As a follow-up to previous work, and in an effort to obtain a more finely-resolved spectra, Nikow and co-workers[167] re-examined the assignments of the vibrational modes using time-resolved FTIR. As mentioned, we have also included that data in 6.1. We find good agreement between our computed frequencies and the experimentally obtained spectra, but note that we have reported harmonic vibrational frequencies that cannot be directly compared to the anharmonic frequencies listed without a scaling factor.

The general harmonic force-field frequencies for ethylene from Duncan and co-workers[156] may be directly compared to our theoretical results. Here we find good agreement between our results and those obtained by experiment, with our computed frequencies deviating by at most 20 cm^{-1} from those obtained by Duncan and co-workers and on average by only 8 cm^{-1}.

Our predicted ZPVE (31.96 kcal mol^{-1}) is also within 0.1 kcal mol^{-1} of their experimental value (31.91 kcal mol^{-1}). Additionally, we predict a ZPVE of 22.95 kcal mol^{-1} for C_2H_3, 30.07 kcal mol^{-1} for C_2H_4, and 6.29 kcal mol^{-1} for H_2.

C_2H_3 [a]	C_2H_3 [b]	C_2H_3 [c]	H_2 [a]	TS 1[a]	C_2H_4[a]	C_2H_4 [d]
				1277i a'		
723 a'	758 ± 5 a'		4402 a_g	267 a'	827 b_{2u}	842.9 b_{2u}
814 a''	895 ± 9 a''	897 ± 6 a''		362 a''	953 b_{2g}	958.8 b_{2g}
916 a''	955 ± 7 a''	944 ± 6 a''		815 a'	967 b_{3u}	968.7 b_{3u}
1068 a'	1099 ± 16 a'	1074 ± 8 a'		896 a''	1052 a_u	1043.9 a_u
1395 a'	1277 ± 20 a'	1401 ± 5 a'		918 a''	1247 b_{3g}	1244.9 b_{3g}
1623 a'	1700 ± 35 a'	1595 ± 10 a'		935 a''	1371 a_g	1369.6 a_g
3078 a'	3103 ± 11 a'			1071 a'	1479 b_{1u}	1473.0 b_{1u}
3184 a'	3164 ± 20 a'			1143 a'	1675 a_g	1654.9 a_g
3256 a'	3235 ± 12 a'			1398 a'	3147 b_{1u}	3146.9 b_{1u}
				1613 a'	3162 a_g	3152.5 a_g
				2067 a'	3228 b_{3g}	3231.9 b_{3g}
				3093 a'	3254 b_{2u}	3234.3 b_{2u}
				3226 a'		
				3237 a'		

[a] This work. Computed at AE-CCSD(T)/cc-pCVQZ level. [b] Fundamental frequencies from IR emission spectroscopy.[166] [c] Experimental data from IR emission spectroscopy.[167] [d] Experimental data (GHFF) from IR crystal spectra.[156]

Table 6.1: Normal Vibrational Frequencies for the Reactants, Products, and Transition State

D. Energetics

For the optimized geometries we have computed the requisite single-point energies for focal point extrapolation to the complete basis-set limit, as described in the Theoretical Methods section. The focal point analyses are listed in Table 2 and Table 3 for the abstraction barrier and exothermicity, respectively. Both extrapolations suggest convergence to within 0.1 kcal mol^{-1}. We have also included four corrections to the computed energy, as mentioned, and these are reported in Tables 2 and 3. After corrections, we predict the activation barrier for abstraction to be 9.65 kcal mol^{-1} and the overall reaction to be exothermic by 5.65 kcal mol^{-1}.

Mebel and co-workers,[159] Li and co-workers,[162] and Tautermann and co-workers[163] report the abstraction barrier to be 10.4 kcal mol^{-1}, 9.95 kcal mol^{-1}, and 10.34 kcal mol^{-1} respectively. Similarly, they report the reaction to be exothermic by 7.1 kcal mol^{-1}, 6.12 kcal mol^{-1}, and 4.84 kcal mol^{-1} respectively. These earlier results contain a correction for the zero-point vibrational energy, and therefore may be directly compared to our results. We find our abstraction barrier to be comparable, but lower, than the previously reported values. Aligned with our initial NRT analysis and prior work, we also find the overall reaction to be exothermic. Our value of 5.65 kcal mol^{-1}, however, is much lower than that of Mebel and co-workers, roughly 0.5 kcal mol^{-1} lower than the value obtained by Li can co-workers, and approximately 0.8 kcal mol^{-1} higher than the value obtained by Tautermann and co-workers. Given the magnitude of the energy values, small differences yield large variations in the resulting kinetics, emphasizing our choice of a such a rigorous treatment of the reaction energies. We estimate our predictions to be accurate to within 0.1 kcal mol^{-1}.

Table 6.2: Valence Focal Point Analysis of the Classical Abstraction Barrier for C_2H_3 + H_2 → TS1 [a]

basis set	ΔE_eHF	+δMP2	+δCCSD	+δCCSD(T)	+δCCSDT	+δCCSDT(Q)	NET
cc-pVDZ	+20.38	−12.78	+1.78	−0.98	+0.02	−0.06	[+8.36]
cc-pVTZ	+21.62	−13.69	+2.10	−1.28	+0.06	−0.08	[+8.72]
cc-pVQZ	+21.72	−13.99	+2.18	−1.35	[+0.06]	[−0.08]	[+8.53]
cc-pV5Z	+21.75	−14.08	+2.21	−1.38	[+0.06]	[−0.08]	[+8.48]
CBS LIMIT	[+21.76]	[−14.18]	[+2.25]	[−1.40]	[+0.06]	[−0.08]	**[+8.40]**

ΔE_a(final) = ΔE_a[CBS CCSDT(Q)] + Δ_{core}[CCSD/cc-pCVQZ] + Δ_{ZPVE}[CCSD(T)/cc-pCVQZ] + Δ_{DBOC}[HF/cc-pVTZ] + Δ_{rel}[CCSD/cc-pCVTZ]

ΔE_a(final) = 8.40 − 0.01 + 0.83 + 0.19 + 0.24 = **9.65 kcal mol^{-1}**

[a] Energies shown in kcal mol^{-1}. Delta (δ) denotes the change in relative energy (ΔE_e) with respect to the preceding level of theory.

Table 6.3: Valence Focal Point Analysis of the Classical Exothermicity for $C_2H_3 + H_2 \rightarrow C_2H_4 + H$ [a]

basis set	ΔE_eHF	$+\delta$MP2	$+\delta$CCSD	$+\delta$CCSD(T)	$+\delta$CCSDT	$+\delta$CCSDT(Q)	NET
cc-pVDZ	−12.92	−1.88	+5.44	−0.40	+0.15	−0.02	[−9.62]
cc-pVTZ	−11.79	−1.63	+5.52	−0.60	+0.19	−0.00	[−8.31]
cc-pVQZ	−11.70	−1.63	+5.47	−0.63	[+0.19]	[−0.00]	[−8.30]
cc-pV5Z	−11.70	−1.59	+5.44	−0.64	[+0.19]	[−0.00]	[−8.31]
CBS LIMIT	[−11.71]	[−1.56]	[+5.40]	[−0.64]	[+0.19]	[−0.00]	**[-8.32]**

$\Delta E_0(\text{final}) = \Delta E_0[\text{CBS CCSDT(Q)}] + \Delta_{\text{core}}[\text{CCSD/cc-pCVQZ}] + \Delta_{\text{ZPVE}}[\text{CCSD(T)/cc-pCVQZ}]$
$+\Delta_{\text{DBOC}}[\text{HF/cc-pVTZ}] + \Delta_{\text{rel}}[\text{CCSD/cc-pCVTZ}]$

$\Delta E_0(\text{final}) = -8.32 - 0.15 + 2.72 - 0.15 + 0.26 =$ **-5.65 kcal mol^{-1}**

[a] Energies shown in kcal mol^{-1}. Delta (δ) denotes the change in relative energy (ΔE_e) with respect to the preceding level of theory.

6.5 Summary

We have examined the reaction $C_2H_3 + H_2 \rightarrow C_2H_4 + H$, an intermediary process that occurs during combustion and in planetary atmospheres. Through focal-point analysis we have obtained molecular energies for this hydrogen abstraction step that are extrapolated to the complete basis-set limit. Additionally we have included several corrections to this energy. Namely, a core-correction to account for "freezing" of the core-electrons in computing the single-point energy, a correction for the zero-point vibrational energy, a relativistic correction, and a correction for the Born-Oppenheimer approximation. Our geometries, obtained at the rigorous CCSD(T)/cc-pCVQZ level, agree reasonably well with prior theoretical work, and our computed vibrational modes for vinyl radical and ethylene generally align with previous experimental and theoretical studies. We report a barrier height of 9.65 kcal mol^{-1} and overall reaction enthalpy of -5.65 kcal mol^{-1} with a suggested accuracy of 0.1 kcal mol^{-1}.

6.6 Acknowledgments

This work was supported by the Department of Energy, Office of Basic Energy Sciences (Grant No. DEFG02-97-ER14748). This research used resources of the National Energy Research Scientific Computing Center (NERSC), which is supported by the Office of Science of the U.S. Department of Energy under Contract No. DE-AC02-05CH11231.

A. Complete Citation for MOLPRO

MOLPRO, version 2006.1, a package of ab initio programs written by H.-J. Werner; P. J. Knowles; R. Lindh; F. R. Manby; M. Schütz; P. Celani; T. Korona; G. Rauhut; R. D. Amos; A. Bernhardsson; A. Berning; D. L. Cooper; M. J. O. Deegan; A. J. Dobbyn; F. Eckert; C. Hampel; G. Hetzer; A. W. Lloyd; S. J. McNicholas; W. Meyer; M. E. Mura; A. Nicklass; P. Palmieri; R. Pitzer; U. Schumann; H. Stoll; A. J. Stone; R. Tarroni and T. Thorsteinsson. See http://www.molpro.net Cardiff, UK, 2006

B. Data for Computed Stationary Points

1. C_2H_3

Atom	X	Y	Z	Atom	X	Y	Z
C	-0.62123814	-0.02540339	0.0	C	0.685260840	0.07583787	0.0
H	-1.26458237	0.84573603	0.0	H	-1.11264680	-0.99658038	0.0
H	1.52921648	-0.59336013	0.0				

2. H_2

Atom	X	Y	Z	Atom	X	Y	Z
H	0.0	0.0	0.37096091	H	0.0	0.0	-0.37096091

3. TS 1

Atom	X	Y	Z	Atom	X	Y	Z
H	-1.25015583	0.0	0.98575444	H	0.81121020	0.0	1.50813847
H	-0.59062640	0.0	-1.53402026	H	1.17034433	0.0	-0.97842070
H	1.50538411	0.0	2.02368323	C	-0.26473042	0.0	0.54511599
C	0.12587314	0.0	-0.71392429				

4. C_2H_4

Atom	X	Y	Z	Atom	X	Y	Z
C	0.0	0.0	-0.66561045	C	0.0	0.0	0.66561045
H	0.0	0.92211762	-1.22955219	H	0.0	-0.92211762	-1.22955219
H	0.0	0.92211762	1.22955219	H	0.0	-0.92211762	1.22955219

5. H

Atom	X	Y	Z
H	0.0	0.0	0.0

Chapter 7

Fundamental Vibrational Frequencies and Spectroscopic Constants for the Methylperoxyl Radical, CH_3O_2 and Related Isotopologues $^{13}CH_3OO$, $CH_3{}^{18}O{}^{18}O$, and CD_3OO [1]

[1] J. Agarwal, A. C. Simmonett, and H. F. Schaefer *Mol. Phys.*, **2012**, 110, 2419-2427. Reproduced by permission of Taylor and Francis.

7.1 Abstract

Accurate spectroscopic and geometric constants for CH_3O_2, and its isotopologues $^{13}CH_3OO$, $CH_3{}^{18}O^{18}O$ and CD_3OO, are predicted. Employing coupled cluster theory with single, double, and perturbative triple excitations [CCSD(T)], we obtain optimized equilibrium geometries using Dunning's cc-pVTZ basis set. A Taylor expansion of the potential energy surface, including all third-order and semidiagonal fourth-order terms in a basis of normal coordinates, yields anharmonic vibrational frequencies and vibrationally-averaged properties including the effects of anharmonicity. We detail the strong influence of Fermi resonances on the problematic ν_6 vibrational mode of CD_3OO, arriving at a value of 993 cm^{-1}; two previous experimental measurements of this mode appear to have been incorrectly assigned. Our computed energies for the low intensity ν_{11} transition are in excellent agreement with experimental measurements performed for $CH_3{}^{18}O^{18}O$ and CD_3OO, inspiring confidence that our results will serve as a guide for experimental measurement of this yet-unobserved quantity for the CH_3OO and $^{13}CH_3OO$ isotopologues. Given the reliability of our force field, and considering the results of other experiments, we make a number of reassignments to previously recorded spectra, which eliminate large disagreements between experimental observations. The vibrational averaging of the rotational constants and geometries are also discussed for each isotopologue.

7.2 Introduction

The continued interest in alkyl peroxyl radicals (RO_2) stems from their importance in atmospheric and combustion chemistries, where they are intermediates in the formation of ozone and agents for low-temperature autoignition, respectively.[197–200] In both instances alkyl peroxyl radicals result from the oxidation of hydrocarbons, which subsequently react with molecular oxygen, O_2.[201–204] Once produced, alkyl peroxyl radicals are involved in the

oxidation of NO to produce NO_2, a precursor to ozone.[205] From an environmental standpoint this is an important process, especially in the troposphere where volatile organic compounds (VOCs) are present from the incomplete combustion of fossil fuels. There, the formation of alkyl peroxyl radicals, and subsequently the production of ozone, contributes to ground-level smog.[205]

Our interest is in the simplest alkyl peroxyl radical, methyl peroxyl radical (CH_3O_2). This species has been investigated in the laboratory by both infrared[206–211] and ultraviolet spectroscopy,[212–221] with the latter observations being more prevalent in the literature. In experiments CH_3O_2 is commonly produced using a precursor to form methyl radical, which subsequently reacts with O_2. This process is similar to the termolecular reaction ($CH_3 + O_2 + M \rightarrow CH_3O_2 + M$) that occurs in the atmosphere. Methyl radical precursors include methyl iodide, azomethane, and acetone. CH_3O_2 may also be formed in the absence of O_2 using hydroperoxides and an oxidizing agent.[222,223]

Much experimental work has also been devoted to understanding the kinetic rates involved in the reactions of CH_3O_2 with O_2, NO, NO_2, HO_2, OH and other peroxyl radicals, since these species are relevant to the production of ozone.[158,217,219,222,224] The experiments required to probe fleeting species are usually highly sophisticated, and the reactive nature of radicals can yield spectra that contain precursor and byproduct signals. Therefore, accurate theoretical data can be of great utility in disentangling such spectra. Motivated by this, several groups have studied methyl peroxyl radical computationally and reported thermochemical, photophysical, and vibrational data.[206,225–230] However, no rigorous theoretical analyses of the spectroscopic constants of CH_3O_2, or isotopologues thereof, have ever been reported.

In the current research, we produce the first detailed survey of spectroscopic data of the isotopologues of CH_3O_2. We have employed state-of-the-art theoretical methodology, paying particular attention to the anharmonic vibrational frequencies. Herein, computed frequencies

are discussed for each isotoplogue, then related to experimentally observed modes. The vibrational contributions to rotational constants and geometric structures are also discussed.

7.3 Theoretical Methods

To obtain reliable vibrational frequencies and geometric parameters, we performed geometry optimizations using coupled cluster theory with single, double and perturbative triple excitations [CCSD(T)][168–173] using Dunning's correlation consistent cc-pVTZ basis set.[176] Because minimal spin contamination was encountered in the reference function ($\langle \hat{S}^2 \rangle = 0.76$), unrestricted Hartree-Fock based methods were used throughout, which permitted the use of analytic second derivatives[231,232] in the vibrational frequency computations. It has been shown that coupled cluster theory with only single and double excitations included can often overcome spin contamination in the reference wavefunction.[233,234]

In keeping with the design of the cc-pVTZ basis set, and for computational efficiency, the lowest energy 1s-like orbitals on the carbon and oxygen atoms were neglected from the computations. To gauge the error introduced by this "frozen core" approximation, we performed an all-electron CCSD(T) harmonic vibrational frequency computation using the cc-pCVTZ basis set.[235] Inclusion of the core correlation effects in these computations changed the vibrational frequencies by 4 cm^{-1} on average, compared to those computed with "frozen core" cc-pVTZ CCSD(T).

To account for anharmonicity in the potential energy surface, second-order vibrational perturbation theory (VPT2) analyses[236] were performed for multiple isotopologues of CH_3OO. The requisite cubic and semidiagonal quartic force fields, in the normal coordinate representation, were obtained by numerical differentiation of analytic second derivatives of the energy with respect to nuclear displacements. The reliability of VPT2 analyses can be diminished in the presence of strong resonances; these were not generally encountered but extra treatments, described in the following section, were required to compute the vibrational frequen-

cies for CD_3OO. The equilibrium rotational constants, $\{A_e, B_e, C_e\}$, were corrected for both zero-point vibrational effects and centrifugal distortion effects, corresponding to Watson's A-reduction Hamiltonian in the I^r representation,[237] yielding our final $\{A^{(A)}, B^{(A)}, C^{(A)}\}$ values. To explore the effect of zero-point vibrations on the geometric parameters, we computed r_g structures for all of the isotopologues considered,[238,239] which would be comparable with experimental geometry determinations at 0K. All computations utilized the CFOUR[185] suite of electronic structure codes.

7.4 Results and Discussion

A. Structures

The equilibrium structure of ground-state ($\tilde{X}\ ^2A''$) CH_3O_2, computed at the cc-pVTZ CCSD(T) level of theory, is shown in Figure 7.4. Additionally, Table 7.1 reports the geometric parameters with zero-point corrections for each isotopologue; five significant figures are provided for comparison purposes, but careful calibration[175] shows that the method used provides errors in bond lengths on the order of 0.001 Å. We note that throughout this work we use C and O to describe the most abundant isotopes (^{12}C and ^{16}O).

The near equivalence of the H_a and $H_{b,c}$ bonds indicates minimal electronic interaction between the oxygen and methyl termini. The O-O bond length (1.324 Å) is roughly halfway between the O-O single bond length in hydrogen peroxide (1.475 Å) and the O-O double bond distance in molecular oxygen (1.208 Å), though closer to the latter. Natural Bond Order (NBO) analysis[186] of the O-O bond using Natural Resonance Theory yields a bond order of 1.49.

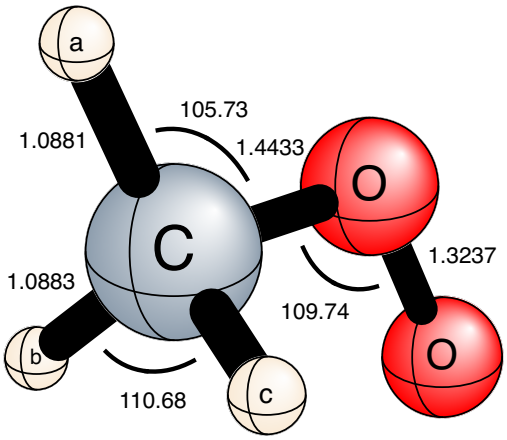

Figure 7.1: Equilibrium geometry (Ångströms and degrees), possessing C_s symmetry, computed at the cc-pVTZ CCSD(T) level of theory. See Table 7.1 for vibrationally-averaged geometry parameters.

Table 7.1: Structural parameters (Ångström and degrees) for selected isotopologs of CH_3O_2. The hydrogen atoms are labeled according to Figure 7.4

		Zero-point corrected[a]			
Parameter	r_e	CH_3OO	$^{13}CH_3OO$	$CH_3{}^{18}O^{18}O$	CD_3OO
$r(H_a\text{-}C)$	1.0880	1.1096	1.1095	1.1096	1.1038
$r(H_{b,c}\text{-}C)$	1.0883	1.1097	1.1097	1.1097	1.1040
r(C-O)	1.4432	1.4546	1.4544	1.4544	1.4540
r(O-O)	1.3237	1.3296	1.3297	1.3293	1.3297
$\angle H_a\text{-}C\text{-}O$	105.72	105.44	105.45	105.44	105.46
$\angle$C-O-O	109.73	109.91	109.91	109.92	109.84
$\angle H_{b,c}\text{-}C\text{-}O$	109.12	108.72	108.73	108.72	108.76

[a] The r_g structure. See references[238,239] for additional information.

The $\angle H_a$-C-O bond angle (105.7°) is distorted from tetrahedral geometry, similar to the related bond angle in methanol.[240] The ∠C-O-O bond angle is approximately 109.7°, larger than the ∠H-O-O bond angle in the hydroperoxyl radical, which is in agreement with previous work.[225,227] Overall, we note good agreement between our structure and those obtained in prior computational studies.[225–229] In fact, the geometric parameters the from the first *ab initio* studies[227] of CH_3O_2 – performed in 1982 using general valence bond (GVB) and configuration interaction (CI) theories – are within 0.01 Å and 0.5° of ours. This highlights the relative insensitivity of the CH_3O_2 structure to choice of the methodology used and suggests confidence in our force field, which was computed with an approach that is commonly termed the "gold standard" of quantum chemistry.

The zero-point corrections manifest themselves mostly in changes in the bond lengths, with angles changing by 0.4° or less for all isotopologues, relative to the equilibrium geometry. Inspection of Table 7.1 reveals that the vibrationally-averaged structure possesses longer bond lengths than the equilibrium structure. The C-H bonds are most strongly affected since they are associated with vibrations involving the highest degree of anharmonicity (*vide infra*).

B. Vibrational Frequencies

The methyl peroxyl radical has twelve normal vibrational modes – eight symmetric and four anti-symmetric – which are described in Table 7.2. The isotopologues investigated have C_s symmetry, rendering all vibrational modes infrared (IR) active. Several groups have performed IR experiments on CH_3O_2, beginning with Ase, Bock and Snelson (ABS, 1986) who examined the parent molecule and nine isotopologues in argon matrices using methyl iodide and azomethane precursors.[209] In later work Nandi and co-workers re-examined the parent and three isotopologues in argon matrices with the same precursors, but reassigned the ν_6 and ν_7 nodes observed by ABS by interchanging them.[207] For the parent molecule, only two studies have reported frequencies in the gas-phase, and in each case the entire

Table 7.2: Descriptions and symmetries for the vibrational modes of CH_3OO

Mode	Description	Symmetry	Mode	Description	Symmetry
ν_1	CH_3 Symmetric Stretch	a'	ν_7	C-OO Stretch	a'
ν_2	CH_3 Symmetric Stretch	a'	ν_8	C-O-O Bend	a'
ν_3	CH_3 Deformation	a'	ν_9	CH_3 Asymmetric Stretch	a''
ν_4	CH_3 Umbrella	a'	ν_{10}	CH_3 Asymmetric Deformation	a''
ν_5	CH_3 Rock + OO Stretch	a'	ν_{11}	CH_2 Wag	a''
ν_6	CH_3 Rock - OO Stretch	a'	ν_{12}	CH_3 Torsion	a''

spectrum has not been completely observed. Blanksby and co-workers reported gas-phase values for the ν_6 and ν_8 modes of CH_3OO and CD_3OO in 2001,[210] and Huang and co-workers reported estimated gas-phase values for eight of the twelve vibrational modes in 2007 using simulated spectra and values from a step-scan Fourier-transform spectrometer.[208]

Our theoretical harmonic and anharmonic frequencies for the parent molecule and three isotopologues are listed in Tables 7.3-7.6, alongside the corresponding experimental values. Overall, the harmonic values are shifted lower by 3.4% on average after anharmonic corrections. In each table, values from ABS are listed as reported,[209] but an additional column is included for our reassignments. The reassigned transitions are the interchange of ν_6 and ν_7, recognized by Nandi and co-workers; the interchange of ν_4 and ν_{10}, determined here; and the reassignment of ν_9 to ν_2, also determined from the present work. Importantly our additional reassignments eliminate the large discrepancy between the results of ABS and Nandi and co-workers; they report the only experimental work for $^{13}CH_3OO$ and $CH_3{}^{18}O{}^{18}O$, for instance. In general our values cannot be directly compared to results obtained via matrix isolation in all cases. While the perturbation of fundamental frequencies due to the presence of the inert matrix is typically small (about 0.2-0.7 % for argon), perturbations exceeding 2% are not unprecedented.[241,242]

CH_3OO

Vibrational frequencies for the parent molecule are listed in Table 7.3 with four sets of experimental values. To our knowledge, no other group has reported anharmonic frequencies for this species, and only eight of the twelve modes have been observed in the gas-phase experimentally. Nandi and co-workers present the most complete set of frequencies observed in an argon matrix, but they were unable to observe ν_{11} and ν_{12} due to low intensity and limits of the detector, respectively. On average our values deviate by 8 cm^{-1} from their reported values, noting perturbations due to the argon matrix.

Our suggested anharmonic frequencies also agree well with reported gas-phase values. Compared to frequencies reported by Blanksby and co-workers,[210] which were obtained using negative-ion photoelectron spectroscopy, our values deviate by 4 cm^{-1} and 11 cm^{-1} for the ν_6 and ν_8 modes, respectively. And, for the estimated gas-phase values reported by Huang and co-workers,[208] our values differ on average by 6 cm^{-1}, with a maximum difference of 11 cm^{-1} for modes ν_1 and ν_6.

With regard to the values reported by ABS,[209] several discrepancies are clear upon inspection of Table 7.3. Nandi and co-workers recognized the incorrect assignment of ν_6 and ν_7, which deviate from other reported values by hundreds of wavenumbers. Moreover, we surmise that two of the three modes around 1400 cm^{-1}, namely ν_4 and ν_{10}, are also incorrectly assigned. We find ABS's ν_4 is roughly 23 cm^{-1} larger than our computed value and ν_{10} is roughly 26 cm^{-1} lower. Based on this comparison, we suggest that they should be interchanged, resulting in differences of just 3 cm^{-1} and 0 cm^{-1}, respectively. Finally, the ν_9 mode is curious. The value reported by ABS shows a discrepancy of (-43, -56, -52) cm^{-1} when compared to our findings, those of Nandi and co-workers, and those of Huang and co-workers, respectively. This level of discrepancy leads us to reassign the value to ν_2, whereupon the disagreement with our findings is reduced to 12 cm^{-1}. A summary of these

Table 7.3: Harmonic and anharmonic vibrational frequencies (in cm^{-1}) for CH_3OO with IR intensities (in km mol^{-1}, listed parenthetically)

Mode	This work[a]		Experiment				
	Harmonic	Anharmonic	Ref. 209[b]	Ref. 209[c]	Ref. 210[d]	Ref. 207[b]	Ref. 208[d]
ν_1	3168 (9.0)	3022 (7.7)				3032	3033±1 (100)
ν_2	3061 (16.8)	2956 (17.4)		2968		2954	2954±1 (250)
ν_3	1497 (8.2)	1456 (5.9)	1453	1453		1448 (71)	1453±2 (100)
ν_4	1449 (1.4)	1417 (2.8)	1440	1414		1410 (8)	1408±1 (54)
ν_5	1212 (10.5)	1181 (9.2)	1183	1183		1180 (37)	1183±1 (68)
ν_6	1160 (9.5)	1128 (9.4)	902	1112	1124±5	1109 (25)	1117±2 (74)
ν_7	949 (14.7)	917 (13.8)	1112	902		902 (78)	
ν_8	493 (6.2)	493 (6.3)	492	492	482±9	492 (30)	
ν_9	3159 (13.1)	3011 (12.6)	2968			3024	3020±2 (70)
ν_{10}	1484 (7.5)	1440 (6.3)	1414	1440		1434 (100)	1441±1 (68)
ν_{11}	1144 (1.1)	1118 (1.1)					
ν_{12}	149 (0.2)	131 (0.1)					

[a]Harmonic and anharmonic (VPT2) vibrational frequencies computed at the cc-pVTZ CCSD(T) level of theory. [b]Observed in Ar matrix. [c]Ordering reassigned, based on our values and other experiments. [d]Observed in the gas-phase.

reassignments is reported in column 4 of Table 7.3. This modification is somewhat complicated by the fact that all modes are IR active, so we cannot discern the activity of each mode solely based on symmetry. Our reassignments lead to a mean absolute deviation of just 7 cm^{-1} between our anharmonic frequencies and the ABS values; the same quantity was 65 cm^{-1} before the reassignment.

$^{13}CH_3OO$

Vibrational frequencies for $^{13}CH_3OO$ are reported in Table 7.4 with two sets of experimental values. We find that ^{13}C isotopic substitution has the most profound effect on the C-OO stretching mode ν_7, reducing its magnitude by 1.6%, with respect to the parent molecule. The mode corresponding to torsional rotation, ν_{12}, is the only mode not shifted after substitution. For reference, isotopic shifts for all modes are shown in Table 7.7.

As before, we reassign Ase and coworkers' values in column 4 of Table 7.4. In addition

Table 7.4: Harmonic and anharmonic vibrational frequencies (in cm^{-1}) for $^{13}CH_3OO$ with IR intensities (in km mol^{-1}, listed parenthetically)

Mode	This work[a]		Experiment		
	Harmonic	Anharmonic	Ref. 209[b]	Ref. 209[c]	Ref. 207[d]
ν_1	3147 (12.6)	3001 (12.2)			3021
ν_2	3059 (16.3)	2951 (17.1)		2960	2948 (31)
ν_3	1495 (8.4)	1454 (6.2)	1451	1451	1447 (59)
ν_4	1442 (1.2)	1409 (2.5)	1438	1407	1404 (19)
ν_5	1204 (11.4)	1174 (9.2)	1175	1175	1173 (37)
ν_6	1155 (7.8)	1123 (8.3)	888	1110	1104 (23)
ν_7	933 (14.0)	902 (13.1)	1110	888	887 (64)
ν_8	489 (6.2)	489 (6.3)	487	487	487 (32)
ν_9	3156 (8.7)	3012 (7.9)	2960		3014
ν_{10}	1481 (7.6)	1438 (6.4)	1407	1438	1432 (100)
ν_{11}	1136 (0.9)	1111 (0.9)			
ν_{12}	149 (0.1)	131 (0.1)			

[a]Harmonic and anharmonic (VPT2) vibrational frequencies computed at the cc-pVTZ CCSD(T) level of theory. [b]Observed in Ar matrix. [c]Ordering reassigned, based on our values and other experiments.

to the transition frequencies, the ABS study presents the various spectra recorded for this isotopologue. The ratio of the intensities for the transitions at 1407 and 1438 cm^{-1} is about 1:3 from ABS's spectra, which correlates well with our reassignment; our computations place that ratio at 1:2.6. Similarly, the ratio of intensities for the transitions at 888 and 1110 cm^{-1} from the spectra reported by ABS is about 1.4:1, which is in agreement with our computed value of 1.6:1. Our values differ from those reported by Nandi and co-workers by 8 cm^{-1}, on average.

To our knowledge, we report the first complete set of anharmonic frequencies for $^{13}CH_3OO$, and the only reported values for ν_{11} (1111 cm^{-1}) and ν_{12} (131 cm^{-1}), which we predict to be relatively low intensity modes. We note that the large degree of anharmonicity in the latter, however, could render the VPT2 analysis suspect.

$CH_3{}^{18}O{}^{18}O$

Vibrational frequencies for $CH_3{}^{18}O{}^{18}O$ are listed in Table 7.5, again with two sets of experimental values from ABS and Nandi and co-workers. For this species, isotopic substitution with ^{18}O in the O_2 moiety affects ν_5 - ν_8 most, as expected. Of this set of four modes ν_6 has the largest shift (4.8%) with respect to the parent molecule, while the remaining modes exhibit shifts of 1.3-3.4%. Surprisingly the torsional mode, ν_{12}, is also shifted by substitution (1.5%), but the remaining modes are unaffected.

Once again, we reassigned the ABS frequencies. The ABS ratio of intensities for the transitions at 880 and 1056 cm^{-1} is about 1.3:1, which matches our computed ratio of 1.3:1. The ordering of both the energies and the intensities justifies our interchange of ν_6 and ν_7 from the ABS study. The ABS transition at 2098 cm^{-1} deviates from our computed value by just 10 cm^{-1} when ascribed to ν_2 instead of ν_9, where the discrepancy is a sizable 43 cm^{-1}.

The mean absolute deviation between our values and those of Nandi and co-workers is 8 cm^{-1}. As mentioned previously, we urge caution about the reliability of our value for ν_{12} due to its highly anharmonic nature and the VPT2 perturbation theory treatment applied.

CD_3OO

Vibrational frequencies for CD_3OO are reported in Table 7.6, alongside three sets of experimental values. Since deuterium substitution results in a significant relative mass change, most vibrational frequencies differ considerably (>20%), with respect to CH_3OO. The modes least affected are those largely impacted by O_2 vibrations, ν_5 - ν_8; these are the modes most affected by $^{18}O_2$ substitution, as identified in the previous section. As with previous species, our suggested anharmonic frequencies generally agree well with reported experimental values, with the exception of ν_2 and ν_6, which differ considerably. Both of these modes are perturbed by Fermi resonances, whose treatment is detailed below. Furthermore, our com-

Table 7.5: Harmonic and anharmonic vibrational frequencies (in cm^{-1}) for $CH_3{}^{18}O{}^{18}O$ with IR intensities (in km mol^{-1}, listed parenthetically)

Mode	This work[a]		Experiment		
	Harmonic	Anharmonic	Ref. 209[b]	Ref. 209[c]	Ref. 207[b]
ν_1	3168 (9.0)	3022 (7.6)			3033
ν_2	3061 (16.8)	2956 (17.3)		2968	2953
ν_3	1497 (7.9)	1455 (5.6)	1450	1450	1448 (85)
ν_4	1447 (1.7)	1413 (3.1)	1438	1412	1408 (10)
ν_5	1196 (5.9)	1166 (6.1)	1169	1169	1165 (39)
ν_6	1102 (12.7)	1073 (10.7)	880	1056	1055 (51)
ν_7	925 (14.1)	895 (13.5)	1056	880	880 (109)
ν_8	476 (5.7)	476 (5.8)	476	476	477 (35)
ν_9	3159 (13.0)	3011 (12.4)	2968		3022
ν_{10}	1483 (7.4)	1440 (6.2)	1412	1438	1434 (100)
ν_{11}	1141 (1.0)	1115 (1.0)	1115	1115	
ν_{12}	147 (0.1)	129 (0.1)			

[a]Harmonic and anharmonic (VPT2) vibrational frequencies computed at the cc-pVTZ CCSD(T) level of theory. [b]Observed in Ar matrix. [c]Ordering reassigned, based on our values and other experiments.

putations yield a relatively low IR intensity for ν_6 which makes spectroscopic identification difficult.

For this isotopologue, the ratio of the ABS intensities for the 1048 cm^{-1} and 1078 cm^{-1} modes is 1:1.2, which agrees qualitatively with our value of 1:5. Without reassignment the difference between the ABS results and ours are (29, -38) for (ν_4, ν_{10}), but these differences drop to just (-6, -1) cm^{-1} upon interchange of these two modes.

As noted previously, our VPT2 analyses were generally free from problematic resonances. However, the ν_6 vibrational mode of CD_3OO suffers from a Fermi type II resonance ($\omega_{11} + \omega_{12} \approx \omega_6$). As is standard practice, we exclude the terms with small denominators from the summations in the VPT2 analysis, and estimate the energetic effect of neglecting such terms via the first-order couplings:[243]

$$\begin{pmatrix} \omega_{11} + \omega_{12} & \frac{\phi_{6-11-12}}{\sqrt{8}} \\ \frac{\phi_{6-11-12}}{\sqrt{8}} & \omega_6 \end{pmatrix} \tag{7.1}$$

Our final ν_6 value is obtained by appending a correction term to the deperturbed ν_6 from the partial VPT2 analysis. This correction is computed by differencing the desired eigenvalue of (7.1) above, whose eigenvector has the maximal ω_6 content, and ω_6. The resulting value of 993 cm^{-1}, coupled with Nandi and co-workers' value of 941 cm^{-1} leads us to also question Blanksby and co-workers' assignment of this mode at 1123 cm^{-1}.

Similarly, the ν_2 vibrational mode of CD_3OO suffers from a Fermi type II resonance ($\omega_4 + \omega_5 \approx \omega_2$), in addition to two Fermi type I resonances ($2\omega_4 \approx \omega_2$ and $2\omega_5 \approx \omega_2$). In this case the type II resonance is not strong, evidenced by the small magnitude of the coupling constant ($\phi_{2-4-5} = -12.9$ cm^{-1}). The type I resonances are both strong ($\phi_{4-4-2} = -157.7$ cm^{-1} and $\phi_{5-5-2} = -84.9$ cm^{-1}), so we use a procedure analogous to that described above to account for them:

$$\begin{pmatrix} 2\omega_4 & \frac{\phi_{4-4-2}}{4} & 0 \\ \frac{\phi_{4-4-2}}{4} & \omega_2 & \frac{\phi_{5-5-2}}{4} \\ 0 & \frac{\phi_{5-5-2}}{4} & 2\omega_5 \end{pmatrix} \tag{7.2}$$

The two type I resonances reduce the deperturbed ν_2 by 10.1 cm^{-1}, resulting in a final estimated value of 2122 cm^{-1}.

The force constant that couples the $\omega_{11} + \omega_{12}$ combination band with the ω_6 fundamental, $\phi_{6-11-12}$ has a magnitude of 35.3 cm^{-1}, which might be considered too small to cause a resonance according to commonly employed criteria. However, the sizable perturbation found in our study reaffirms the notion[244] that both the energetic separation of the resonating terms and the magnitude of the coupling should be taken into consideration simultaneously.

To our knowledge, our data represent the first complete set of anharmonic frequencies for CD_3OO and suggest new frequencies for the ν_2 (2102 cm^{-1}), ν_6 (993 cm^{-1}), and ν_{12} (107 cm^{-1}) modes. The latter, ν_{12}, may be difficult to directly detect experimentally, given the low intensity predicted, and its highly anharmonic nature is problematic for theoretical treatments too.

Table 7.6: Harmonic and anharmonic vibrational frequencies (in cm^{-1}) for CD_3OO with IR intensities (in km mol^{-1} listed parenthetically).

Mode	This work[a]		Experiment			
	Harmonic	Anharmonic	Ref. 209[b]	Ref. 209[c]	Ref. 210[d]	Ref. 207[b]
ν_1	2353 (6.9)	2272 (6.3)				2280 (42)
ν_2	2190 (11.7)	2122 (11.2)		2176		2172 (76)
ν_3	1183 (12.9)	1158 (11.0)		1146		1144 (119)
ν_4	1116 (11.3)	1086 (10.4)	1048	1078		1076 (124)
ν_5	1078 (0.9)	1056 (0.8)				1050 (24)
ν_6	1007 (5.5)	993 (0.2)	821		1123±7	941 (31)
ν_7	849 (8.9)	829 (8.6)	1146	821		822 (190)
ν_8	448 (4.4)	446 (4.4)	445	445	440±7	446 (30)
ν_9	2346 (9.2)	2265 (8.9)	2176			2273 (163)
ν_{10}	1072 (2.6)	1049 (2.3)	1078	1048		1046 (100)
ν_{11}	879 (2.2)	863 (2.0)	860	860		880 (32)
ν_{12}	117 (0.0)	107 (0.0)				

[a]Harmonic and anharmonic (VPT2) vibrational frequencies computed at the cc-pVTZ CCSD(T) level of theory. [b]Observed in Ar matrix. [c]Ordering reassigned, based on our values and other experiments. [d]Observed in the gas-phase.

Table 7.7: Isotopic shifts (in cm^{-1}) with respect to parent molecule

Mode	$^{13}CH_3OO$	$CH_3{}^{18}O^{18}O$	CD_3OO
ν_1	-21	0	-750
ν_2	-5	0	-834
ν_3	-2	-1	-298
ν_4	-8	-4	-331
ν_5	-7	-15	-125
ν_6	-5	-55	-129
ν_7	-15	-22	-88
ν_8	-4	-17	-47
ν_9	1	0	-746
ν_{10}	-2	0	-391
ν_{11}	-7	-3	-255
ν_{12}	0	-2	-24

Table 7.8: Rotational constants (MHz) from the equilibrium geometry, and with vibrational zero-point corrections (MHz).

Parameter	CH_3OO	$^{13}CH_3OO$	$CH_3{}^{18}O{}^{18}O$	CD_3OO
A_e	51437	51156	47956	38579
B_e	11469	11131	10894	9695
C_e	9976	9709	9411	8599
$A^{(A)}$	51386	51110	47929	38446
$B^{(A)}$	11322	10989	10759	9582
$C^{(A)}$	9861	9598	9307	8515

C. Rotational Constants

Rotational constants for the species under study, with and without corrections for centrifugal distortion and zero-point vibrational effects, are shown in Table 7.8. The zero-point corrections are obtained from the vibration-rotation interaction constants α_r^x, which describe coupling of rotations about the principal axis x and the vibrational normal mode r, by retaining only the leading term in the expansion:

$$B_0 \approx B_e - \frac{1}{2}\sum_r \alpha_r^B + \ldots \tag{7.3}$$

These corrections are the largest for the equilibrium rotational constants, changing $\{A_e, B_e, C_e\}$ by $\{51, 147, 115\}$ MHz, respectively, for the parent isotopologue. The remaining corrections, due to centrifugal distortion, contribute just $\{-0.1, 0.2, -0.1\}$ MHz. The corrected rotational constants are lower than their equilibrium counterparts by $\{0.1, 1.2, 1.2\}\%$, which is consistent with the bond elongation observed in the vibrationally averaged structure, relative to the equilibrium structure. Similar trends are observed for the other isotopologues, although the corrections to A_e for CD_3OO are a more sizable -0.3% due to the heavier deuterium atoms distributed about the A principal axis.

7.5 Summary

As the simplest peroxyl radical, CH_3O_2 is a prototypical species for study in both atmospheric and combustion chemistry. In the present research we have focused on the infrared signature of this species and three related isotopologues using reliable computational methods. Namely, we have examined CH_3OO, $^{13}CH_3OO$, $CH_3{}^{18}O{}^{18}O$, and CD_3OO using vibrational perturbation theory, VPT2, to obtain anharmonic vibrational frequencies, zero-point corrected rotational constants, and zero-point corrected structural parameters. We find good agreement between our computed frequencies and the most recent experimental values. However, we have reassigned several values from original work by Ase and co-workers, including the ν_4, ν_9, and ν_{10} modes (previously the ν_6 and ν_7 modes had been reassigned by Nandi and co-workers) on the basis of inspection of the original spectra and comparison to computed values and intensities. These reassignments eliminate the large discrepancies between experimental studies, especially for $^{13}CH_3OO$ and $CH_3{}^{18}O{}^{18}O$. We also suggest a value for the ν_6 mode for CD_3OO, which appears to have been incorrectly assigned by two previous groups. Overall, we predict the first complete set of anharmonic frequencies for the parent species and three isotopologues, in addition to spectroscopic constants. It is hoped that this research will guide further characterization of this important molecule.

7.6 Acknowledgments

This work was supported by the Department of Energy , Office of Basic Sciences (Grant No. DEFG02-97-ER14748). J. A. thanks D. S. Hollman for helpful discussions.

Chapter 8

Conclusions

Vinyl radical and methyl peroxy radical are key combustion intermediates, and prototypical species for fundamental investigations because they are small enough to be tractable with high-accuracy quantum-mechanical methods, yet large enough to exhibit some of the complexities found in larger, more relevant, molecules. For the hydrogen abstraction mechanism, $C_2H_3 + H_2 \rightarrow C_2H_4 + H$, presented in Chapter 6 a barrier of 9.65 kcal mol^{-1} and overall reaction enthalpy of -5.65 kcal mol^{-1} is suggested. The estimated accuracy of these values is within 0.1 kcal mol^{-1}. These results should eliminate discrepancies in the rate constant, which varies over several orders of magnitude in different studies due to small (on the order of 1-2 kcal mol^{-1}) changes in reaction energies.

For the methyl peroxy radical presented in Chapter 7, the first complete set of frequencies for the parent isotopologue and three related isotopologues is reported. Furthermore, several important modes were reassigned by comparing reported values to computed frequencies and intensities in addition to examination of the original spectra. As a result, large discrepancies between studies were eliminated. A new value for the ν_6 transition was suggested for the

deuterated isotopologue, CD_3OO. This mode was likely incorrectly assigned in previous work.

Importantly, the anharmonic frequencies for methyl peroxy radical were subsequently used to verify its presence in a helium nanodroplet.[138] This is a key result since the reaction of methyl radical and oxygen is barrierless and exothermic, and could have evaporated the helium nanodroplet that enclosed it. Interrogation with infrared light, yielding fundamental transitions that were compared directly with values from our investigation, confirmed the presence of methyl peroxy radical within the cold droplet. This is a great example of the interplay between theory and experiment, and an illustration of the important cooperation necessary for furthering fundamental combustion research.

Bibliography

[1] van Helmont, J. B. *Ortus Medicinae*; ca. 1650.

[2] Cavendish, H. *Philos. Trans. R. Soc. London* **1766**, *56*, 141–184.

[3] Priestly, J. *Philos. Trans. R. Soc. London* **1772**, *62*, 147–264.

[4] Lavoisier, A. L. *Opuscules Physiques et Chimiques*; Paris, 1774.

[5] Faraday, M. *Philos. Trans. R. Soc. London* **1823**, *113*, 189–198.

[6] Ashcroft, A. T.; Cheetam, A. K.; Green, M. L. H.; Vernon, P. D. F. *Nature* **1991**, *352*, 225–226.

[7] Jessop, P. G.; Ikariya, T.; Noyori, R. *Nature* **1994**, *368*, 231–233.

[8] Arakawa, H. *et al.*, *Chem. Rev.* **2001**, *101*, 953–996.

[9] Sakakura, T.; Choi, J. C.; Yasuda, H. *Chem. Rev.* **2007**, *107*, 2365–2387.

[10] Olah, G. A.; Goeppert, A.; Prakash, G. K. S. *J. Org. Chem.* **2009**, *74*, 487–498.

[11] Topham, S. *Carbon Dioxide. Ullmann's Encyclopedia of Industrial Chemistry.*; Wiley-VCH Verlag GmbH & Co. KGaA, 2000.

[12] Klironomos, J. N.; Allen, M. F.; Rillig, M. C.; Piotrowski, J.; Makvandi-Nejad, S.; Wolfe, B. E.; Powell, J. R. *Nature* **2005**, *433*, 621–624.

[13] Matthews, H. D.; Gillett, N. P.; Stott, P. A.; Zickfeld, K. *Nature* **2009**, *459*, 829–832.

[14] Melillo, J. M.; McGuire, A. D.; Kicklighter, D. W.; Moore, B.; Vorosmarty, C. J.; Schloss, A. L. *Nature* **1993**, *363*, 234–240.

[15] Schimel, D. S. *Glob. Change Biol.* **1995**, *1*, 77–91.

[16] Levin, S. A. *Ecology* **1992**, *73*, 1943–1967.

[17] Gurney, K. R. *et al.*, *Nature* **2002**, *415*, 626–630.

[18] Stauffer, B.; Blunier, T.; Dallenbach, A.; Indermuhle, A.; Schwander, J.; Stocker, T. F.; Tschumi, J.; Chappellaz, J.; Raynaud, D.; Hammer, C. U.; Clausen, H. B. *Nature* **1998**, *392*, 59–62.

[19] Langley, J. A.; Megonigal, J. P. *Nature* **2010**, *466*, 96–99.

[20] Khatiwala, S.; Primeau, F.; Hall, T. *Nature* **2009**, *462*, 346–349.

[21] Bates, N. R.; Pequignet, A. C.; Johnson, R. J.; Gruber, N. *Nature* **2002**, *420*, 489–493.

[22] Retallack, G. J. *Nature* **2001**, *411*, 287–290.

[23] Meinshausen, M.; Meinshausen, N.; Hare, W.; Raper, S. C. B.; Frieler, K.; Knutti, R.; Frame, D. J.; Allen, M. R. *Nature* **2009**, *458*, 1158–1162.

[24] Horvath, H. *Atmos. Environ.* **1993**, *27A*, 293–317.

[25] Balkan, S.; Hintzpeter, H. *Atmospheric Radiation. Landolt-Börnstein's Numerical Data and Functional Relationships in Science and Technology, Vol. 4, Meteorology, Subvol. b, Physical and Chemical Properties of the Air*; Springer, Berlin, 1988.

[26] Members, P. P. *Nature* **2012**, *491*, 683–691.

[27] Song, C. *Catalysis Today* **2006**, *115*, 2–32.

[28] Leitner, W. *Angew. Chem. Int. Edit.* **1995**, *34*, 2207–2221.

[29] Fujita, E. *Coord. Chem. Rev.* **1999**, *185*, 373–384.

[30] Hara, K.; Kudo, A.; Sakata, T. *J. Electroanal. Chem.* **1995**, *391*, 141–147.

[31] Chen, Y.; Kanan, M. W. *J. Am. Chem. Soc.* **2012**, *134*, 1986–1989.

[32] Li, C. W.; Kanan, M. W. *J. Am. Chem. Soc.* **2012**, *134*, 7231–7234.

[33] Chen, Y.; Li, C. W.; Kanan, M. W. *J. Am. Chem. Soc.* **2012**, *134*, 19969–19972.

[34] Grodkowski, J.; Neta, P. *J. Phys. Chem. A* **2000**, *104*, 4475–4479.

[35] Grodkowski, J.; Behar, D.; Neta, P.; Hambright, P. *J. Phys. Chem. A* **1997**, *101*, 248–254.

[36] Behar, D.; Dhanasekaran, T.; Neta, P.; Hosten, C. M.; Ejeh, D.; Hambright, P.; Fujita, E. *J. Phys. Chem. A* **1998**, *102*, 2870–2877.

[37] Khenkin, A.; Efremenko, I.; Weiner, L.; Martin, J.; Neumann, R. *Chem. Eur. J.* **2010**, *16*, 1356–1364.

[38] Tanaka, K.; Ooyama, D. *Coord. Chem. Rev.* **2002**, *226*, 211–218.

[39] Kitamura, N.; Tazuke, S. *Chem. Lett.* **1983**, *7*, 1109–1112.

[40] Ishida, H.; Tanaka, K.; Tanaka, T. *Chem. Lett.* **1988**, *6*, 339–342.

[41] Ishida, H.; Terada, T.; Tanaka, K.; Tanaka, T. *Inorg. Chem.* **1990**, *29*, 905–911.

[42] Tinnemans, A. H. A.; Koster, T. P. M.; Thewissen, D. H. M. W.; Mackor, A. *Recl. Trav. Chim. Pay. B* **1984**, *103*, 288–295.

[43] Kimura, E.; Wada, S.; Shionoya, M.; Okazaki, Y. *Inorg. Chem.* **1994**, *33*, 770–778.

[44] Maidan, R.; Willner, I. *J. Am. Chem. Soc.* **1986**, *108*, 8100–8101.

[45] Hayashi, Y.; Kita, S.; Brunschwig, B.; Fujita, E. *J. Am. Chem. Soc.* **2003**, *125*, 11976–11987.

[46] Gibson, D. H. *Coord. Chem. Rev.* **1999**, *185-6*, 335–355.

[47] Johnson, F. P. A.; George, M. W.; Hartl, F.; Turner, J. J. *Organometallics* **1996**, *15*, 3374–3387.

[48] Doherty, M. D.; Grills, D. C.; Fujita, E. *Inorg. Chem.* **2009**, *48*, 1796–1798.

[49] Doherty, M. D.; Grills, D. C.; Muckerman, J. T.; Polyansky, D. E.; Fujita, E. *Coord. Chem. Rev.* **2010**, *254*, 2472–2482.

[50] Agarwal, J.; Johnson, R. P.; Li, G. *J. Phys. Chem. A* **2011**, *115*, 2877–2881.

[51] Fujita, E.; Brunschwig, B. S.; Ogata, T.; Yanagida, S. *Coord. Chem. Rev.* **1994**, *132*, 195–200.

[52] Fisher, B. J.; Eisenberg, R. *J. Am. Chem. Soc.* **1980**, *102*, 7361–7363.

[53] Morris, A. J.; Meyer, G. J.; Fujita, E. *Acc. Chem. Res.* **2009**, *42*, 1983–1994.

[54] Fujita, E.; Creutz, C.; Sutin, N.; Szalda, D. J. *J. Am. Chem. Soc.* **1991**, *113*, 343–353.

[55] Creutz, C.; Schwarz, H. A.; Wishart, J. F.; Fujita, E.; Sutin, N. *J. Am. Chem. Soc.* **1991**, *113*, 3361–3371.

[56] Fujita, E.; Creutz, C.; Sutin, N.; Brunschwig, B. S. *Inorg. Chem.* **1993**, *32*, 2657–2662.

[57] Matsuoka, S.; Yamamoto, K.; Ogata, T.; Kusaba, M.; Nakashima, N.; Fujita, E.; Yanagida, S. *J. Am. Chem. Soc.* **1993**, *115*, 601–609.

[58] Ogata, T.; Yanagida, S.; Brunschwig, B. S.; Fujita, E. *J. Am. Chem. Soc.* **1995**, *117*, 6708–6716.

[59] Sato, S.; Morikawa, T.; Kajino, T.; Ishitani, O. *Angew. Chem. Int. Ed.* **2012**, *52*, 988–992.

[60] Hull, J. F.; Himeda, Y.; Wang, W.-H.; Hashiguchi, B.; Periana, R.; J., S. D.; Muckerman, J. T.; Fujita, E. *Nature Chemistry* **2012**, *4*, 383–388.

[61] Meshitsuka, S.; Ichikawa, M.; Tamaru, K. *J. Chem. Soc. Chem. Commun.* **1974**, 158–159.

[62] Beley, M.; Collin, J. P.; Ruppert, R.; Sauvage, J. P. *J. Am. Chem. Soc.* **1986**, *108*, 7461–7467.

[63] Simón-Manso, E.; Kubiak, C. P. *Organometallics* **2005**, *24*, 96–102.

[64] Fujita, E.; Haff, J.; Sanzenbacher, R.; Horst, E. *Inorg. Chem.* **1994**, *33*, 4627–4628.

[65] Kelly, C. A.; Mulazzani, Q. G.; Venturi, M.; Blinn, E. L.; Rodgers, M. A. J. *J. Am. Chem. Soc.* **1995**, *117*, 4911–4919.

[66] Kelly, C. A.; Blinn, E. L.; Camaioni, N.; D'Angelantonio, M.; Mulazzani, Q. G. *Inorg. Chem.* **1999**, *38*, 1579–1584.

[67] Schneider, J.; Jia, H.; Kobiro, K.; Cabelli, D.; Muckerman, J. T.; Fujita, E. *Energy. Environ. Sci.* **2012**, *5*, 9502–9510.

[68] Wulfsberg, G. *Inorganic Chemistry*; University Science Books: Sausalito, CA.

[69] Takeda, H.; Ishitani, O. *Coord. Chem. Rev.* **2010**, *254*, 346–354.

[70] Smieja, J. M.; Kubiak, C. P. *Inorg. Chem.* **2010**, *49*, 9283–9289.

[71] Takeda, H.; Koike, K.; Inoue, H.; Ishitani, O. *J. Am. Chem. Soc.* **2008**, *130*, 2023–2031.

[72] Hori, H.; Johnson, F. P. A.; Koike, K.; Ishitani, O.; Ibusuki, T. *J. Photochem. Photobio. A* **1996**, *96*, 171–174.

[73] Bourrez, M.; Molton, F.; Chardon-Noblat, S.; Deronzier, A. *Angew. Chem. Int. Ed.* **2011**, *50*, 9903–9906.

[74] Smieja, J. M.; Sampson, M. D.; Grice, K. A.; Benson, E. E.; Froehlich, J. D.; Kubiak, C. P. *Inorg. Chem.* **2013**, Articles ASAP.

[75] Gibson, D. H.; Yin, X. *J. Am. Chem. Soc.* **1998**, *120*, 11200–11201.

[76] Gibson, D. H.; He, H. Y. *Chem. Commun.* **2001**, 2082–2083.

[77] Gibson, D. H.; Yin, X. L.; He, H. Y.; Mashuta, M. S. *Organometallics* **2003**, *22*, 337–346.

[78] Schwarz, H. A.; Dodson, R. W. *J. Phys. Chem.* **1989**, *93*, 409–414.

[79] Schneider, J.; Vuong, K. Q.; Calladine, J. A.; Sun, X.-Z.; Whitwood, A. C.; George, M. W.; Perutz, R. N. *Inorg. Chem.* **2011**, *50*, 11877–11889.

[80] Dhanasekaran, T.; Grodkowski, J.; Neta, P.; Hambright, P.; Fujita, E. *J. Phys. Chem. A.* **1999**, *103*, 7742–7748.

[81] Gholamkhass, B.; Mametsuka, H.; Koike, K.; Tanabe, T.; Furue, M.; Ishitani, O. *Inorg. Chem.* **2005**, *44*, 2326–2336.

[82] Bian, Z.-Y.; Sumi, K.; Furue, M.; Sato, S.; Koike, K.; Ishitani, O. *Dalton Trans.* **2009**, 983–993.

[83] Whitten, D. G. *Acc. Chem. Res.* **1980**, *13*, 83–90.

[84] Ogata, T.; Yamamoto, Y.; Wada, Y.; Murakoshi, K.; Kusaba, M.; Nakashima, N.; Ishida, A.; Takamuku, S.; Yanagida, S. *J. Phys. Chem.* **1995**, *99*, 11916–11922.

[85] Richardson, R. D.; Carpenter, B. K. *J. Am. Chem. Soc.* **2008**, *130*, 3169–3180.

[86] Carpenter, B. K. *J. Phys. Chem. A* **2007**, *111*, 3719–3726.

[87] Sullivan, B. P.; Bolinger, C. M.; Conrad, D.; Vining, W. J.; Meyer, T. J. *J. Chem. Soc., Chem. Commun.* **1985**, 1414–1416.

[88] Fujita, E.; Muckerman, J. T. *Inorg. Chem.* **2004**, *43*, 7636–7647.

[89] Kumar, B.; Smieja, J. M.; Kubiak, C. P. *J. Phys. Chem. C* **2010**, *114*, 14220–14223.

[90] Frisch, M. J. et al. Gaussian 09 Revision B.01. Gaussian Inc. Wallingford CT 2009.

[91] Barone, V.; Cossi, M. *J. Phys. Chem. A* **1998**, *102*, 1995–2001.

[92] Cossi, M.; Rega, N.; Scalmani, G.; Barone, V. *J. Comp. Chem.* **2003**, *24*, 669–81.

[93] Fukui, K. *Acc. Chem. Res* **1981**, *14*, 363–368.

[94] Hratchian, H. P.; Schlegel, H. B. *J. Chem. Phys.* **2004**, *120*, 9918–9924.

[95] Hratchian, H. P.; Schlegel, H. B. *J. Chem. Theory and Comput.* **2005**, *1*, 61–69.

[96] Becke, A. D. *J. Chem. Phys.* **1993**, *98*, 5648–5652.

[97] Becke, A. D. *J. Chem. Phys.* **1996**, *104*, 1040–1046.

[98] Lee, C. T.; Yang, W. T.; Parr, R. G. *Phys. Rev. B* **1988**, *37*, 785–789.

[99] Zhao, Y.; Truhlar, D. G. *J. Chem. Phys.* **2006**, *125*, 194101.

[100] Sieger, M.; Kaim, W.; Stufkens, D. J.; Snoeck, T. L.; Stoll, H.; Záliš, S. *Dalton Trans.* **2004**, *22*, 3815–3821.

[101] Roy, L. E.; Hay, P. J.; Martin, R. L. *J. Chem. Theory Comput.* **2008**, *4*, 1029–1031.

[102] Pantazis, D. A.; Neese, F. *J. Chem. Theory Comput.* **2009**, *5*, 2229–2238.

[103] Choua, S.; Djukic, J.; Dalléry, J.; Bieber, A.; Welter, R. *Inorg. Chem.* **2008**, *48*, 149–163.

[104] Cramer, C. J.; Truhlar, D. G. *Phys. Chem. Chem. Phys.* **2009**, *11*, 10757–10816.

[105] Li, X.; Liu, X.; Wu, Z.; Zhang, H. *J. Phys. Chem. A* **2008**, *112*, 11190–11197.

[106] Rodríguez, L.; Ferrer, M.; Rossell, O.; Duarte, F. J. S.; Santos, A. G.; Lima, J. C. *J. Photochem. Photobio. A* **2009**, *204*, 174–182.

[107] Radosevich, A. T.; Melnick, J. G.; Stoian, S. A.; Bacciu, D.; Chen, C.-H.; Foxman, B. M.; Ozerov, O. V.; Nocera, D. G. *Inorg. Chem.* **2009**, *48*, 9214–9221.

[108] Dill, J. D.; Pople, J. A. *J. Chem. Phys.* **1975**, *62*, 2921–2923.

[109] Francl, M. M.; Pietro, W. J.; Hehre, W. J.; Binkley, J. S.; Gordon, M. S.; Defrees, D. J.; Pople, J. A. *J. Chem. Phys.* **1982**, *77*, 3654–3665.

[110] Sullivan, B. P.; Meyer, T. J. *Organometallics* **1986**, *5*, 1500–1502.

[111] Tryk, D. A.; Yamamoto, T.; Kokubun, M.; Hirota, K.; Hashimoto, K.; Okawa, M.; Fujishima, A. *Appl. Organometal. Chem.* **2001**, *15*, 113–120.

[112] Zhao, Y.; Truhlar, D. G. *Theor. Chem. Account* **2008**, *120*, 215–241.

[113] Leitner, W. *Coord. Chem. Rev.* **1996**, *153*, 257–284.

[114] Cokoja, M.; Bruckmeier, C.; Reiger, B.; Herrmann, W. A.; Kühn, F. E. *Angew. Chem. Int. Ed.* **2011**, *50*, 8510–8537.

[115] Kumar, B.; Smieja, J. M.; Sasayam, A. F.; Kubiak, C. P. *Chem. Commun.* **2012**, *48*, 272–274.

[116] Gibson, D. H.; Yin, X. *Chem. Commun.* **1999**, 1411–1412.

[117] Shaver, R. J.; Rillema, D. P. *Inorg. Chem.* **1992**, *31*, 4101–4107.

[118] IR v_{CO} (KBr, cm^{-1}): 2008 (s), 1916 (sh), 1880 (s). ^{1}H NMR (DMSO-d_6, 25 °C): δ 9.02 (1H, s), 8.79 (2H, d, J=4Hz), 8.58 (2H, s), 7.50 (2H, d, J=4Hz), 2.53 (6H, s).

[119] Reaction of Re(dmb)CO_3COOH and CO_2 in dark after 2 h. ^{1}H NMR (DMSO-d_6, 25 °C): δ 9.11 (1H, br), 8.86 (2H, d, J=5Hz), 8.59 (2H, s), 7.58 (2H, d, J=5Hz), 2.53 (6H, s). ^{13}C NMR (DMSO-d_6, 25 °C): δ 198.33, 194.61, 158.61 (OCO_2H), 154.95, 152.68, 152.46, 128.09, 124.56, 20.97. IR v_{CO} (KBr, cm^{-1}): 2028 (s), 1905 (s), 1857 (s), 1621 (m), 1416 (m), 1346 (m)

Reaction of Re(dmb)CO_3COOH and $^{13}CO_2$ in dark after 2 h. ^{1}H NMR (DMSO-d_6, 25 °C): δ 9.10 (1H, br), 8.86 (2H, d, J=8Hz), 8.61 (2H, s), 7.58 (2H, d, J=8Hz), 2.54 (6H, s). ^{13}C NMR (DMSO-d_6, 25 °C): δ 198.33, 194.62, 158.62 ($O^{13}CO_2H$), 154.94, 152.66, 152.46, 128.08, 124.57, 20.96. IR v_{CO} (KBr, cm^{-1}): 2027 (s), 1904 (s), 1858 (s), 1574 (m), 1393 (w), 1330 (m).

[120] Agarwal, J.; Fujita, E.; Schaefer, H. F.; Muckerman, J. T. *J. Am. Chem. Soc.* **2012**, *134*, 5180–5186.

[121] Saidur, R.; Atabani, A. E.; Mekhilef, S. *Renew. Sust. Energ. Rev.* **2011**, *15*, 2073–2086.

[122] U.S. Energy Information Administration. Few Transportation Fuels Surpass the Energy Densities of Gasoline and Diesel. http://www.eia.gov/todayinenergy/detail.cfm?id=9991, 2013.

[123] Westbrook, C. K. *Annu. Rev. Phys. Chem.* **2013**, *64*, 201–219.

[124] Marinov, N. M.; Pitz, W. J.; Westbrook, C. K.; Vincitore, A. M.; Castaldi, M. J.; Senkan, S. M.; Melius, C. F. *Combust. Flame* **1998**, *114*, 192–213.

[125] Miller, J. A.; Melius, C. F. *Combust. Flame* **1992**, *91*, 21–39.

[126] Sherwood, L. *Human Physiology. From Cells to Systems. 7th ed.*; Brooks/Cole: Belmont, CA, 2010.

[127] Atkinson, R. *Atmos. Environ.* **2000**, *34*, 2063–2101.

[128] Laufer, A. H.; Fahr, A. *Chem. Rev.* **2004**, *104*, 2813–2831.

[129] Császár, A. G.; Allen, W. D.; Schaefer, H. F. *J. Chem. Phys.* **1998**, *108*, 9751–9764.

[130] Bennet, C. J.; Jamieson, C. S.; Osamura, Y.; Kaiser, R. I. *Astrophys. J.* **2006**, *653*, 792–811.

[131] Schuurman, M. S.; Muir, S. R.; Allen, W. D.; Schaefer, H. F. *J. Chem. Phys.* **2004**, *120*, 11586–11599.

[132] Gonzales, J. M.; Pak, C.; Cox, R. S.; Allen, W. D.; Schaefer, H. F.; Császár, A. G.; Tarczay, G. *Chem. Eur. J.* **2003**, *9*, 2173–2192.

[133] Császár, A. G.; Tarczay, G.; Leininger, M. L.; Polyansky, O. L.; Tennyson, J.; Allen, W. D. In *Spectroscopy from Space*; Demaison, J., Sarka, K., Eds.; Kluwer: Dordrecht, 2001; p 317.

[134] Bomble, Y.; Kállay, M.; Gauss, J.; Stanton, J. F. *J. Chem. Phys.* **2005**, *123*, 054101.

[135] Kállay, M.; Gauss, J. *J. Chem. Phys.* **2005**, *123*, 214105.

[136] Kállay, M.; Gauss, J. *J. Chem. Phys.* **2008**, *129*, 144101.

[137] Kim, H. K.; Kim, Y.; Lee, S. M.; Ahn, K. Y. *P. Combust. Inst.* **2007**, *31*, 3377–3384.

[138] Morrison, A. M.; Agarwal, J.; Schaefer, H. F.; Douberly, G. E. *J. Phys. Chem. A* **2012**, *116*, 5299–5304.

[139] Fermi, E. *Z. Phys.* **1931**, *71*, 250–259.

[140] Darling, B. T.; Dennison, D. M. *Phys. Rev.* **1940**, *57*, 128–139.

[141] Aliev, M. R.; Watson, J. K. G. *Molecular Spectroscopy: Modern Research*; Vol. 3, ed. K.N. Rao: Academic Press, New York, 1985.

[142] Clabo Jr., D. A.; Allen, W. D.; Remington, R. B.; Yamaguchi, Y.; Schaefer, H. F. *Chem. Phys.* **1988**, *123*, 187–239.

[143] Mills, I. M. *Molecular Spectroscopy: Modern Research*; Vol. 1, eds. K.N. Rao and C.W. Mathews: Academic Press, New York, 1972.

[144] Vázquez, J.; Stanton, J. F. *Mol. Phys.* **2006**, *104*, 377–388.

[145] Willetts, A.; Handy, N. C.; Green Jr., D., W. H.and Jayatilaka *J. Phys. Chem.* **1990**, *94*, 5608–5616.

[146] Noll, K. S.; Knacke, R. F.; Tokunaga, A. T.; Lacy, J. H.; Beck, S.; Serabyn, E. *Icarus* **1986**, *65*, 257–263.

[147] Hanel, R. A.; Conrath, B. J.; Flaser, F. M.; Hearth, L.; Kunde, V.; Maguire, W.; Pearl, J.; Pirraglia, J.; Samuelson, R.; Gautier, D.; Gierasch, P.; Kumar, S.; Ponnamperuma, C. *Science* **1979**, *206*, 952–956.

[148] Hanel, R. A.; Conrath, B. J.; Flaser, F. M.; Hearth, L.; Kunde, V.; Maguire, W.; Pearl, J.; Pirraglia, J.; Samuelson, R.; Gautier, D.; Gierasch, P.; Kumar, S.; Ponnamperuma, C. *Science* **1979**, *204*, 972–976.

[149] Atreya, S. K. *Atmospheres and Ionospheres of the Outer Planets and their Sattelites*; Springer-Verlag, 1986.

[150] Romani, P. N.; Atreya, S. K. *Icarus* **1988**, *74*, 424–445.

[151] Strobel, D. F. *Int. Rev. Phys. Chem.* **1983**, *3*, 145–176.

[152] Baker, A. D.; Baker, C.; Brundle, C. R.; Turner, D. W. *Int. J. Mass Spec. Ion Physics* **1968**, *1*, 285–301.

[153] Gordon, M. S.; Truong, T. N.; Pople, J. A. *Chem. Phys. Lett.* **1986**, *130*, 245–248.

[154] Ahern, A. M.; Garrell, R. L.; Jordan, K. D. *J. Phys. Chem.* **1988**, *92*, 6228–6232.

[155] Sosa, C.; Schlegel, H. B. *Int. J. Quantum Chem.* **1986**, *29*, 1001–1015.

[156] Duncan, J. L.; McKean, D. C.; Mallinson, P. D. *J. Mol. Spectrosc.* **1973**, *45*, 221–246.

[157] Callear, A. B.; Smith, G. B. *J. Phys. Chem.* **1986**, *90*, 3229–3237.

[158] Tsang, W.; Hampson, R. F. *J. Phys. Chem. Ref. Data* **1986**, *15*, 1087–1279.

[159] Mebel, A. M.; Morokuma, K.; Lin, M. C. *J. Chem. Phys.* **1995**, *103*, 3440–3449.

[160] Fahr, A.; Monks, P. S.; Stief, L. J.; Laufer, A. H. *Icarus* **1995**, *116*, 415–422.

[161] Knyazev, V. D.; Bencsura, A.; Stoliarov, S. I.; Slagle, I. R. *J. Phys. Chem.* **1996**, *100*, 11346–11354.

[162] Li, Q. S.; Lü, R. H.; Wang, C. Y. *J. Mol. Struct.* **2004**, *668*, 35–39.

[163] Tautermann, C. S.; Wellenzohn, B.; Clary, D. C. *Mol. Phys.* **2006**, *104*, 151–158.

[164] Weissman, M. A.; Benson, S. W. *J. Phys. Chem.* **1988**, *92*, 4080–4084.

[165] Moran, D.; Simmonett, A. C.; Leach, F. E.; Allen, W. D.; Schleyer, P. v. R.; Schaefer, H. F. *J. Am. Chem. Soc.* **2006**, *128*, 9342–9343.

[166] Letendre, L.; Liu, D. K.; Pibel, C. D.; Halpern, J. B.; Dai, H. L. *J. Chem. Phys.* **2000**, *112*, 9209–9212.

[167] Nikow, M.; Wilhelm, M. J.; Dai, H. L. *J. Phys. Chem. A* **2009**, *113*, 8857–8870.

[168] Raghavachari, K.; Trucks, G. W.; Pople, J. A.; Head-Gordon, M. *Chem. Phys. Lett.* **1989**, *157*, 479–483.

[169] Stanton, J. F. *Chem. Phys. Lett.* **1997**, *281*, 130–134.

[170] Watts, J. D.; Gauss, J.; Bartlett, R. J. *Chem. Phys. Lett.* **1992**, *200*, 1–2.

[171] Watts, J.; Gauss, J.; Bartlett, R. *J. Chem. Phys.* **1993**, *98*, 8718–8733.

[172] Hampel, C.; Peterson, K. A.; Werner, H.-J. *Chem. Phys. Lett.* **1992**, *190*, 1–2.

[173] Deegan, M. J. O.; Knowles, P. J. *Chem. Phys. Lett.* **1992**, *227*, 321–326.

[174] Woon, D. E.; Dunning, T. H. *J. Chem. Phys.* **1995**, *103*, 4572–4585.

[175] Bak, K. L.; Gauss, J.; Jørgensen, P.; Olsen, J.; Helgaker, T.; Stanton, J. F. *J. Chem. Phys.* **2001**, *114*, 6548–6556.

[176] Dunning, T. H. *J. Chem. Phys.* **1989**, *90*, 1007–1023.

[177] Feller, D. *J. Chem. Phys.* **1993**, *98*, 7059–7071.

[178] Helgaker, T.; Klopper, W.; Koch, H.; Noga, J. *J. Chem. Phys.* **1997**, *106*, 9639–9646.

[179] Handy, N. C.; Yamaguchi, Y.; Schaefer, H. F. *J. Chem. Phys.* **1986**, *84*, 4481–4484.

[180] Sellers, H.; Pulay, P. *Chem. Phys. Lett.* **1984**, *103*, 463–465.

[181] Perera, S. A.; Bartlett, R. J. *Chem. Phys. Lett.* **1993**, *216*, 606–612.

[182] Cowan, R. D.; Griffin, D. C. *J. Opt. Soc. Am.* **1976**, *66*, 1010–1014.

[183] Werner, H.-J. et al. MOLPRO, version 2006.1, a package of ab initio programs. see http://www.molpro.net.

[184] Kállay, M.; Surján, P. *J. Chem. Phys.* **2001**, *115*, 2945–2954.

[185] CFOUR, a quantum chemical program package written by J.F. Stanton, J. Gauss, J.D. Watts, P.G. Szalay, R.J. Bartlett with contributions from A.A. Auer, D.E. Bernholdt, O.Christiansen, M.E. Harding, M. Heckert, O. Heun, C. Huber, D. Jonsson, J. Jusélius, W.J. Lauderdale, T. Metzroth, C. Michauk, D.P. O'Neill, D.R. Price, K. Ruud, F. Schiffmann, A. Tajti, M.E. Varner, J. Vázquez and the integral packages: Molecule (J. Almlöf and P.R. Taylor), Props (P.R. Taylor), Abacus (T. Helgaker, H.J. Aa. Jensen, P. Jørgensen, and J. Olsen), and ECP routines by A.V. Mitin and C. van Wüllen. For the current version see, http://www.cfour.de.

[186] Glendening, E. D.; Badenhoop, J. K.; Reed, A. E.; Carpenter, J. E.; Bohmann, J. A.; Morales, C. M.; Weinhold, F. NBO 5.0. Theoertical Chemistry Institute, University of Wisconsin, Madison (2001).

[187] Hammond, G. S. *J. Am. Chem. Soc.* **1955**, *77*, 334–338.

[188] Shepherd, R. A.; Doyle, T. J.; Graham, W. R. M. *J. Chem. Phys.* **1988**, *89*, 2738–2742.

[189] Kanamori, H.; Endo, Y.; Hirota, E. *J. Chem. Phys.* **1990**, *92*, 197–205.

[190] Zhang, J. S.; Xu, K. S. *J. Chem. Phys.* **1999**, *111*, 3783–3786.

[191] Pibel, C. D.; McIllroy, A.; Taatjes, C. A.; Alfred, S.; Patrick, K.; Halpern, J. B. *J. Chem. Phys.* **1999**, *110*, 1841–1843.

[192] Ahmed, M.; Peterka, D. S.; Suits, A. G. *J. Chem. Phys.* **1999**, *110*, 4248–4253.

[193] Fahr, A.; Hassanzadeh, P.; Atkinson, D. B. *Chem. Phys.* **1998**, *236*, 43–51.

[194] Fahr, A.; Laufer, A. H. *J. Phys. Chem.* **1988**, *92*, 7229–7232.

[195] Hunziker, H. E.; Kneppe, H.; McLean, A. D.; Siegbahn, P.; Wendt, H. R. *Can. J. Chem.* **1983**, *61*, 993–995.

[196] Sattelmeyer, K. W.; Schaefer, H. F. *J. Chem. Phys.* **2002**, *117*, 7914–7916.

[197] Wallington, T. J.; Dagaut, P.; Kurylo, M. J. *Chem. Rev.* **1992**, *92*, 667–710.

[198] Sharp, E. N.; Rupper, P.; Miller, T. A. *Phys. Chem. Chem. Phys.* **2008**, *10*, 3955–3981.

[199] Ravishankara, A. R. *Annu. Rev. Phys. Chem.* **1988**, *39*, 367–394.

[200] Wang, S.; Miller, D. L.; Cernansky, N. P.; Curran, H. J.; Pitz, W. J.; Westbrook, C. K. *Combust. Flame* **1999**, *118*, 415–430.

[201] Lightfoot, P. D.; Cox, R. A.; Crowley, J. N.; Destriau, M.; Hayman, G. D.; Jenkin, M. E.; Moortgat, G. K.; Zabel, F. *Atmos. Environ.* **1992**, *26A*, 1805–1961.

[202] Rienstra-Kiracofe, J. C.; Allen, W. D.; Schaefer, H. F. *J. Phys. Chem. A* **2000**, *104*, 9823–9840.

[203] Stark, M. S. *J. Am. Chem. Soc.* **2000**, *122*, 4162–4170.

[204] Wilke, J. J.; Allen, W. D.; Schaefer, H. F. *J. Chem. Phys.* **2008**, *128*, 074308.

[205] Finlayson-Pitts, B. J.; Pitts, J. N. *Science* **1997**, *276*, 1045–1051.

[206] Hunziker, H. E.; Wendt, H. R. *J. Chem. Phys.* **1976**, *64*, 3488–3490.

[207] Nandi, S.; Blanksby, S. J.; Zhang, X.; Nimlos, M. R.; Dayton, D. C.; Ellison, G. B. *J. Phys. Chem. A* **2002**, *106*, 7547–7556.

[208] Huang, D.-R.; Chu, L.-K.; Lee, Y.-P. *J. Chem. Phys.* **2007**, *127*, 234318.

[209] Ase, P.; Bock, W.; Snelson, A. *J. Phys. Chem.* **1986**, *90*, 2099–2109.

[210] Blanksby, S. J.; Ramon, T. M.; Davico, G. E.; Nimlos, M. R.; Kato, S.; Vierbaum, V. M.; Lineberger, W. C.; Ellison, G. B.; Okumura, M. *J. Am. Chem. Soc.* **2001**, *123*, 9585–9596.

[211] Pushkarsky, M. B.; Zalyubovsky, S. J.; Miller, T. A. *J. Chem. Phys.* **2000**, *112*, 10695.

[212] Hartmann, D.; Karthäuser, J.; Zellner, R. *J. Phys. Chem.* **1990**, *94*, 2963–2966.

[213] Maricq, M. M.; Wallington, T. J. *J. Phys. Chem.* **1992**, *96*, 986–992.

[214] Hochandel, C. J.; Ghormley, J. A.; Boyle, J. W.; Ogren, P. J. *J. Phys. Chem.* **1977**, *81*, 3–7.

[215] McAdam, K.; Veyret, B.; Lesclaux, R. *Chem. Phys. Lett.* **1987**, *133*, 39–44.

[216] Dagaut, P.; Kurylo, M. J. *J. Photochem. Photobiol. A* **1990**, *51*, 133–140.

[217] Parkes, D. A.; Paul, D. M.; Quinn, C. P.; Robson, R. C. *Chem. Phys. Lett.* **1973**, *23*, 425–429.

[218] Fu, H. B.; Hu, Y. J.; Bernstein, E. R. *J. Chem. Phys.* **2006**, *125*, 014310.

[219] Fernandes, R. X.; Luther, K.; Jürgen, T. *J. Phys. Chem. A* **2006**, *110*, 4442–4449.

[220] Just, G. M. P.; McCoy, A. B.; Miller, T. A. *J. Chem. Phys.* **2007**, *127*, 044310.

[221] Chung, C. Y.; Cheng, C. W.; Lee, Y. P.; Liao, H. Y.; Sharp, P., E. N. Rupper; Miller, T. A. *J. Chem. Phys.* **2007**, *127*, 044311.

[222] Vaghjiani, G. L.; Ravishankara, A. R. *J. Phys. Chem.* **1989**, *93*, 1948–1959.

[223] Niki, H.; Maker, P. D.; Savage, C. M.; Breitenbach, L. P. *J. Phys. Chem.* **1983**, *87*, 2190–2193.

[224] Lightfoot, P. D.; R., L.; Veyret, B. *J. Phys. Chem.* **1990**, *94*, 700–707.

[225] Besler, B. H.; Sevilla, M. D.; MacNeille, P. *J. Phys. Chem.* **1986**, *90*, 6446–6451.

[226] Nizovtsev, A. S.; Bogdanchikov, G. A.; Baklanov, A. V. *Combust. Flame* **2010**, *157*, 1382–1389.

[227] Bair, R. A.; Goddard, W. A. *J. Am. Chem. Soc.* **1982**, *104*, 2719–2724.

[228] Boyd, S. L.; Boyd, R. J.; Barclay, L. R. *J. Am. Chem. Soc.* **1990**, *112*, 5724–5730.

[229] Jafri, J. A.; Phillips, D. H. *J. Am. Chem. Soc.* **1990**, *112*, 2586–2590.

[230] Lay, T. H.; Bozzelli, J. W. *J. Phys. Chem. A* **1997**, *101*, 9505–9510.

[231] Szalay, P. G.; Gauss, J.; Stanton, J. F. *Theor. Chem. Acc.* **1998**, *100*, 5–11.

[232] Harding, M. E.; Metzroth, T.; Gauss, J.; Auer, A. A. *J. Chem. Theory Comput.* **2008**, *4*, 64–74.

[233] Stanton, J. F. *J. Chem. Phys.* **1994**, *101*, 371–374.

[234] Krylov, A. I. *J. Chem. Phys.* **2000**, *113*, 6052–6062.

[235] Woon, D. E.; Dunning, T. H. *J. Chem. Phys.* **1995**, *103*, 4572–4585.

[236] Nielsen, H. H. *Rev. Mod. Phys.* **1951**, *23*, 90–136.

[237] Watson, J. K. G. *J. Mol. Spectrosc.* **1977**, *65*, 123–133.

[238] Mills, I. M. *J. Phys. Chem.* **1976**, *80*, 1187–1188.

[239] Gauss, J.; Cremer, D.; Stanton, J. F. *J. Phys. Chem. A* **2000**, *104*, 1319–1324.

[240] Florián, J.; Leszczynski, J.; Johnson, B. G.; Goodman, L. *Mol. Phys.* **1997**, *91*, 439–447.

[241] Jacox, M. *Chem. Soc. Rev.* **2002**, *31*, 108–115.

[242] Jacox, M. *Acc. Chem. Res.* **2004**, *37*, 727–734.

[243] Nielsen, H. H. *Phys. Rev.* **1945**, *68*, 181–191.

[244] Martin, J. M. L.; Lee, T. J.; Taylor, P. R.; François, J.-P. *J. Chem. Phys.* **1995**, *103*, 2589–2602.